PhD Thesis

Investigation of individual donors in silicon at cryogenic temperature with atomic-scale resolution for atomic electronic devices

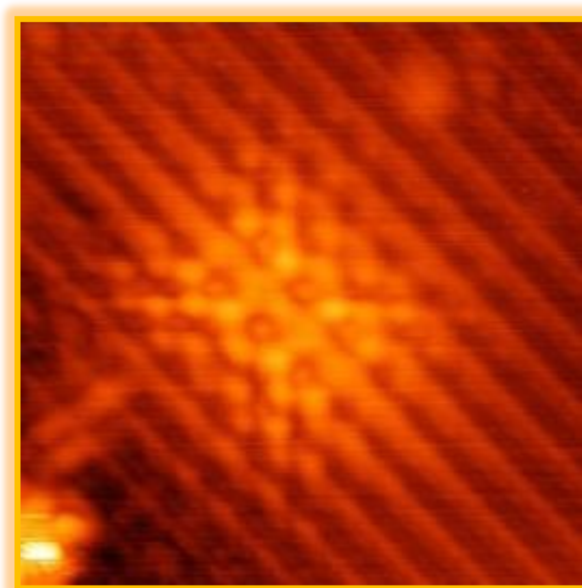

Kitiphat Sinthiptharakoon
PhD in Electronic and Electrical Engineering
London Centre for Nanotechnology
University College London

Supervisors:
Dr. Neil Curson
Dr. Steven Schofield

Declaration

I confirm that the works presented in this thesis is my own. Wherever information has been derived from other sources, it has been indicated in the thesis.

Kitiphat Sinthiptharakoon

Acknowledgements

I would like to thank all the people supporting me during the PhD study, with scientific and technical advice or simply encouraging words. Completing the PhD study at this high standard would not have been possible without you. My deepest gratitude is attributed to Neil Curson for the opportunity to be part of his vibrant and creative research group in one of the world-leading research institutes called London Centre for Nanotechnology (LCN) and for his close support throughout my PhD study. I am also greatly indebted to Steven Schofield for his continuous guidance and advice, always pointing me in the right direction and helping me to focus on the relevant points. I would like to thank Phillip Studer, Adam Rahnejat, and Lim Tingbin for supporting me in the lab, showing me everything to know about Scanning Tunneling Microscope (STM) techniques, and always being there whenever I need help with my experiments. Further I would like to thank the whole STM lab, Ben, Fadi, Reyes, Jenny, Benjamin, and many more for their warm welcome and friendship, the coffee breaks and the wonderful time here. I would also like to thank my collaborators, Veronika Brazdova and David Bowler for valuable discussions and for providing all DFT calculations and simulated STM images, making my work even more interesting for the research community. Thanks for a valuable support from Surrey University for their help with ion implantation. I am also grateful to my parents for always supporting me throughout my whole life, being with me whenever I need warm hands from trustworthy people. The last but not least, I would like to thank all the people coming into my life both inside and outside the academia. Without some of you directly and indirectly supporting me at some points during my PhD study, I would have never reached the goals I would like to achieve.

Abstract

There is an urgent need for characterisation of group V donors in silicon necessary for the development of quantum information processing (QIP) devices [1-3], and my PhD work has been contributed towards this objective. In this thesis, three different group V donors were individually studied with scanning tunnelling microscopy (STM) and spectroscopy (STS), combined with DFT calculation and simulated STM images where necessary.

Si(001) dosed with phosphine (PH_3) at room temperature prior and imaged at 77 K a few minutes later was investigated. Novel phosphine-related features were observed and compared to the room-temperature results [4]. Some features were the same as the room-temperature dissociative products but a new dissociative mechanism was proposed and novel bonding configurations were assigned to the features. A transformation between adsorbates was seen to occur on the surface at 77 K and was attributed to a tip-induced effect. The appearance of the Si-P heterodimer was found to be different at 77 K and room temperature [5] and the reasons for this difference was discussed.

Subsurface As and Bi donors below the Si(001):H surface were separately investigated at 77 K. Special sample annealing (flashing) procedures were created for both studies. There were two classes of As features commonly observed while there were three types for Bi. The appearance of the As features related to the As wavefunction informed that the subsurface As donors were electrically neutral but could be reversibly switched to being ionised (positively-charged) by changing the sample bias. Some subsurface As donors can also be negatively-charged, depending on their distances from the surface. DFT calculations were performed and simulated STM images were generated to compare with the experimental data, allowing us to assign the features to As donors at their exact lattice positions.

The appearance of the Bi features indicated that the Bi donors were negatively-charged but could be changed to being positively-charged. With the unequal rate of tunnelling in and off the donor energy level, the Bi donors could be switched back to being negatively-charged again. The Bi wavefunction projection was speculated, based on the Bi features.

Publications arising from this PhD work

1. **K. Sinthiptharakoon**, S. R. Schofield, *et al.*, *Investigating individual arsenic dopant atoms in silicon using low-temperature scanning tunnelling microscopy*, Journal of Physics: Condensed Matters 26, 012001 (2014).

2. **K. Sinthiptharakoon**, S. R. Schofield, *et al.*, *Interaction of phosphine-related molecules on Si(001) investigated by low-temperature scanning tunnelling microscopy*, (In preparation).

3. V. Brazdova, **K. Sinthiptharakoon**, *et al.*, *Exact subsurface dopant sites identified by means of scanning tunnelling microscopy on the Si(001):H surface*, (In Preparation).

4. M. Siegl, **K. Sinthiptharakoon**, *et al.*, *Charged states of subsurface Bi donors below Si(001):H investigated with scanning tunneling microscope at 77 K*, (In preparation).

Conference presentations

1) **Poster**; *The 2nd Meeting on Silicon Quantum Information Processing (SiQIP2012)*, University of Surrey, UK.
2) **Poster**; *Postgraduate Symposium on Nanotechnology (PSN2012)*, University of Birmingham, UK.
3) **Poster**; *The 18th International Conference on Microscopy of Semiconducting Materials (MSM2013)*, University of Oxford, UK.
4) **Talk**; *The 39th International Conference on Micro and Nano Engineering (MNE2013)*, Imperial College London, UK.
5) **Poster**; *The 3rd Meeting on Silicon Quantum Information Processing (SiQIP2013)*, University of Surrey, UK.
6) **Talk** and **Poster**; *The 1st International Conference on Advanced Materials for Demanding Applications (AMDA2014)*, Glyndwr University, UK.
7) **Poster**; *The 4th Meeting on Silicon Quantum Information Processing (SiQIP2014)*, University College London, UK, 2014.
8) **Talk**; *The 4th International Conference on Thailand Nanotechnology Conference (NanoThailand2014)*, Thailand Science Park, Thailand.

Table of Contents

Acknowledgement 3

Abstract 4

Publication arising from this PhD work 5

Conference presentations 6

Chapter 1 Introduction 12

1.1 Nanotechnology 12

1.2 Silicon-based quantum computer 13

1.3 Atomically controlled placement of donors in silicon 16

1.4 Single subsurface donor atoms in silicon 18

Chapter 2 Background 21

2.1 Scanning tunnelling microscope 21

2.1.1 Quantum Tunnelling 23

2.1.2 Quantum Tunnelling in STM 24

2.1.3 Energy-Dependence of the Tunnelling Current 25

2.1.4 Distance-dependence of the Tunnelling Current 27

2.1.5 Constant-current and constant-height modes of imaging 27

2.1.6 Interpretation of the tunnelling current 28

2.1.7 Scanning Tunnelling Spectroscopy (STS) 30

2.1.8 Current Imaging Tunnelling Spectroscopy (CITS) 31

2.1.9 Tip-Induced Band Bending (TIBB) 32

2.1.10 Double-Tip Effect 33

2.2 Si(001) surface 35

2.2.1 Reconstruction of Si(001) 35

2.2.2 Si(001) at room temperature 37

2.2.3 Si(001) appearance at low temperature 39

2.2.4 Energy-band structure of Si(001) 39

2.2.5 Defects of Si(001) 42

2.3 Si(001):H surface 44

2.3.1 Three types of structures from H-termination 45

2.3.2 Energy-Band Structure of the Si(001):H surface 48

2.4 Phosphine (PH_3) on Si(001) 49

2.5 Subsurface dopants below Si(001) 54

Chapter 3 Experiment Methods 59

3.1 Low Temperature STM 59

3.1.1 Ultra High Vacuum Chambers 60

3.1.2 Vibration Isolation System 61

3.2 Sample Preparation 62

3.2.1 Si(001) Preparation 62

3.2.2 Si(001):H Preparation 63

3.3 Tip Preparation 63

3.3.1 Ex-situ 64

3.3.2 In-situ 66

3.4 Phosphine Dosing 68

3.5 RGA Spectrometer 68

3.6 STM Data Processing 69

Chapter 4 Phosphine on Si(001) at 77 K 70

4.1 Introduction 70

4.2 Saturation PH_3-dosed Si(001) 72

4.2.1 Two distinctive PH_3-related features 72

4.2.2 Voltage-dependent imaging of the saturation-dosed surface 74

4.3 Low PH_3-dosed Si(001) 74

Individual phosphine-related features 76

4.3.1 Group A features 79

4.3.2 Group U features 84

4.3.3 Group C features 86

4.3.4 PH3-related hemihydride structure 90

4.4 Tip-induced structural transformation 92

4.5 Si-P heterodimer at 77 K 99

4.5.1 Ejected Si dimer rows and redundant H atoms 100

4.5.2 The ground state of Si-P heterodimer 102

Chapter 5 Subsurface As dopants below Si(001):H at 77 K 107

5.1 Introduction 107

5.2 Low-temperature flash for sample preparation 108

5.3 Subsurface As-dopant induced features 112

5.4 Feature As1 114

5.4.1 Electrically neutral As donors (D^0) 116

5.4.1.1 Voltage-dependent appearance of As^0 features 117

5.4.1.2 How As donors in silicon can be electrically neutral 119

5.4.2 Positively-Charged As donors (D^+) 121

5.4.3 Band-gap states related to As1 122

5.5 Feature As2 124

5.5.1 Negatively-charged As donors (D^-) 126

5.5.2 Origin of the negatively-charged As donors 128

5.6 DFT calculation for the neutral As features 131

5.6.1 Calculation Methods 131

5.6.2 Stable substitutional sites for As 132

5.6.3 Simulated STM images 134

5.7 Dimer-row shift of the Si(001):H surface 138

Chapter 6 Subsurface Bi dopants below Si(001):H at 77 K 140

6.1 Introduction 140

6.2 Sample preparation 141

6.2.1 Ion implantation 142

6.2.2 Two-step flashing procedure 143

6.2.3 Checking subsurface Bi concentration using STS curves 145

6.2.3.1 Checking Bi concentration below Si(211) with X-STM 145

6.2.3.2 Checking Bi concentration below Si(001) without X-STM 147

6.2.4 Removing the surface states of Si(001) with H-termination 149

6.3 Subsurface Bi-induced features at 77 K 149

6.3.1 Many Bi features in the same image 151

6.3.2 Three classes of subsurface Bi-induced features 151

6.3.3 Mechanism inducing the subsurface Bi features 155

6.3.3.1 Filled-stated appearance 155

6.3.3.2 Empty-stated appearance 157

Chapter 7 Conclusion and future work 161

7.1 Conclusion 161

7.1.1 The study of phosphine on Si(001) at 77 K 161

7.1.2 Subsurface As donors in Si 164

7.1.3 Subsurface Bi donors in Si 166

7.2 Possible future work 168

7.2.1 Possible future work for PH_3 on Si(001) 168

7.2.2 Possible future work for subsurface As and Bi donors in Si 168

Appendix A The density of subsurface As donors 169

Lists of Figures 171

List of Tables 175

Bibliography 176

Chapter 1

Introduction

1.1 Nanotechnology

The field of nanoscience and nanotechnology was first introduced by Richard Feynman back in 1959 in the annual meeting of American Physical Society [6] in which he gave a ground-breaking lecture entitled "*There's plenty of room at the bottom*". It was pointed out in the lecture that when we went down to nanoscale dimensions, the properties of individual atoms would be different from what they had been in macroscopic and microscopic systems, and the laws having been used for understanding these systems would not be the same as the laws used for the nanoscopic system. The prediction has been experimentally proved to be true in the last few decades with a good example being variation of the *wavefunction symmetry* of Mn acceptors in GaAs, which depends on the distance of the dopants with respect to the surface layer [7] as shown in Figure 1.1. Another good example of Feynman's prediction is the variation of the *ionisation energy* of Si donors in GaAs which depends on the depth of the dopants with respect to the semiconductor surface [8]. Some Si donors in GaAs can even express the negatively-charged state when observed with STM [9, 10], which has been surprising for the conventional concepts in which the charge state of donors in semiconductors can only be electrically neutral (non-ionised) and positively-charged (ionised) [11].

There have been many definitions of nanotechnology, however, in the context of the present work it could be defined as "*The capability of measuring and making things with controllable atomic precision by exploiting novel properties of individual atoms or molecules found at the nanoscale*". Nanotechnology has been envisaged as a new enabling technology similar to the electronics technology and the Internet technology. It will have significant impacts on human living with its capabilities of enhancing other existing

technologies such as processing chips in computers – Desktop, Laptop, Tablet, and Smart Phone – that would lead to the next generation of computation.

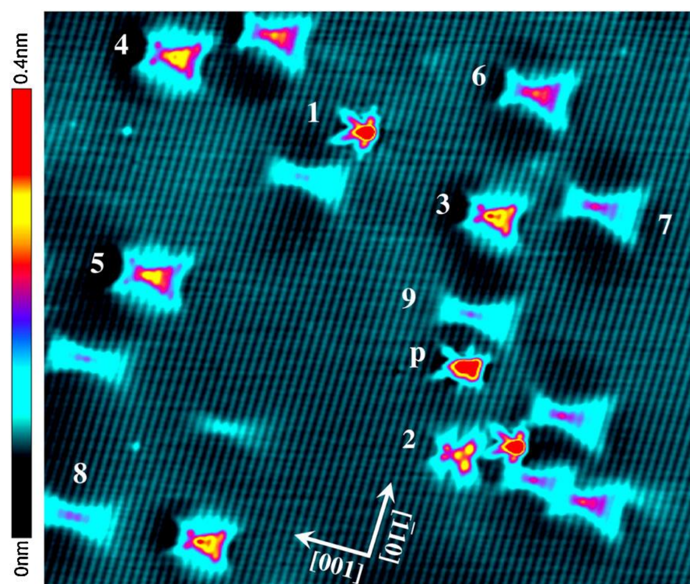

Figure 1.1 An STM image of 45 × 35 nm² of an GaAs(110) surface doped with the Mn acceptors measured at 5 K revealing the variation of the projection of the wavefunction of the Mn acceptors located in the subsurface layers beneath GaAs(110). This STM image is taken from Ref. [7].

1.2 Silicon-based quantum computer

As the miniaturisation of semiconductor devices continues, the properties of individual dopants, the interactions among them, and the influences of the environment at the atomic scale becomes vitally important for device functionality. For conventional electronic devices, it has been known that the variation of the properties of individual dopants can be negligible since the device functionality is based on the averaged properties of many thousands of dopants in the semiconductor substrate. However, for atomic electronic devices, variation of properties of individual dopants, coupling interactions among the dopant atoms, and effects of environment to the dopants at the atomic scale can significantly affect the device operation. For example, it has been reported that when dopants are located near the interface, their ionisation energies are varied when measured with STM [8], and when two dopants are positioned with the inter-dopant distance

smaller than 10 nm, the electrostatic interaction between the dopants and their altered electronic properties due to the semiconductor surface provide a bistable charge switching behaviour of the two-donor system [12]. The characteristics of individual dopants are essential not only for the highly-scaled electronic devices [13, 14], but also for the Quantum Information Processing (QIP) concept [1, 2] that is expected to form the next generation of computation devices.

The first scheme of constructing a quantum computer in silicon using the P atoms as quantum bits (qubits) for storing information was proposed by B. E. Kane in 1998 [1] as shown in Fig. 1.2 (a). The device has to operate at about 100 mK so that each P atom is in its non-ionised state with the fifth valence electrons still weakly bound to the nucleus. In this proposal, the information is encoded on the nuclear-spin states of P atoms, based on the fact that the nuclear spin has 2 quantum states which are "spin up" and "spin down" represented as 1 and 0 respectively. The P atoms are embedded in the silicon substrate and separated by ~ 20 nm from adjacent P atoms. Metal gate electrodes called the A gates are placed on the insulating layer above each P qubit with the J gates placed between two A gates as shown in Fig. 1.2 (a). To change the nuclear-spin state of a particular P atom, a voltage is applied to the A gate above that P qubit. The electrostatic influence will alter the charge distribution of the fifth valence electron bound to that P atom, in-turn changing the resonance frequency of the P nucleus, via the hyperfine interaction. The interaction between the P-bound electron and the P nuclear spin also allows coupling between two adjacent P qubits via the overlap of their valence electrons, which occurs because the electron wavefunctions extend up to tens of nanometres in silicon. By applying negative bias to the J gate, the electron charge is repelled from the region between two adjacent qubits, reducing the wavefunction overlap of the adjacent valence electrons, and hence turning off the interaction between these two qubits. For Kane's proposal, each P atom must be placed with atomic-scale precision in the silicon substrate with close proximity to the insulating oxide layer and the metal gates (no more than ~ 20 nm). This requirement emphasises the need of experimentally investigating the effects of the interface on the properties of the individual P dopants and the interactions of adjacent dopant atoms.

However, since the operation temperature of the quantum computer proposed by Kane is very low (~ 100 mK), and furthermore the metal gates and the insulating layer may create atomic-scale defect at the interfaces that might disturb the operation of the device, a new proposal for Quantum Information Processing (QIP) is preferable. More recently a scheme proposed by A. M. Stoneham *et al.* in 2003 [2] (see Fig. 1.2 (b)))) making use of energetically deep donors such as Bi instead of P to enable the device to operate at higher temperature e.g. 77 K which is the temperature of liquid nitrogen. The scheme also makes use of control atoms instead of the metal gates for controlling the qubit interactions, removing the gate-related defects that might cause problems for device operation.

The donors used in the QIP scheme proposed by Stoneham *et al.* are placed together within the proximity of 10 nm as shown in Fig. 1.2(b). It consists of three dopant atoms embedded in a silicon substrate. Dopant A and Dopant B have the same ionisation energy and form the quantum bits (qubits) with dopant C having different ionisation energy from dopant A and B acting as a control switch. The information is encoded in the spin states of the fifth valence electrons bound to the A dopant and the B dopant. To encode the information in the spin of the donor valence electrons, the scheme requires these three impurities to be at their ground state (the non-ionised state) when there is not any external influence applied to the device. In the ground state, none of the dopants interact with one another. However, with optical excitation of the valence electron of the control atom into its orbital excited state, the wavefunction of this electron is greatly expanded and extends across both neighbouring dopants, being able to create an exchange interaction between the electron spin of each qubit since both qubits are placed away from each other in the range of less than 10 nm. The optical excitation and stimulated de-excitation of dopant C are used to switch the interaction between the qubits on and off respectively. Some promising candidates for these dopants are group V donors with large ionisation energy such as As (54 meV) and Bi (71 meV) atoms.

According to both QIP schemes, one proposed by Kane and the other by Stoneham, it is necessary to fabricate the device such that the separation between adjacent qubits is around 10-20 nm. Furthermore, the dopant atoms must also be

embedded within the silicon substrate, which makes the knowledge of how individual dopant atoms behave with atomic-scale resolution when they are in the subsurface layers below the device surface essential. Understanding the interaction between the dopants and the influence of the interface on the dopants is also necessary.

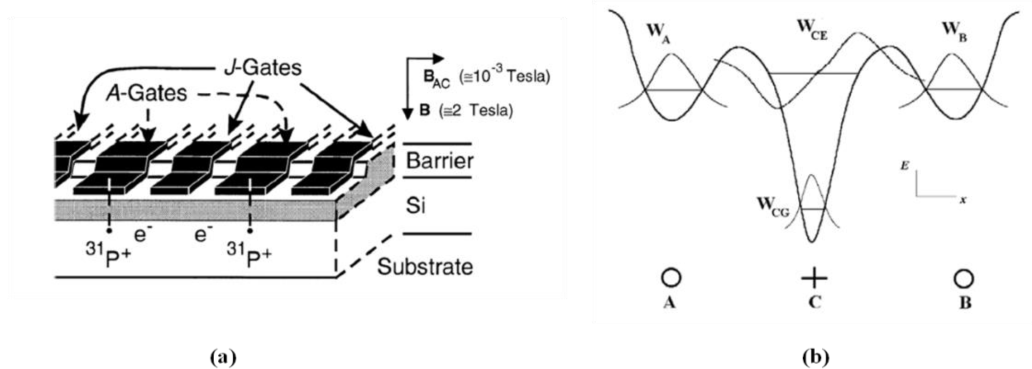

Figure 1.2 **(a)** The Quantum Computer device proposed by Kane in which two P dopants are precisely embedded below a silicon substrate with each metal gate precisely placed with respect to each P atom. The diagram is taken from Ref. [1]. **(b)** The Quantum Computer scheme introduced by Stoneham *et al.* in which the C atom is the control switch instead of the metal gates, and atoms A and B have a larger binding energy than for C, enabling device operation at higher temperature. (taken from Ref. [2]).

1.3 Atomically controlled placement of donors in silicon

Since the operation of the Quantum Information Processing (QIP) device significantly relies on the electronic states of donors, the capability of placing dopant atoms with atomic-scale spatial accuracy and the capability of characterising the properties of individual dopants in the silicon are necessary. There already exists a technique allowing the placement of P donors in silicon with the atomic-scale precision using a scanning tunnelling microscope (STM) [15, 16]. The schematic diagram illustrating the fabrication steps is shown in Fig. 1.3. Firstly, a well-reconstructed and clean Si(001) surface is prepared (Fig. 1.3 (a)). Then, it is terminated by a single layer of H atoms, following by using the

STM tip to selectively desorb individual H atoms from the H layer as seen in Fig. 1.3 (b). Phosphine (PH_3) gas is subsequently dosed to the surface and can only be adsorbed onto the hydrogen-free surface areas before the sample is then be thermally annealed so as to incorporate the P donor atoms into the Si(001) surface layer (see Fig. 1.3 (c)). Then, the sample is heated up to remove the H resist before that Si layers are grown on top of the Si(001) surface to encapsulate the P dopants without making them significantly diffuse from the original positions, resulting in an atomic device with the P dopants in the silicon substrate.

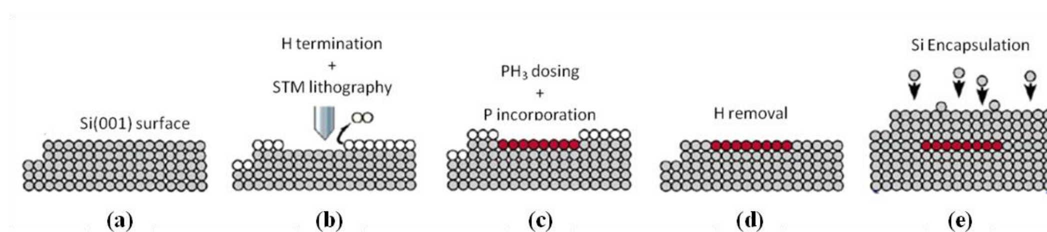

Figure 1.3 (a)-(e) The fabrication steps toward an atomic-scale electronic device in silicon. The grey, white, and red circles represent Si, H, and P atoms respectively. The P atoms are selectively placed on the Si(001) surface and Si layers are subsequently grown on top of the surface to bury the P donor atoms. The figure is taken from Ref. [16].

The technique described above has met the requirement for building a QIP device in which individual donor atoms must be precisely placed at the intended positions. However, each step of the fabrication requires comprehensive understanding of how the dopants behave. A part of this PhD work is contributed to the study of phosphine-related structures on the Si(001) surface with the STM imaging being performed at 77 K. In the past, these structures have been comprehensively studied with room-temperature imaging, electronic structure calculations, and theoretically simulated STM images [4]. Although the study has led to the underlying mechanism of the PH_3 dissociation on the Si(001) surface, there are still some key structures that have never been experimentally observed. Moreover, while all observed structural transformations of the phosphine dissociative products are thermally induced, the possibility exists for structural transformations to occur that are induced by the electrostatic influence. These two

aspects of the PH_3 dissociation will be studied in Chapter 4, enabled by the advantage of investigating the phosphine-dosed Si(001) surface at 77 K.

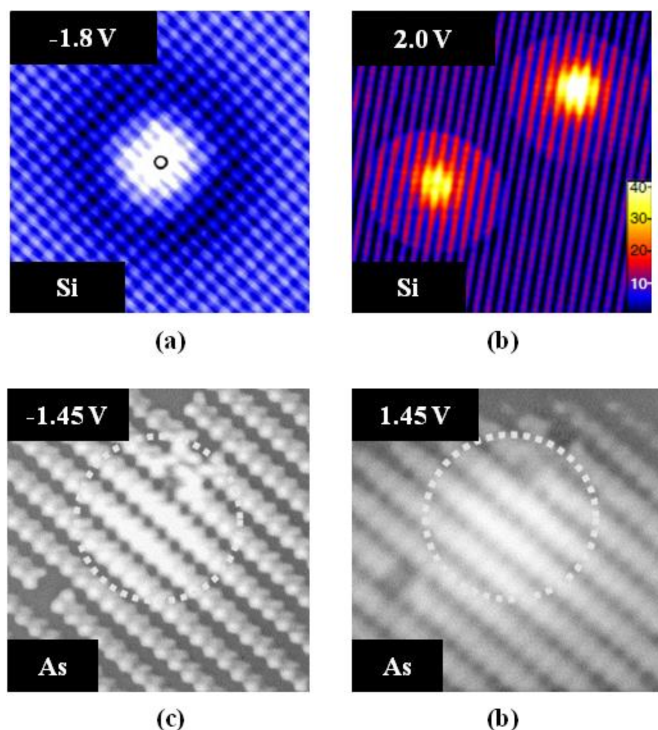

Figure 1.4 **(a)** and **(b)** filled- and empty-state images of Si donors in GaAs below the (110) surface orientation measured at ~ 5 K . **(c)** and **(d)** filled- and empty-state images of As donors in Si below the Si(001):H surface measure at room temperature. Images are taken and adapted from Ref. [11, 17, 18].

1.4 Single subsurface donor atoms in silicon

Beside the capability of placing donor atoms in silicon with the atomic-scale precision and the understanding of donor behaviours during the fabrication process, the determination of the properties of the resulting subsurface dopants beneath the semiconductor surfaces is another challenging step towards desirable device operation.

Subsurface donors such as Si [18] and Te [19] have been extensively studied below the GaAs(110) surface. This surface has no surface states, making the observation of electronic states associated with the subsurface dopants in the

semiconductor bandgap possible, as shown in Fig. 1.4 (a) and 1.4 (b). However, for subsurface donors in Si, only a small number of studies have been reported such as for P [20] and As [17], illustrated in Fig. 1.4 (c) and 1.4 (d). Unlike the GaAs(110) surface that could be prepared by cleavage, the Si(001) surface that is of interest to us has to be thermally prepared to obtain flat and clean characteristics [21, 22] preferable for the STM measurement. This is provides a challenge since the thermal diffusion of the donors with inappropriate sample temperature may result in the depletion of the dopants in the surface region where they could be observed by STM [23].

In Chapter 5 and 6, the As donor and the Bi donor in the subsurface layers below the H-terminated Si(001) surface will be discussed. The thermal preparation of the silicon sample for obtaining a surface suitable for STM measurement and a sufficient density of donors in the subsurface layers is revealed. The study of subsurface As in Chapter 5 unveils images of a neutral donor wavefunction (or to be more precise the projection onto the surface of the square of the amplitude of the wavefunction) in silicon for the first time. The ability to image neutral dopant wavefunctions in silicon is of great interest and potential use for researchers developing the QIP schemes described above. Also observed in Chapter 5 is the striking discovery that the As donor in its electrically neutral state (its ground state) at 77 K, but can be reversibly switched to the positively-charged ionised state merely by changing the sample bias. The experiment also leads us to a strange discovery of negatively-charge As donors for which we have proposed some possible interpretations. In Chapter 6, we studied Bi donors in the subsurface layers below the H-terminated Si(001) surface at 77 K. The Bi donors were embedded in the silicon sample by ion implantation to create 5 layers of the donors down to 600 nm below the Si(001) surface. The preparation of the Si(001) surface had the requirement that there were sufficient Bi dopants remaining in the subsurface layers after preparation, which was a significant challenge. A multi-flash method for the sample preparation is discussed in Chapter 6. The STM images revealing subsurface Bi donors observed are very promising although the interpretation of the observed features is still a real mystery. We have suggested some ideas that could lead to clearer explanation of their appearance and their charge state. In Chapter 5 and Chapter 6, the

influence of the interface between the semiconductor and the vacuum on the subsurface donor properties will also be discussed for the full interpretation of the subsurface donor behaviour which is opposed to the conventional understanding of dopants in silicon.

Chapter 2

Backgrounds

Properties of atomic-scale electronic devices are dramatically influenced by individual dopant atoms such that the understanding of the behaviour of the dopants individually, the interaction among them, and the influence of the environment on individual dopants could pave way for the fabricating of new electronic devices, along with their characterisation, at the atomic-scale precision. In this Chapter, the principles of scanning tunnelling microscopy (STM) widely used for studying and even manipulating individual atoms in the sample surface regions of conducting samples will be discussed, which is vitally important for the interpretation of our data presented in the later chapters of this thesis. We will also review the essential characteristics of the sample surfaces used in this PhD work, the clean Si(001) surface and the hydrogen-terminated Si(001) surface. Finally, we will review the past work on the study of the interaction of phosphine molecules (PH_3) with the Si(001) surface, and the work contributing to the study of subsurface dopants in semiconductors. This basic understanding has allowed us to distinguish the intrinsic features of the surfaces under study from those additional features which appeared on the surfaces after the samples had undergone some molecular dosing or special thermal treatment.

2.1 Scanning tunnelling microscope

Scanning tunnelling microscope (STM) is an instrument exploiting the tunnelling current created by the tunnelling of electrons between two electrodes – one is a sharp metal tip (or probe) and the other is a conducting sample – to measure and manipulate the sample surfaces and additional adsorbates on the particular surfaces. Since its invention in 1982 [24], followed by the first image of a silicon surface revealing individual Si atoms of the surface [25], the STM has made a significant impact on various fields of study, not just semiconductor

physics, such as biology [26], electrochemistry [27], and organic chemistry [28]. The reason why STM is widely used in such diverse fields is its remarkable capability of providing topographical images of surfaces at high spatial resolution. Even individual atoms and their electronic properties can be examined with the atomic-scale resolution. Apart from the imaging capability, STM can also be used to manipulate individual atoms and molecules in the surface region [29]. For example, the tip has been utilised to tailor the electronic states of subsurface dopant atoms below semiconductor surfaces [11, 30, 31], to controllably cause the phase transition of the surface [32], and even to create an artificial molecule on the surface [33].

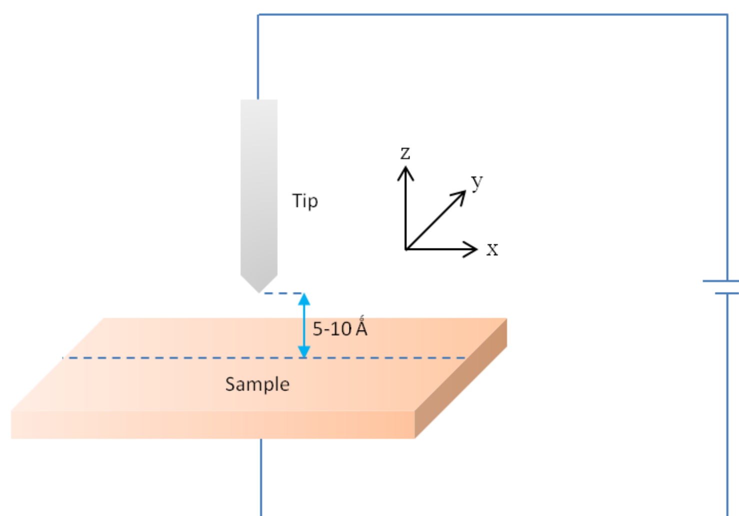

Figure 2.1 (a) A simple diagram illustrating an STM structure consisting of a sharp metal tip positioned over a conducting sample surface within a separation of a few angstroms and a power supply providing voltages across the tip and the sample, which generates tunnelling current flowing between the tip and the sample.

The principle of STM that provides the atom-by-atom measurement is illustrated in Fig. 2.1. To allow electrons to tunnel between the tip and the sample, a sharp metal tip is approached to the conducting sample within proximity of a few angstroms with respect to the planar surface with a vacuum gap acting as an insulator between these two electrodes. When a bias voltage is applied across the sample and the tip, electrons tunnel from the tip to the sample or vice versa

through the vacuum barrier, which forms the so-called *tunnelling current*. By scanning the tip over the surface, we can image the sample surface and measure local electronic properties.

2.1.1 Quantum Tunnelling

In this section, we will briefly discuss the concept of the quantum tunnelling of a particle in one dimension which is important for obtaining an insight into electron tunnelling – the crucial basic mechanism that one has to understand before he can interpret the results from the STM measurement.

The diagram of a particle tunnelling in one dimension is illustrated in Fig. 2.2. There are three regions. In Region I and Region III, the potential V is equal to zero ($V = 0$), meaning the particle in these regions has no potential energy; thus, the particle can be called a free particle. In Region II, the potential is not zero but equal to V_0, ($V = V_0$). If the particle is classically considered, the probability of the particle to move from Region I to Region III through the potential barrier (Region II) is zero if the total energy E of the particle is less than the energy required to cross the barrier which is equal to potential barrier height qV_0 in which q is the charge of the particle. We assume that the total energy of the particle is less than the potential barrier height ($E < qV_0$), so the particle is always reflected from the barrier. However, in quantum mechanics where a particle is considered as a wave, the probability of the particle to transmit through the potential barrier is not zero if the barrier width is sufficiently narrow.

The schematic representation of the wavefunction of the particle in all three regions is shown in Fig. 2.2 in which the amplitude of the wavefunction inside the barrier exponentially decreases from position $z = 0$ to $z = d$. If the width d of the potential barrier is small enough, the amplitude of the wavefunction tunnelling through the barrier will not be decreased to zero before it reaches the boundary $z = d$, so the particle successfully tunnels across the barrier.

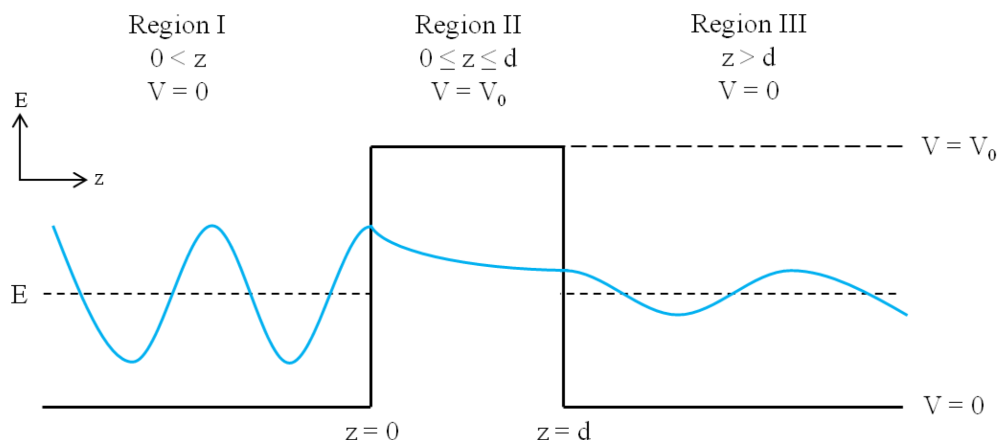

Figure 2.2 Tunnelling of a particle of mass m and energy E from a zero-potential region (Region I) to another zero-potential region (Region III) through a one-dimensional rectangular potential barrier (Region II) showing an amplitude decay of the wavefunction of the particle.

2.1.2 Quantum Tunnelling in STM

Figure 2.3 shows energy-band diagrams of an STM system consisting of a metal sample and a metal tip separated by a vacuum region. For simplicity, the energy levels up to the Fermi levels of the sample (E_{F_s}) and the tip (E_{F_t}) are occupied by electrons (filled states) whereas the energy levels above the Fermi levels are unoccupied (empty states).

When the sample and the tip are far from each other such that there is no interaction between them, the Fermi levels of the tip and the sample are not aligned with each other as shown in Fig. 2.3 (a). In equilibrium for which the tip is approached towards the sample such that the separation between the tip and the sample surface is approximately a few angstroms, the tip Femi level and the sample Fermi level become aligned (see Fig. 2.3 (b)).

Once a bias voltage V is applied across the tip and the sample, the Fermi levels are shifted away from each other. Consider Fig. 2.3 (c) as an example, if a negative bias is applied to the sample, the tip Fermi level will be shifted downwards with respect to the sample Fermi level, allowing some filled states of the sample to lie above the tip Fermi level. Due to the driving force from the power supply, electrons can tunnel from the sample to the tip, generating a

tunnelling current. The applied voltage V is considered to be so small that the shift of the Fermi levels does not significantly alter the vacuum levels with respect to the Fermi levels. Hence, the shape of the vacuum potential barrier can be considered rectangular so that the concept of a particle tunnelling in one dimension is also applicable for the STM system.

For the STM system, the tunnelling current for a particle with a certain energy level can be written as

$$I = |\psi(z)|^2 e^{-2\beta d} \tag{2.1}$$

$|\psi(z)|^2$ is a constant representing the probability of finding the particle at the distance z. β associated with the particle energy and the potential barrier the particle tunnelling through is expressed as $\frac{\sqrt{2m(qV_0-E)}}{\hbar}$. d is the tunnelling distance.

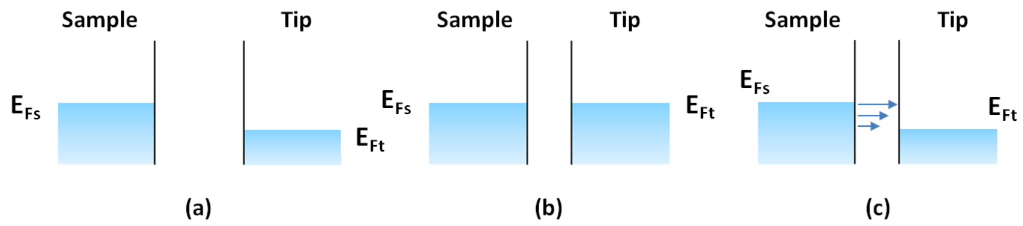

Figure 2.3 Energy-band diagrams of an STM system consisting of a metal sample and a metal tip: **(a)** separated such that there is no interaction between them, **(b)** brought close to each other until they are in thermal equilibrium, **(c)** with a negative bias applied to the sample.

2.1.3 Energy-Dependence of the Tunnelling Current

For the tunnelling current, I, of an STM system such as Fig. 2.3 under the condition that the tunnelling distance is constant, we have

$$I \propto e^{-2E^{1/2}} \tag{2.2}$$

where E represents the energy magnitude of the electronic state contributing to the tunnelling current. From Eq. (2.2), the magnitude of the tunnelling current is inversely proportional to the energy of the level contributing to the tunnelling

current. The further away from the vacuum level the energy level *E* is, the weaker the tunnelling current *I* becomes. Therefore, at negative sample bias as shown in Fig. 2.4 (a), most of the tunnelling current is contributed by those electrons tunnelling from the filled states of the sample lying at and just below the Fermi level. Similarly, at the positive sample bias as shown in Fig. 2.4 (b), most of the tunnelling current is contributed by those electrons tunnelling from the filled states of the tip lying at and just below the tip Fermi level. The magnitudes of relative tunnelling current produced by electrons tunnelling from different energy levels are qualitatively represented by the length of the blue arrows in the vacuum part between the sample and the tip surfaces.

The concept of the dominance of the tunnelling current associated with the electrons in the higher energy levels will be useful when we discuss the results of our experiments on the subsurface dopants below semiconductor surfaces to show how the tunnelling current contributed by the dopant energy levels in the band gap can dominate the total tunnelling current, allowing the surface features induced by the subsurface dopants to be visible.

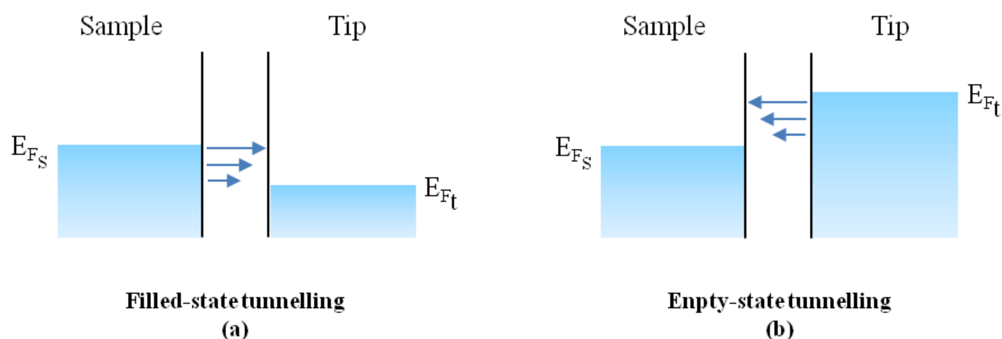

Figure 2.4 Energy-band diagrams of a sample and a tip: **(a)** the sample is negatively biased, so electrons tunnel out of the filled states of the sample; **(b)** the sample is positively biased, so electrons tunnel into the empty states of the sample.

2.1.4 Distance-dependence of the Tunnelling Current

For the tunnelling current of an STM system considered in the previous section when only one energy level is considered and the tunnelling distance (tip-sample separation) is varied, we have

$$I \propto e^{-2d} \tag{2.3}$$

The tunnelling current exponentially decreases with increasing the tip-sample separation d. This means that an increase of the tip-sample separation by 1 Å can result in a decrease of the tunnelling current by almost one order of magnitude. To keep the current constant, the separation between the tip and the sample surface must be kept constant. If the separation distance suddenly changes and so the current, the control system will detect the change of the current and accordingly adjust the vertical position of the tip to keep the current at the set constant value. The variation of the tip position over the sample surface is used to create the topographical image of the surface. Hence, with the precise control over the movement of the tip along the z-axis (the axis perpendicular to the surface plane) and in the $x - y$ plane (the sample surface plane), atomic-resolution images of the surface can be acquired.

2.1.5 Constant-current and constant-height modes of imaging

In using STM to image the surface, there are two modes of operation; constant-current imaging mode and constant-height imaging mode. Fig. 2.5 (a) illustrates the movement of the tip over the scanned surface in the constant-current mode. The tip is moving from the left to right and the tunnelling current is set to a constant setpoint value. At a given applied voltage, the tip vertical position is regulated to maintain the current at the setpoint value. In the other word, the tip-surface separation (h) is kept constant by adjusting the tip vertical position with respect to the surface while scanning, using a feedback mechanism. The voltage signal required to change the vertical tip position is used to generate the STM image. The contrast of the image is directly related to the local density of states

(LDOS) of the sample surface, and of the tip (which usually assumed to be constant).

For the constant-height imaging mode shown in Fig 2.5 (b), the tip vertical position is constant; thus, the tip-sample separation is changing while scanning, depending on the topography and LDOS of the sample at each scanned point. The vertical position of the tip can be fixed by turning off the feedback mechanism. The change of the tunnelling current is exploited to create the STM image. Since the regulation of the vertical tip position is not required, the height-constant mode provides faster scan rate. However, unlike the images acquired with the constant-current mode, the contrast of the image obtained with the height-constant mode is not directly related to the LDOS of the surface.

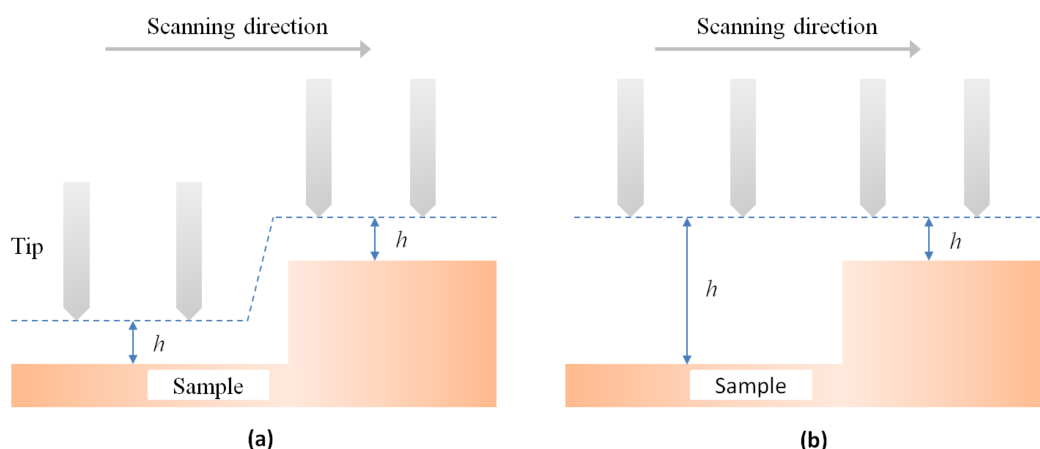

Figure 2.5 Modes of STM imaging: **(a)** Constant-Current, the tip-surface separation is controlled to keep the setpoint tunnelling current constant by adjusting the tip vertical position during the scan. **(b)** Constant-Height, the tip vertical position is constant, leading the alteration of the tunnelling current during the scan.

2.1.6 Interpretation of the tunnelling current

Fig. 2.6 (a) and 2.6 (b) show filled- and empty-state images of a clean Si(001) surface taken at the sample bias of -2.0 V and +2.0 V respectively. While the topography of the surface apparently changes when the bias voltage switches from negative and positive and vice versa, we also have to consider the LDOS

when interpreting the images. The electronic energy levels associated with the tunnelling current are those lying between the sample Fermi level and the tip Fermi level for which the electrons tunnel out of the filled states (shaded area) of the sample to the empty states (empty area) of the tip for the negative bias. Therefore, the topographic image of the surface is strongly associated with the energetic states of the sample.

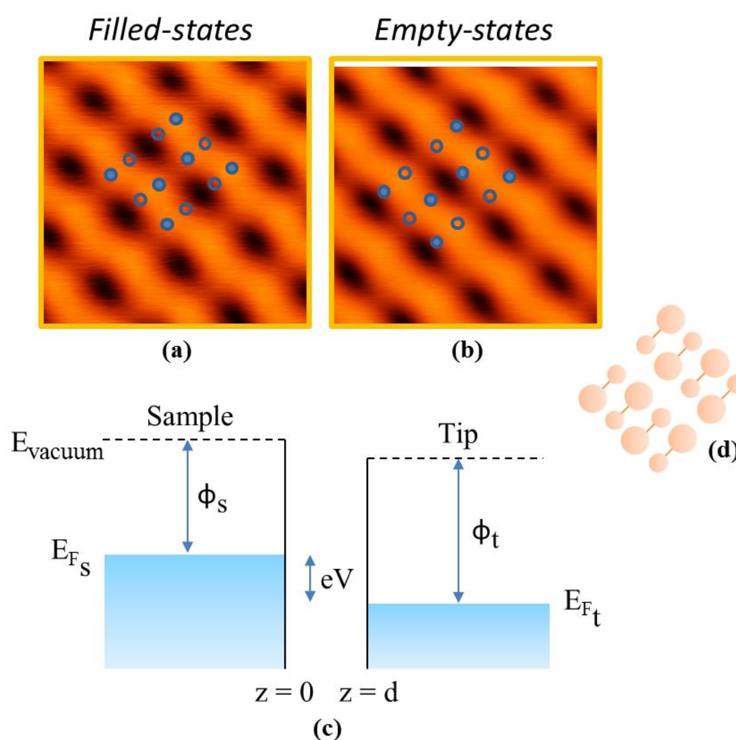

Figure 2.6 Topography images of a Si(001) surface taken with the sample bias of **(a)** -2.0 V and **(b)** +2.0 V, showing the dependence of the appearance of the surface corrugation on the sample bias. The filled and empty circles on top of each image represent up and down buckling Si dimer atoms respectively as depicted in **(d)** where the up and down atoms are represented the big and small circles respectively. **(c)** An energy-band diagram for filled-state imaging with a negative sample bias of magnitude V equivalent to the downward shift of the tip Fermi level from the sample Fermi level by eV.

Considering the tunnelling model shown in Fig. 2.6 (c) taking the negative sample bias for the discussion, the sample electronic states in the interval of the sample Fermi level E_{F_s} to the energy level $E_{F_s} - eV$ can contribute to the

tunnelling current. The tunnelling current is estimated by summing over all the states within the tunnelling interval. With the condition that the bias voltage is small, we have got a relation that

$$I \propto \rho_s(d, E_F) \tag{2.4}$$

i.e. the tunnelling current is proportional to the LDOS of the sample, ρ_s, at the sample Fermi level which is the highest energy level contributing to the tunnelling current in this negative-bias case (see Fig. 2.6(c)).

Nevertheless, without the approximation that the applied voltage is sufficiently small, and the tip wave function and the transmission coefficient are constant, the interpretation of the tunnelling current will be more complex. The tunnelling current will involve the electronic structure of the tip and the transmission function rather than solely the electronic structure of the sample. Thus, when the bias voltage is high, the tunnelling current is given by

$$I \propto \int_{E_F - eV}^{E_F} \rho_s(\vec{r}, E)\rho_t(\vec{r}, E - eV)T(\vec{r}, E, V)dE \tag{2.5}$$

where ρ_s and ρ_t are the local density of states of the sample and tip at location $\vec{r}$ and the energy E. T is the tunnelling transmission probability for electrons with energy E and the applied bias V at a distance z from the sample surface.

2.1.7 Scanning Tunnelling Spectroscopy (STS)

Consider Eq. (2.5), if the tip position $\vec{r}$ is constant, the current I will be dependent on the LDOS of the surface which is solely associated with the sample energy levels E in the interval from $E_F - eV$ to E_F that can be varied by changing the sample bias. Hence, the LDOS at a particular point of the surface with different tunnelling energy intervals can be probed by recording the tunnelling current at different bias voltage. The result of the measurement is an I-V spectrum and this measuring technique is called scanning tunnelling spectroscopy (STS). To gain an I-V spectrum, the tip is placed over a particular point over the surface with the vertical tip position being constant while varying the voltage bias over a

range of interest. The tip vertical position corresponding to a tunnelling-current setpoint and an applied sample bias is set by the feedback loop. The feedback loop is then disabled, fixing the tip position while varying the voltage and measuring the tunnelling current for each voltage value.

Assuming that the LDOS of the tip is constant, Eq. (2.5) can be written as

$$I(V) \propto \int_{E_F - eV}^{E_F} \rho_s(E) T(E, V) dE \tag{2.6}$$

The derivative dI/dV normalised by dividing with I/V has the form of

$$\frac{dI}{dV} \cdot \frac{V}{I} = \frac{d \ln I}{d \ln V} \propto \rho_s(\Delta E) \tag{2.7}$$

The normalised derivative of the tunnelling current I at a surface point as a function of applied voltage V is proportional to the local density of states of the sample ρ_s at that point varied with the interval of tunnelling energy states ΔE. Thus, by potting $d \ln I / d \ln V$ as a function of V, we obtain a graph approximately revealing the surface LDOS at each bias in the voltage range of interest.

2.1.8 Current Imaging Tunnelling Spectroscopy (CITS)

In addition to the STS technique we can simultaneously take an STM image and an I-V spectrum of each surface point while scanning the tip over the surface. This technique is called Current Imaging Tunnelling Spectroscopy (CITS).

Consider Fig. 2.7. the surface area is divided into 100×100 pixels of an equal size. The scan starts from pixel (1, 1). While the tip is moving from pixel (1, 1) to pixel (1, 2), the feedback loop is enabled so that the tip-sample separation is regulated so that the separation is always constant in order to maintain the tunnelling current for a set imaging bias. Once the tip is over pixel (1, 2), the feedback loop is disabled, which fixes the vertical tip position. Then, the sample bias is modulated while the tunnelling current of pixel (1, 2) is measured for each bias value. This procedure is repeated until every pixel in the first row is

measured; from pixel (1, 1) to pixel (1, 100). Subsequently, the tip will start measuring in row 2; from pixel (2, 1) to pixel (2, 100). This process will continue until the (100, 100) pixel is measured.

Due to the time required for taking the I-V curve of each pixel, this scanning technique can take up to many hours before its completion. The data we obtain from CITS are firstly $\Delta z(x, y)$, which is the variation of the vertical tip position with respect to each point of the surface plane, and secondly $I(V, x, y)$, which is the variation of the current with respect to the modulated bias at each point of the surface plane.

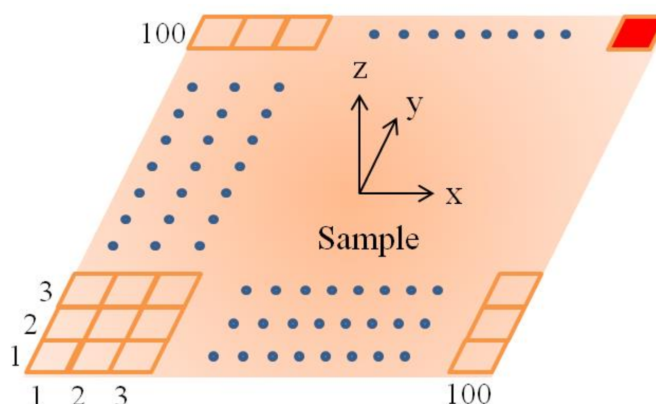

Figure 2.7 A schematic illustrating the CITS measurement. A sample surface divided into 100 × 100 pixels. The scan starts from pixel (1, 1) to pixel (1, 100) and then from pixel (2, 1) to pixel (2, 100) until pixel (100, 100) is measured as described in the text. The tip stops over each pixel with the feedback loop turned off. By varying the sample bias in a range of interest, the tunnelling current for each bias is recorded, which results in an STS data (I-V curve) at each pixel.

2.1.9 Tip-Induced Band Bending (TIBB)

It has been stated that the tunnelling energy interval is reduced by the voltage drops. In practice, there is a small voltage drop across the vacuum barrier, but in addition to this there is also a large voltage drop associated with band bending of the sample caused by an electrostatic influence of the tip. This effect is known as tip-induced band bending (TIBB) and plays a crucial role in an STM system with the sample being a semiconductor as shown in Fig. 2.8. Energy-band

diagrams for STM that have been proposed so far cannot be applied to the semiconductor cases in which the energy bands of the sample have a non-negligible bandgap; for example, 1.12 eV for silicon. Fig. 2.8 shows an STM system consisting of a metal tip and a semiconductor sample separated by a vacuum gap. With a positive bias applied to the sample, the tip Fermi level is shifted upwards with respect to the sample Fermi level. It has been widely accepted that the energy levels near the sample surface are bent upwards with the tip Fermi level while the sample Fermi level remains unchanged. The upward bending of the energy bands reduces the tunnelling energy window, which is alternatively known as the voltage drop. According to Fig. 2.8, the voltage drop due to the upward band bending is ΔV which is equivalent to $e\Delta V$ in the diagram. The shift of the sample energy levels near the surface compared to the bulk levels will play a vitally important role in the interpretation of our data that will be shown later throughout the thesis.

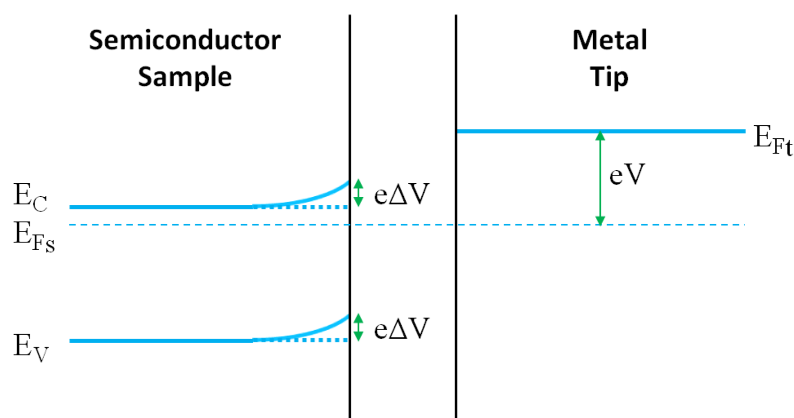

Figure 2.8 An energy-band model with the TIBB effect of the sample showing voltage drop ΔV which reduces the tunnelling energy window by $e\Delta V$ at a positive bias V applied to the sample.

2.1.10 Double-Tip Effect

As mentioned above, the sensitivity of the tunnelling current to the tip-sample separation is so high that variation of the distance of just 1 Å can cause a an order-of-magnitude change of the tunnelling current. If the metal tip is so rough that there is more than a single atom or a few atoms acting like a single probing point at the tip apex, there will be several probing points on the tip. As a

result of the multi probes, the resolution of the surface images will become very low and the atomic resolution cannot be obtained.

However, although the tip is sharp and there are only few atoms on the tip apex, the surface images can also be badly imaged due to the double-tip effect. If on the apex of the sharp tip there are two distinguishable probing points (Fig. 2.9), a feature of the surface will be displayed twice in the STM image of the surface. This effect is known as a double-tip effect. Sometimes, it becomes a multi-tip effect if there are more than two distinguishable probing points, resulting in a feature appearing more than twice in the STM images such as three times or four times. Realising that the scanning tip is affected by the double-tip effect is crucial. This can be checked by scanning the tip over a large surface area. If the double-tip effect is found, then the tip must be optimised before starting to collect data to prevent misinterpretation of features observed on the surface. The methods of optimising the tip performance will be discussed in the Experimental Methods chapter.

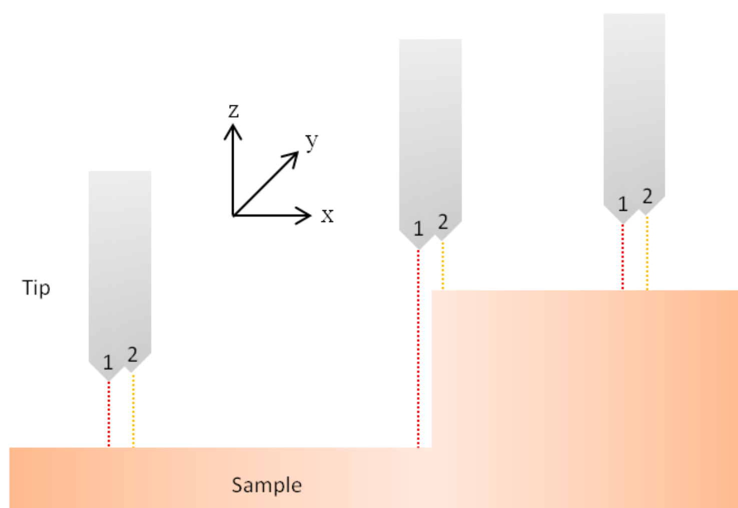

Figure 2.9 When the apex of the tip is not singular such that there are at least two points being able to measure the tunnelling current nearly at the same level, features of the surface are scanned twice and appear double in the respective STM image.

2.2 Si(001) surface

Silicon is the second most abundant element on Earth and the most commonly used substrate material for the electronics industry. In a single crystal of silicon, each silicon atom bonds to four surrounding silicon atoms with its sp^3 hybridised orbital, allowing the crystal to form the diamond structure. The (001) surface plane of the Si crystal, Si(001), is one of the most widely studied surfaces due to its importance to the electronic industry and is the silicon surface proposed for use in quantum computer schemes. In this section, we review Si(001) which is the surface used for all the studies in this thesis.

2.2.1 Reconstruction of Si(001)

Each Si atom in the bulk crystal has two bonds to the Si atoms in the plane below and the other two bonds to the Si atom in the plane above as illustrated in Fig. 2.10. However, for a Si atom in the (001) surface plane, the atoms above it have been removed, leaving two half-filled bonds protruding from the surface plane as shown in Fig. 2.10 (a). The half-filled bond is known as the dangling bond which makes the Si(001) surface, which has the 1×1 reconstruction depicted in Fig. 2.10 (e), high in energy and thus very unstable. To lower the surface energy, one dangling bond of each surface Si atom bonds with one dangling bond of a neighbouring surface Si atom, forming a Si-Si dimer as illustrated in Fig. 2.10 (b). The strong bond between the two neighbouring Si surface atoms is called a σ bond. With the Si-Si dimers formed, the surface structure becomes the 2×1 reconstruction comprised of dimer rows as shown in Fig. 2.10 (f) which is more stable than the 1×1 reconstruction. However, in each Si-Si dimer, the remaining two dangling bonds of the Si atoms are not isolated from each other, but they form a weak π bond with each other [Fig. 2.10 (c)]. The surface energy can be further reduced by a charge transfer between the two Si atoms of a dimer with one electron is transferred from one of the half-filled dangling bonds to the other. As a result of the transfer mechanism, the Si atom gaining one more electron into its dangling bond protrudes outwards from the surface plane and is called the *up* atom of the dimer whereas the other Si atom

having no electron left in its dangling bond depresses inwards and hence is called the *down* atom, which forms a buckling configuration illustrated in Fig. 2.10 (d). With the charge transfer, the reconstruction of the surface can be the $p(2 \times 2)$ reconstruction or the $c(4 \times 2)$ reconstruction shown in Fig. 2.10 (g) and 2.10 (h), respectively. Calculations have shown that the surface energy of the $p(2 \times 2)$ reconstruction is lower than that of the 2×1 reconstruction. However, the surface energy can even be minimised by forming the $c(4 \times 2)$ reconstruction which is now widely accepted as the most stable surface reconstruction of the Si(001) surface.

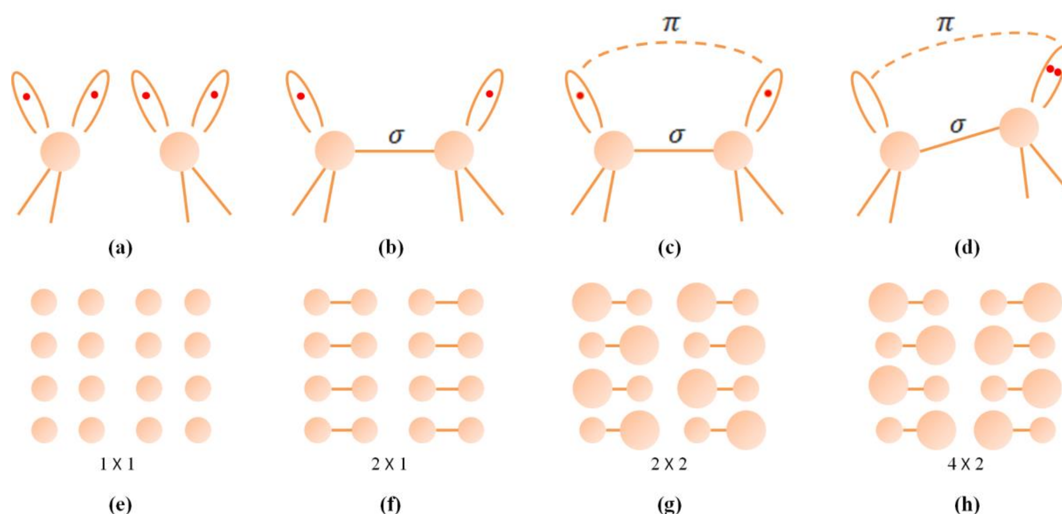

Figure 2.10 (a) Two surface silicon atoms, each of which has two half-filled dangling bonds and two bonds with two silicon atoms in the layer below. **(b)** The two silicon atoms bond to each other, creating a σ bond and forming a silicon dimer. **(c)** A weak π bond is created between the remaining dangling bonds. **(d)** To further reduce the structure energy, an electron is transferred from one dangling bond to the other, making the silicon atom of the filled dangling bond an up Si atom of the silicon dimer. **(e)** The (1×1) surface reconstruction associated with the surface silicon atoms in the state shown in (a). **(f)** The (2×1) reconstruction consisting of rows of silicon dimers associated with the surface silicon atoms in the state shown in (b) and (c). **(g)** $p(2 \times 2)$ surface reconstruction associated with the surface silicon atoms in the state shown in (d). **(h)** $c(4 \times 2)$ surface reconstruction associated with the surface silicon atoms in the state shown in (d) with a buckling orientation different from (g) as illustrated.

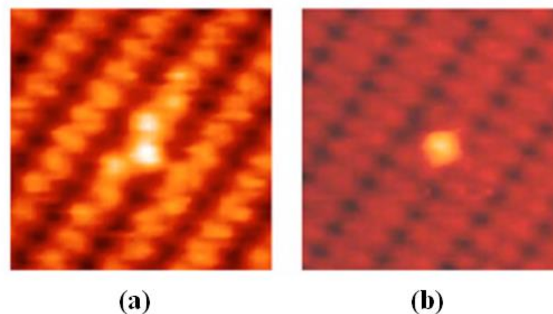

Figure 2.11 (a) A filled-state and **(b)** empty-state images of a clean Si(001) surface taken with a sample bias of -1.6 V and +1.2 V respectively at room temperature revealing the 2×1 reconstruction due to the rapid switch between the *up* and *down* Si atoms. There is a H atom bonded to the surface at the centre of the image, forming a hemihydride structure. The structure can pin the buckling orientation of the surrounding Si dimers such that the up and down atom can be distinguished in the filled-state image. The images are taken and adapted from Ref. [4].

2.2.2 Si(001) at room temperature

While the $c(4 \times 2)$ reconstruction is the ground state of the Si(001) surface, when the sample is at room temperature, the thermal energy is high enough to effectively alter the charge transfer configuration of the Si dimers. At room temperature, the two electrons are transferred back-and-forth between the dangling bond orbitals such that the *up* and *down* atoms alternately changes (in a flip-flop motion) so rapidly that the STM measurement cannot see the buckling aspect of the dimers; in the other word, the tip cannot distinguish the *up* atom from the *down* atom while scanning over each Si dimer. Therefore, the Si(001) surface at room temperature are normally observed in the symmetric 2×1 reconstruction. Fig. 2.11 shows the filled- and empty-state images of the Si(001) surface taken at room temperature. The images reveal the 2×1 reconstruction in that the up and down Si dimer atoms cannot be distinguished. In the filled-state image, a Si dimer appears as a single protrusion while it appears as a double protrusion in the empty-state image. However, there are some aspects of the surface that can pin the buckling orientation of the adjacent Si dimers, thereby allowing the *up* and *down* Si atoms to be distinguished. Those aspects can be step

edges, intrinsic surface defects such as dimer vacancies, and extrinsic surface defects introduced by dosing some molecules onto the surface [4] as seen at the centre of the images in Fig. 2.11. This defect is the hemihydride structure consisting of a single H atom bonded to a Si dimer atom. In the filled-state image, the zig-zag characteristic extends up to a few Si dimers away from the feature dimer.

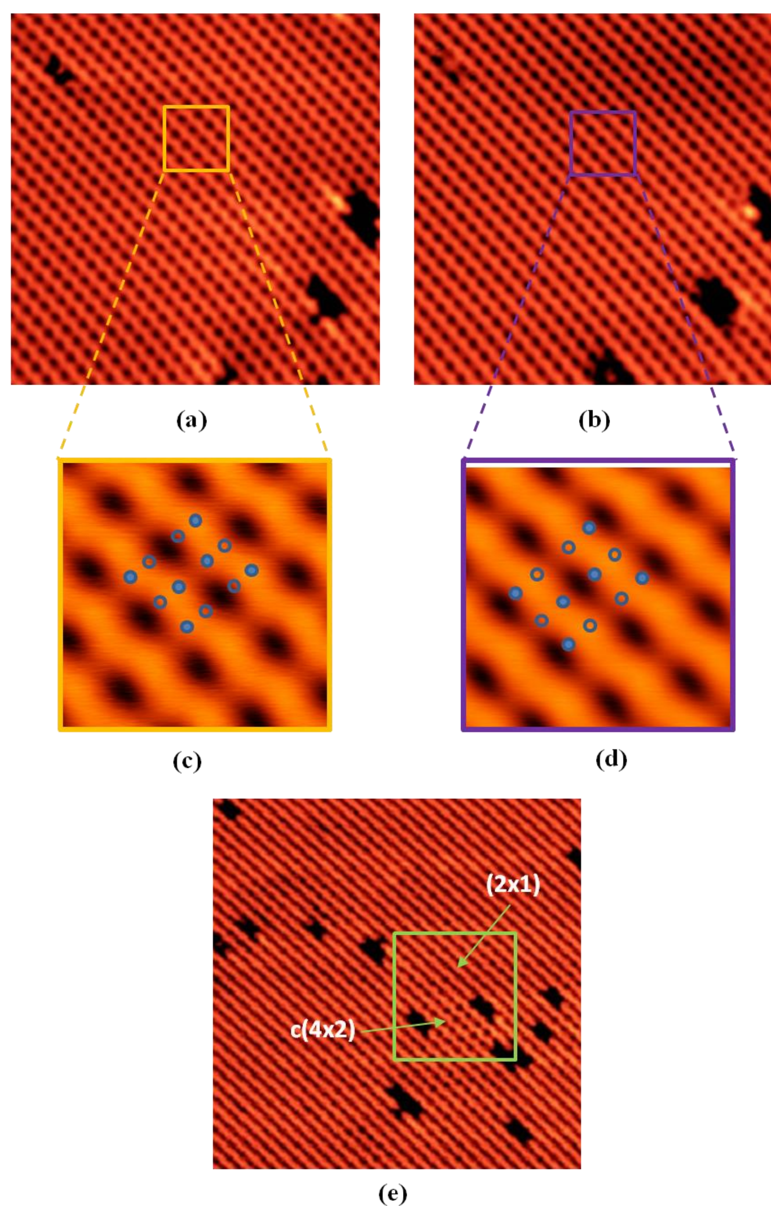

Figure 2.12 Surface reconstruction of Si(001) at 77 K taken at the sample bias of **(a)** -1.6 V and **(b)** +0.6 V showing the $c(4 \times 2)$ reconstruction. **(c)** and **(d)** are the enlargements of the boxes in (a) and (b) respectively. **(e)** Surface reconstruction of a highly As-doped Si(001) revealing the $2 \times$

1 reconstruction and the $c(4 \times 2)$ reconstruction on the same surface area. Images obtained by the author.

2.2.3 Si(001) appearance at low temperature

At low temperature such as 77 K, the appearance of the Si(001) reconstruction is different from the room-temperature appearance. The thermal energy at 77 K is so low that it cannot alter the configuration of the Si dimers, allowing the reconstruction of the surface to be in its most stable state which is the $c(4 \times 2)$ reconstruction as shown in Fig. 2.12 (a) and 2.12 (b) for the imaging of filled and empty states, respectively. In Fig. 2.12 (c) and 2.12 (d) which are the enlargements of the coloured boxes in Fig. 2.12 (a) and Fig. 2.12 (b), the $c(4 \times 2)$ reconstruction can be clearly seen. The up Si atoms appear bright in Fig. 2.12 (c) while the Si down atoms appear dark. For Fig. 2.12 (d), the down Si atoms appear bright whereas the up Si atoms become dark. This appearance can be compared to the 4×2 reconstruction illustrated in Fig. 2.10 (h).

However, for a degenerately-doped silicon sample, it is possible that the $c(4 \times 2)$ reconstruction does not appear throughout the surface but the appearance of the surface consists of the 2×1, $p(2 \times 2)$, and $c(4 \times 2)$ reconstructions randomly as depicted in Fig. 2.12 (e). This is crucial in our experiment since all the Si(001) samples we used are degenerately doped; thus, we do not attribute the random appearance of the other reconstructions apart from the $c(4 \times 2)$ structure to the poor performance of the tip.

2.2.4 Energy-band structure of Si(001)

Due to the charge transfer between both Si atoms in a dimer through the π bond, the dimer configuration becomes buckled. The π bond has two electronic states; the bonding π state and the anti-bonding π^* state. The energy levels of these electronic states in a simple energy-band structure are illustrated in Fig. 2.13 (a). In this figure, the π^* state lies above the Fermi level the Si(001) sample which is assumed to be at the centre of the bandgap for simplicity, whereas the π state lies below the Fermi level. Due to the π^* state positioned far above from the

Fermi level towards the conduction-band edge consisting of the unoccupied electronic states, the π^* state is also considered as an energy band of unoccupied states. Unlike the anti-bonding π^* state, the π state lies far below the Fermi level towards the valence band; thus, the bonding state is a band of occupied states. The existence of these surface states results in the intrinsic upward band bending seen in Fig. 2.13 (a). We have stated that the electrostatic influence from the tip causes the energy bands of the sample to bended but the band bending induced by the π-bond surface states is created without the presence of the tip, and thus it can be called the intrinsic band bending.

Considering the buckling configuration of a Si dimer, the unoccupied π^* state in the energy band represents the down Si atom that has an empty dangling bond while the π state represents the up Si atom having a fully-filled dangling bond. The strong σ bonding and anti-bonding states lies further below and above the valence band edge and conduction band edge respectively.

For the STM tunnelling with negative and positive sample bias at low temperature (77K) shown in Fig 2.13 (b) and 2.13 (e), the surface contrast appears different. At negative sample bias, the tip Fermi level is lower than the sample Fermi level and electrons tunnelling from occupied states of the sample to unoccupied states of the tip. Electrons from the occupied π states and those occupied states in the valence band tunnel through the vacuum barrier to the empty states of the tip lying above the tip Fermi level, providing filled-state STM images as shown in Fig. 2.13 (c) for low negative bias and (d) for high negative bias. In this negative-bias regime, the π states have the highest energy levels, so the these states dominate the tunnelling current such that increasing the magnitude of the negative bias to obtain more tunnelling contribution from the valence band states does not change the appearance of the surface corrugation. The Si(001) surface contrast at negative bias is depicted in Fig. 2.13 (c) and 2.13 (d) where the up Si atoms appear bright but the down atoms appear dark; thus, each dimer row appears with a zig-zag characteristic.

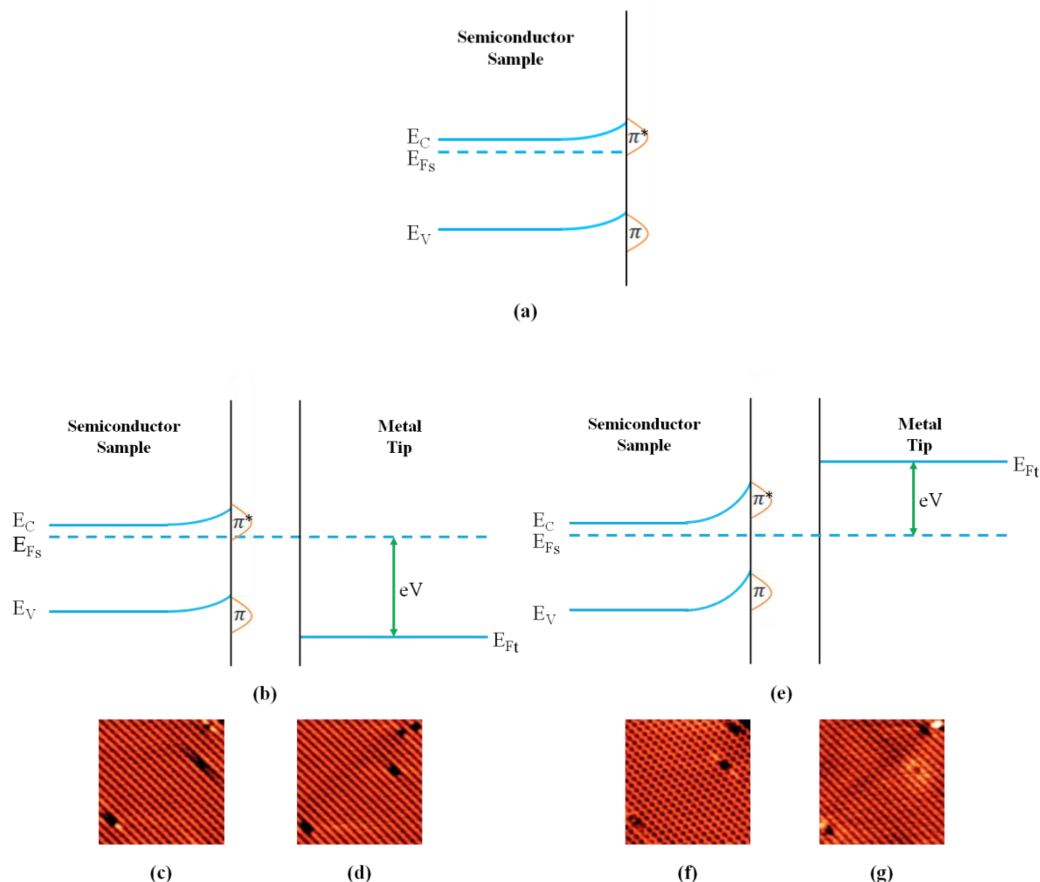

Figure 2.13 **(a)** The surface energetic states of an n-type Si(001) sample with the π-bond states inducing an intrinsic upward band bending. **(b)** At negative sample bias, the sample energy bands are not bended down since the pinning effect of the sample Fermi level**.** **(c)** and **(d)** filled-state images of an As-doped Si(001) sample surface at -1.0 V (low-bias) and -2.0 V (high-bias) respectively. **(e)** At positive sample bias, without the sample Fermi level pinning the conduction band edge, the sample energy bands are normally bended upwards. **(f)** and **(g)** empty-state images of the same sample at 0.5 V (low-bias) and 2.0 V (high-bias) respectively. The high-bias empty-state image reveals the trough state or the surface area between dimer rows. Images obtained by the author.

However, for positive sample bias in which the tip Fermi level is shifted above the sample Fermi level, electrons tunnel from the occupied states of the tip to the unoccupied states of the sample, providing empty-state STM images. The surface appearance is not monotonous but categorised into two tunnelling regimes; low positive bias Fig. 2.13 (f) and high positive bias Fig. 2.13 (g). When the sample bias is small such that the tip Fermi level is shifted above the sample Fermi level but still lies about the conduction band edge, most of the tunnelling

current is contributed from electrons tunnelling into the unoccupied π^* states. The Si(001) surface contrast at the low positive sample bias is illustrated in Fig. 2.13 (f) where the down Si atoms appear bright but the up atoms appear dark such that the orientation of the zigzag characteristic is opposite to the negative-bias image.

When the sample bias is high and the tip Fermi level is shifted further above the conduction band edge, the unoccupied σ^* states in dominates the tunnelling current. The σ bonding states of a Si dimer represent a bright appearance between the two Si dimer atoms whereas the σ^* anti-bonding states represent a dark appearance between both atoms in the dimer. At high negative bias, the tunnelling contribution of the σ states cannot be observed due to the dominance of the π states higher in energy. However, at high positive bias, the tunnelling contribution of the σ^* states can be observed since the band is higher in energy than the π^* states; thus, the surface area between the dimer rows appears bright while the dimer rows themselves appear dark, Fig 2.13 (g). Since the area between the dimer rows is called trough, the states in the energy-band diagram contributing the tunnelling resulting in the appearance of the trough area are called *trough states*.

2.2.5 Defects of Si(001)

In this section we discuss all the intrinsic defects of the Si(001) surface reported so far. Identifiying the intrinsic defects will allow us to judge whether those features appearing on the surface after dosing the surface with a certain kind of molecules result from the dosing molecules, or from intrinsic defects. The mono-atomic step edge can be considered a defect but we do not include it in this discussion.

A dimer vacancy (DV) occurs when there is at least one Si dimer missing from the surface reconstruction. The dimer-vacancy defect can be classified according to the number of the missing dimers. If there is only one dimer missing, the DV is called a single dimer vacancy (1-DV). If there are two or three neighbouring dimers missing from the surface, the dimer vacancy is called a double dimer vacancy (2-DV) and a triple dimer vacancy (3-DV) respectively.

Often, there are also split-off dimer vacancy defects appearing in the surface. This type of intrinsic defects is comprised of a single missing dimer separated from the other one missing dimer or two missing dimers by a single Si dimer and can be respectively called 1+1-DV and 1+2-DV. All of the above-mentioned DV defects are shown in Fig. 2.14 (a)-(d). A low density of the DV defects in the surface is preferable since it allows extrinsic surface features such as those appearing after dosing to be effectively studied. The surface with low density of the DV defects can be achieved by the annealing procedure described in Chapter 3.

Another type of surface defect which is not intrinsic but it is commonly observed in the surface is called the C defect and Fig. 2.14 (e) and 2.14 (f) show how this defect appears in the STM images. It is caused by the residual water molecules left inside the vacuum chambers of the STM machine adsorbed onto Si(001) and subsequently dissociated and inserted into the surface. To allow the dosing structures on the surface to be examined, the number of the C defect must also be minimised. The annealing procedure mentioned above effectively removes all C defects in the surface. However, if there are residual water molecules throughout the chambers, the C defects will start to form again after the sample cools down. Thus, it is necessary to properly bake out the STM machine and pump out the residual molecules inside the chambers until the pressure inside reaches the ultra-high-vacuum (UHV) level before running any experiment with the STM.

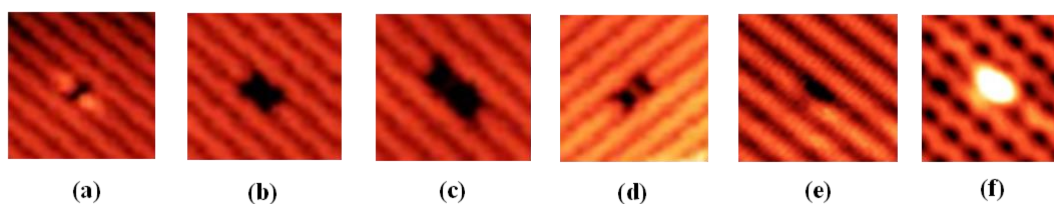

Figure 2.14 **(a)** a 1-DV, **(b)** a 2-DV, **(c)** a 3-DV, **(d)** a Split-off (1+1) DV, **(e)** and **(f)** a C defect imaged at 77 K with the sample bias of -2.0 V and 0.5 V respectively. All of these features were taken on an As-doped Si(001) surface by the author.

2.3 Si(001):H surface

The surface states associated with dangling bonds cause Fermi level pinning which hinders the spectroscopic imaging of certain features (such as buried charges) below the surface. Thus it is sometimes advantageous to remove the surface dangling bonds, and hence the surface states, in order to allow other phenomena of the surface to be observed. One method for the removal of dangling bonds is to terminate the Si(001) surface with an atomic layer of hydrogen atoms. This process is called *hydrogen termination* or *H-termination* and the resulting surface covered by a single monolayer of hydrogen is known as Si(001):H or H-terminated Si(001).

To obtain the Si(001):H surface, hydrogen molecules (H_2) are injected into the chamber through an instrument called a cracker, which breaks the H_2 molecules to produce individual H atoms, which then react with the heated Si(001). Under appropriate conditions, the Si(001):H surface will be attained. The full details of H-termination used in this work will be described in Chapter 3. In this section, we review the possible structures resulting from the hydrogen atoms adsorbed onto the surface and bonding with the surface Si atoms via the chemically active dangling bonds.

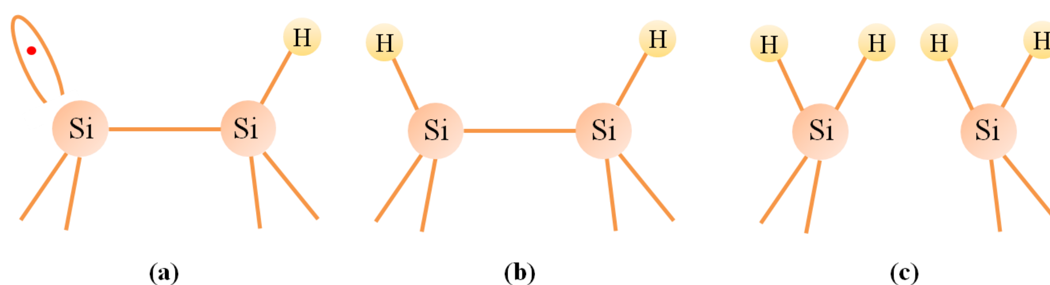

Figure 2.15 Structure of **(a)** the hemidydride dimer, **(b)** monohydride dimer, and **(c)** dihydride dimer in which the σ bond between the Si dimer atoms is broken.

2.3.1 Three types of structures from H-termination

By dosing H atoms to the Si(001) at elevated temperature, the H atoms will bond with the Si atoms on the surface and form H-containing structures. There are three resulting structures;

1. *Hemihydride*, in which there is only one H atom bonded with one of the Si atoms in a Si dimer, Fig. 2.15 (a)
2. *Monohydride*, in which each Si dimer atom is bonded with one H atom, Fig. 2.15 (b)
3. *Dyhydride*, in which are two H atoms bonding with each Si dimer atom, Fig. 2.15 (c)

The hemidydride structure occurs if the coverage is less than a full monolayer and the temperature of the sample during the H-termination is below 300 ℃ where H atoms do not diffuse on Si(001). For the filled-state image (Fig. 2.16 (a)), the bright side of the hemihydride dimer is the half-filled dangling bond. The bonding electronic state of this dangling bond has its energy level slightly closer to the sample Fermi level than the bonding electronic state of the π bond, so it appears brighter than the up atoms of the Si dimers. The dark end of the hemihydride dimer is the Si-H bond. Its bonding electronic state is so far below the sample Fermi level that its contribution to the tunnelling current is negligible. Compared to the Si dimers, the dangling-bond side is on the up atom position while the Si-H bond side is on the down atom position. Thus, at high negative bias where the tunnelling contribution of the valence-band states becomes significant, the difference between the tunnelling current from the bonding state of the dangling bond and the bonding state of the π bond is not observable. Consequently, the hemihydride dimers cannot be distinguished from the Si dimers. For the empty-state image (Fig. 2.16 (b)), in which the buckling configuration of the surface changes to the Si down atoms being brighter than the Si up atoms, the dangling-bond anti-bonding state lies above the sample Fermi level as the π^* anti-bonding state does. Therefore, the dangling-bond side of the hymidydide dimer appears bright as the down Si atoms do. In contrast, the Si-H bond has its anti-bonding state so far above the Fermi level into the conduction

band that even at high positive voltages of the STM system, the tunnelling of the state cannot still contribute to the tunnelling current.

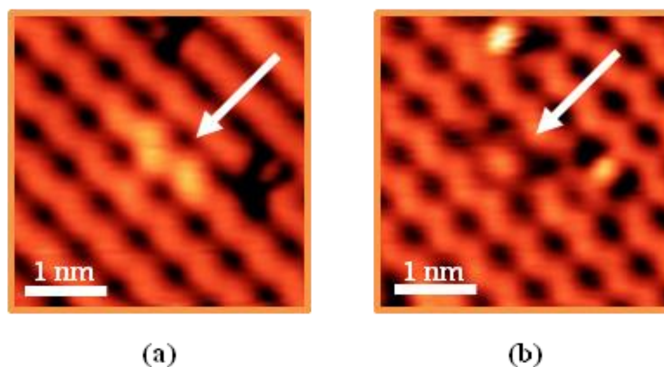

Figure 2.16 A hemihydride dimer appearing on the (001) surface indicated by the white arrows imaged at **(a)** -2.0 V and **(b)** +1.3 V. The bright side of the Si-Si-H image is the half-filled dangling bond while the depression is on the side of the Si-H bond. Images obtained by the author.

Above the temperature of 300 ℃, H atoms become mobile on Si(001). If the temperature of the sample during the H-termination is ~ 400 ℃, the monohydride structure can be formed on Si(001). In the formation of the mohydride structure, the incoming H atoms break the π bond of the Si dimer with subsequently each Si dimer atoms being bonded to one H atom. Since the π bond is discarded and the dangling bonds are removed, there is no the charge transfer between the two Si dimer atoms, and so there is no dimer buckling. Consequently, the reconstruction of a Si(001):H covered with a monolayer of H atoms in the form of the monohydride structure is a 2×1 reconstruction. A monohydride dimer appears as a bean-shaped protrusion in the filled-state image and double protrusions in empty-state image as illustrated in Fig 2.17 (a) and (b) respectively. However, on a clean Si(001), an isolated monohydride dimer appears as a depression with one dimer width like a 1-DV defect due to the electronic states of the Si-H bonds are so far away from the Fermi level and deep inside the valence and conduction bands that they cannot contribute to the tunnelling current.

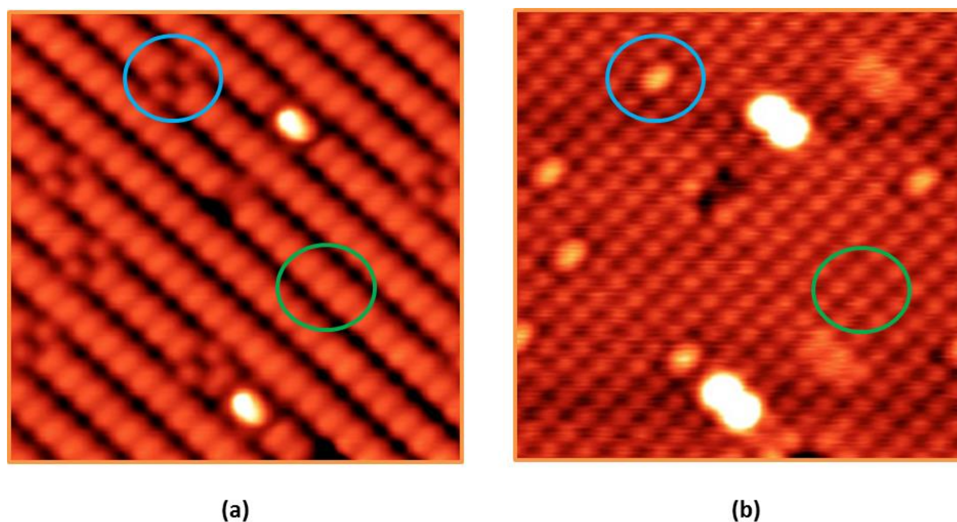

Figure 2.17 (a) a filled-state and **(b)** empty-state 7 nm × 7 nm images of a Si(001):H surface measured at 77 K. The blue circles shows an example of the dihydride dimer on the surface while the green circles show some example of the monohydride dimer. See the text for more details about their appearance. Images obtained by the author.

With the full coverage, if the sample temperature during the H-termination process is above 300 °C but still below ~400 °C, there are drihydride and monohydride structures appearing on the surface with a large amount of the dihydride structure. The dihydride structure appears as double protrusions in filled-state imaging and appears as a single bean-shaped protrusion in empty-state imaging shown in Figure 2.17 (a) and 2.17 (b) respectively. In practice, we need to control the temperature of the sample during H-termination such that the amount of the dihydride structure is minimised. The formation of this structure breaks the σ bonds paving a way for incoming H atoms to remove the surface Si atoms resulting in the etching of the surface.

Nevertheless, it is also important to control the sample temperature to be lower than ~475 °C. At the temperature above ~475 °C, most of the H atoms become dramatically mobile and even unable to stick to the Si(001) surface, resulting in the Si(001) partially terminated by H atoms. Therefore, to achieve a desirable H-terminated Si(001) surface, the sample temperature must be controlled to be around ~400 °C during the termination process.

2.3.2 Energy-Band Structure of the Si(001):H surface

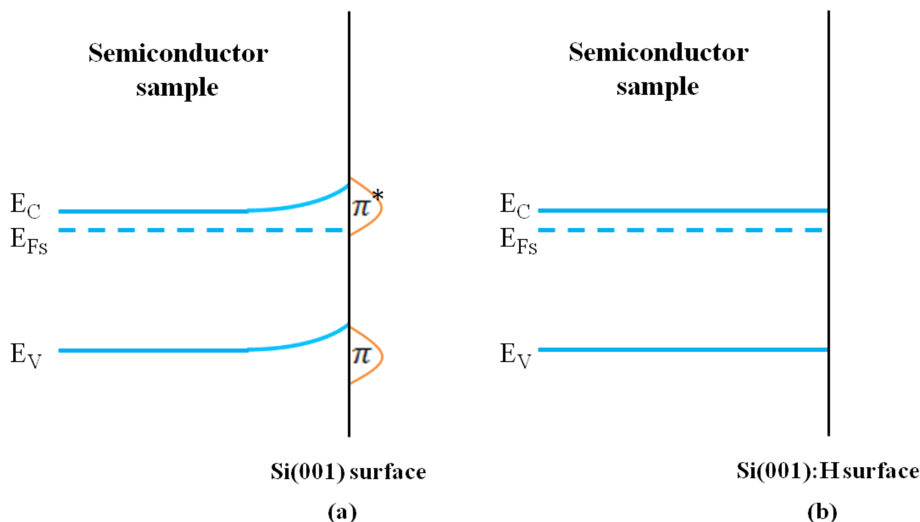

Figure 2.18 Energy-band models of **(a)** the Si(001) surface and **(b)** the Si(001):H surface showing that with the absence of the surface π-bond states, there is no longer the intrinsic band bending.

We have already discussed the band structure of Si(001) having the intrinsic upward band bending due to the presence of the surface π-bond states. We also introduced the H-termination used to remove the surface states and make the surface chemically inert. Thus, for Si(001):H, the energy-band structure is different from the Si(001) in that there are no surface π-bond states and thus the intrinsic upward band bending disappears as shown in Fig. 2.18. In terms of the STM system, the absence of the π states allows other surface states to be observable by the metal tip both due to the absence of the tunnelling current produced by the π states themselves and due to the absence of the pinning of the sample Fermi level to the conduction edge or valence band edge. In this work, we will show that with Si(001):H surface features induced by subsurface dopants that cannot be observed on clean Si(001) are able to be resolved for the first time, contributing to the road toward fabrication of the quantum computer [2, 34].

2.4 Phosphine (PH_3) on Si(001)

Phosphine molecules (PH_3) have been used for introducing phosphorous atoms (P) onto semiconductor surface such as Si(001) [34, 35] to, for example, study and use the P atom as a qubit of the silicon quantum computer [1, 2]. The procedure includes an incorporation of the P atoms adsorbed onto the surface into the sample surface with an annealing process. Then, layers of Si atoms are grown on top of the surface to bury the incorporated P atoms, thus making them subsurface dopants. The positions of the incorporated dopant atoms with respect to one another and the depth measured from the new surface layer are crucial since they are one of the parameter defining the electronic properties of the atomic device examined after the fabrication. During this procedure, understanding the behaviours of phosphine-related structures resulted from the dissociation of the PH_3 molecules on the surface is one of the keys towards complete control of the dosing process.

Room-temperature measurement of phosphine-related structures resulting from PH_3 dosed onto the Si(001) surface at room temperature has been comprehensively reported [4, 35-37]. Fig. 2.19 shows three distinct features commonly observed on the surface after the dosing. With complete calculation of the stable bonding configurations and related simulated STM images, Warschkow *et al.* convincingly proposed that the appearances of the features resulted from imaging PH_2+H, PH+2H, and P+3H structures. They also proposed that each of these three structures can have various bonding configurations possessing different energy values (i.e. different degrees of stability) as shown in Fig. 2.20. However, at the room-temperature, they only observed those with the most stable configurations of each structure, which are the B1 bonding configuration for the PH_2+H structure, the C1 configuration for the PH+2H structure, and the D2 configuration for P+3H structure (see Fig. 2.20). These configurations are described in detail in Chapter 4, where we will show that with measurement at 77 K, we have been able to observe some of those intermediate states of each phosphine-related structure that have not previously been experimentally observed. We provide more background discussion on the PH_3-Si(001) in Chapter 4 where it aids the explanation of our results.

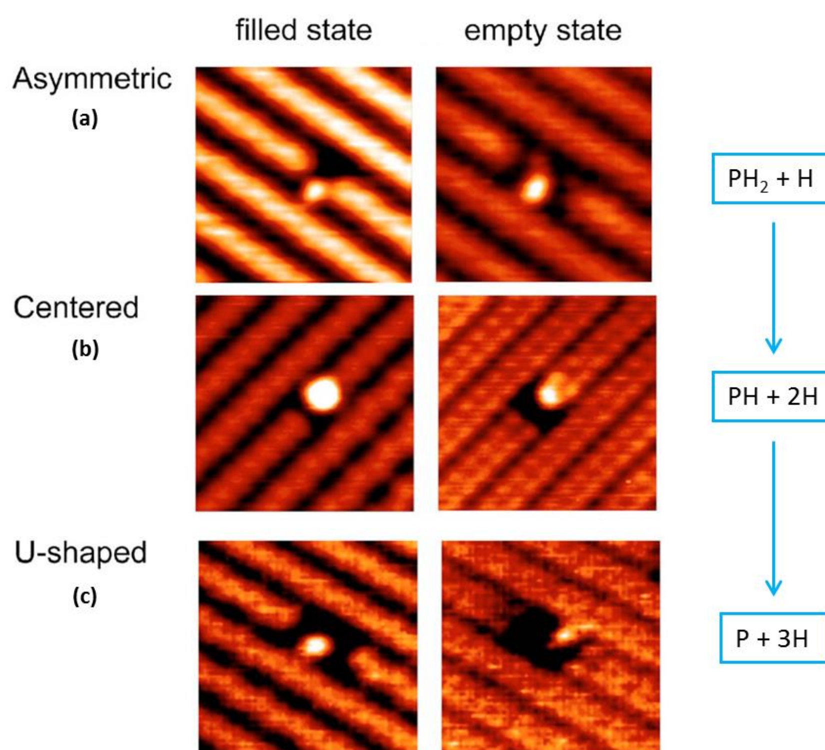

Figure 2.19 Three features commonly observed on Si(001) dosed with PH_3, imaged at room temperature **(a)** the PH_2+H structure called the asymmetric feature, **(b)** the PH+2H structure called the centred feature, **(c)** the P+3H structure called the U-shaped feature. The imaging bias is -1.6 V and +1.2 V for the filled-state and empty-state images respectively. The STM images are adapted from Ref. [4].

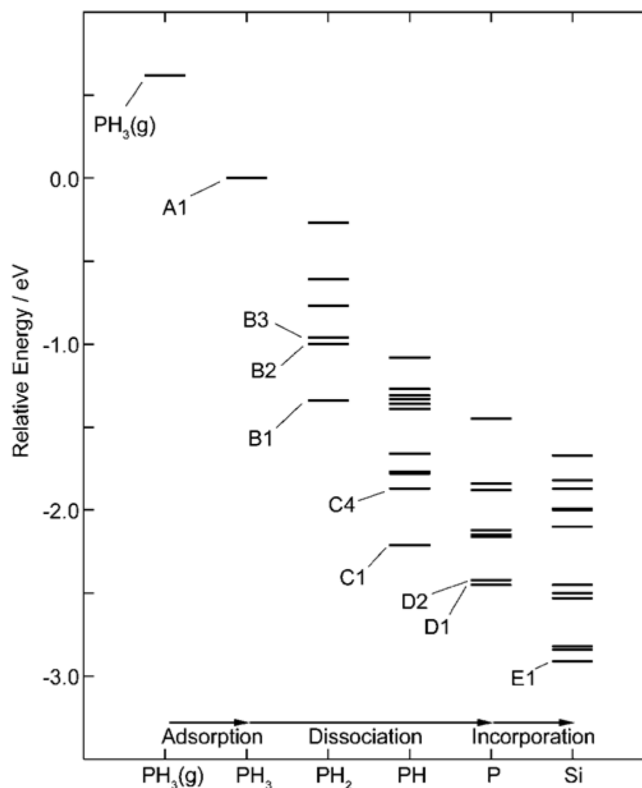

Figure 2.20 The computed energies for possible structures of stable PH_3 adsorption and dissociation products on the Si(001) surface. Low energy configurations along the dissociation series from left to right are labelled. The asymmetric feature is attributed to the B1 structure, the centred feature is attributed to the C1 structure, and the U-shaped feature is thought to be the D2 structure. The diagram is taken from Ref. [4].

Besides identifying the individual dissociative products shown in Fig. 2.19, the authors of Ref. [4] also proposed the observation of the PH_2+H feature transforming to the PH+H feature and subsequently to the P+3H structure on a time scale of minutes as shown in Fig. 2.21. They attribute the cause of the transformation to thermal energy; thus, the structural transition is thermally-driven, forward, and time dependent. At 77 K, where the thermal energy is insufficient for encouraging any changes in the surface structures, we will show a reverse structural transformation observed on the surface that we believe is caused by the electrostatic influence of the tip while the tip is scanning over the features.

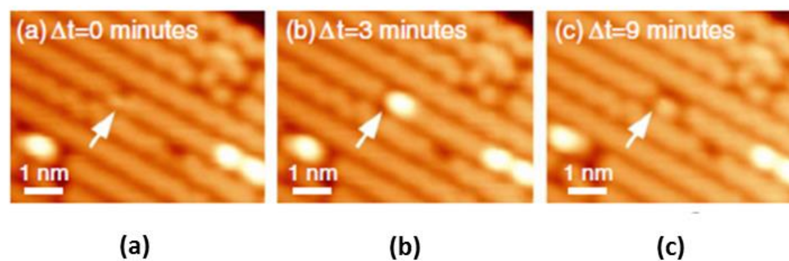

Figure 2.21 A series of STM images showing the transformation of **(a)** the asymmetric feature to **(b)** the centred feature and to **(c)** the U-shaped feature. All images were acquired with -2.0 V sample bias and 0.2 nA. The process is time dependent as indicated in the images. The figure is taken from Ref. [35].

The saturation-dosed Si(001) surface has also been studied and reported in Ref. [37]. The report states that on the Si(001) surface dosed with phosphine to the saturation level, only PH_2+H and PH+2H are observed as small protrusions and big protrusions respectively arranged with respect to Si dimer rows of the background surface as illustrated in Fig. 2.22 [37]. In our work, with the aid of voltage-dependent imaging, we observed that the big protrusions attributed to the PH+H structure actually showed two different behaviours while the voltage was varied. Thus, there are three distinct features on the surface. In Fig. 2.22 (B), the area on the left bottom corner of the image is H-terminated so the arrangement of the big and the small protrusions on the non-terminated part of the surface can be aligned with respect to the Si dimer rows of the background surface.

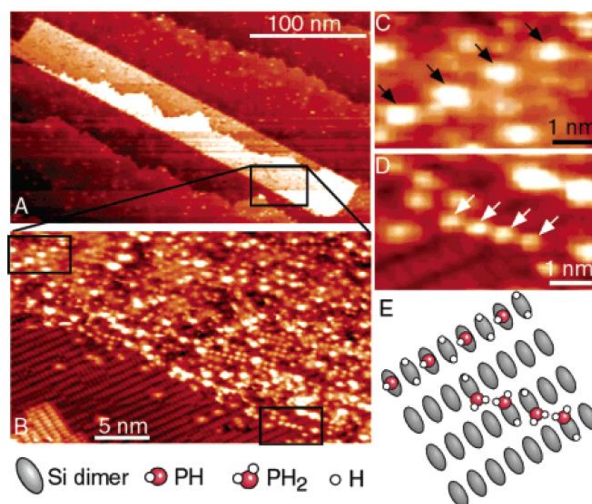

Figure 2.22 **(A)** A 300 × 50 nm^2 lithographic area of exposed Si(001) surface surrounded by H-terminated Si(001). **(B)** Enlargement of the boxed region in (A) after exposure to PH_3 at a saturation-dosing level. **(C)** Enlargement from top left boxed region of (B) showing four PH + 2H structures in a line. **(D)** Enlargement from bottom right boxed region of (B) showing four PH_2 + H structures. All images were taken at -2.0 V sample bias and 0.2 nA tunnelling current. (E) bonding configuration of the big protrusions and the small protrusion with respect to the background dimer rows. This figure is taken from Ref. [37].

The dissociative products are not the final step of the fabrication process of atomic electronic devices based on using P donors [34]. The silicon sample is subsequently thermally annealed after the dissociation to incorporate the phosphorous atoms into the Si(001) surface and also activate their electrical properties [38, 39]. The features commonly observed on the surface after P incorporation is Si-P heterodimer as depicted in Fig. 2.23. The Si-P heterodimer has been thoroughly experimentally and theoretically studied at room temperature [5, 40, 41], which shows the ground state of the Si-P structure and its appearance due to the influence of the tip. In our study, we will show that at 77 the appearance of the Si-P heterodimer are not the same as it is at room temperature. We discuss the details of the difference in Chapter 4.

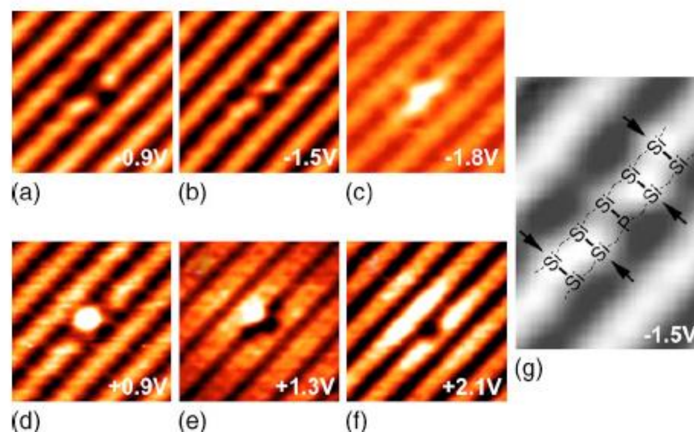

Figure 2.23 **(a)-(c)** filled-state images and **(d)-(f)** empty-state images of a Si-P heterodimer observed at room temperature. **(g)** A magnified view of (b) with an atomic reconstruction and the black arrows indicating the Si up atoms showing that the protruding side of the heterodimer is the Si atom. The figure is taken from Ref. [5].

2.5 Subsurface dopants below Si(001)

The study of dopants in silicon has been of scientific interest and technological importance for many decades. In recent years, there has been strong interest in measuring the properties of individual dopants due to the continued miniaturization of integrated circuit components, and the development of quantum information processing. For example, phosphorous atoms in silicon are seen as potential building blocks for a quantum computer, whose quantum bits may be comprised of the electron [2] or nuclear spins [1] of donor atoms. These proposals were recently made even more promising by the measurement of very long spin lifetimes of P in Si [3]. The capability of fabricating atomic-scale devices by deterministically placing individual dopant atoms in silicon with scanning tunnelling microscopy (STM), is well established [15, 42, 43]. When combined with scanning tunnelling spectroscopy (STS) this technique provides the capability for measuring the structural and electronic properties of substitutional dopant atoms in semiconductors via the ability to map the local density of states (LDOS) at the atomic scale.

Subsurface dopants have been studied with STM/STS in a variety of semiconductors, with the majority of work concentrating on the cleaved

GaAs(110) surface shown in Fig. 2.24. In general, the appearance of such dopants in STM images is dependent on whether they are donors or acceptors, and whether their intrinsic electronic states are shallow (~<50 meV) or deep (~> 50 meV). Shallow donors in GaAs, such as Si [18] and Te [19], are always imaged as isotropic circular protrusions surrounded by a dark halo in low-bias filled-state images and dark depressions in high-bias filled-state STM images. This has been interpreted as imaging the screened Coulomb potential of the ionized donors [18]. In contrast, shallow acceptors in GaAs, such as Zn [7, 44-49], Cd [45], Be [46], and C [47], were seen to induce anisotropic triangular-shaped protrusions at low positive sample bias (empty state), and dark isotropic depressions in high-bias empty-state images. These triangular dopant features were first observed nearly two decades ago [44]; however, the origin of their triangular shape in empty-state images remains controversial. It has been suggested that their characteristic appearance results from a direct image of the acceptor ground state [44, 45]; tunnelling through an excited state of the acceptor that originates from the highly anisotropic heavy hole band [46]; resonant tunnelling through evanescent gap states [48, 49]; or coupling between the acceptor wavefunction and the surface strain [7]. Notwithstanding these varied interpretations, most agree that the occurrence of the triangular imaging contrast coincides with a tunnelling regime where tunnelling into the conduction band is largely suppressed [50]. In case of energetically deep acceptors such as Mn in GaAs, a cross-like (i.e. 'X' shaped) protrusion [31] and a trapezoidal protrusion [7] were observed in low-bias empty-state images, which is believed to arise due to imaging the projection on the surface of the wavefunction of the neutral Mn acceptor that is either uncoupled, or coupled, with relaxation induced surface strain, respectively. Generally, the features induced by subsurface dopant atoms become less pronounced at large biases in both filled- and empty-state images due to the dominance of tunnelling currents arising from the valence and conduction bands, respectively. The interpretation of the appearance of the deep Mn acceptor in GaAs is the basis for interpretation of our subsurface data discussed later in this report.

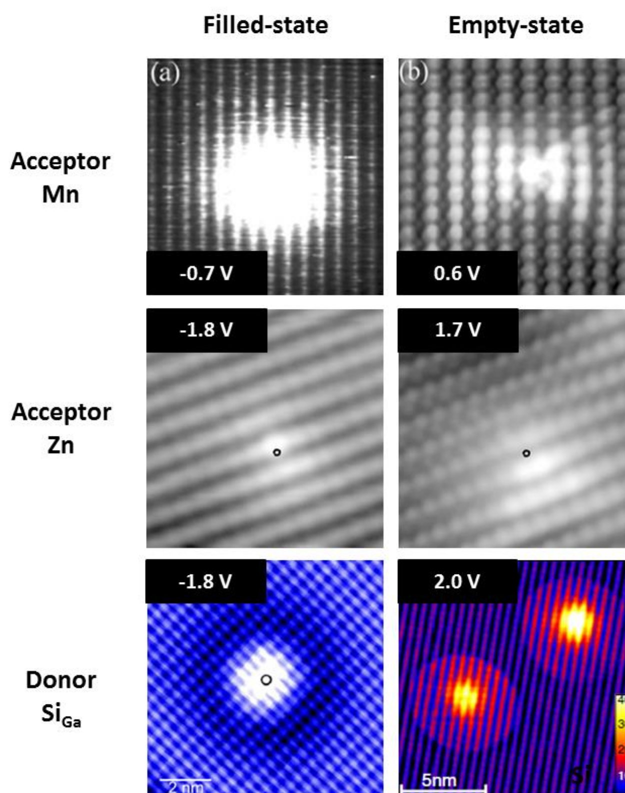

Figure 2.24 Some of the subsurface dopants below GaAs(110) that have been intensively studied by STM both at room temperature and low temperature. Note that the appearance of Mn and Zn acceptors is different although both of them act as acceptors in GaAs. Images are taken from Ref. [11, 18, 31, 46].

The STM/STS observation of dopant atoms in silicon has received less attention in the literature, and to date there have been no reports of imaging dopant wavefunctions. This may be caused by the hardship in observing subsurface dopant-induced features on the Si(001) surface due to the influence of the π-bond surface states both in terms of the tunnelling current and the energy-band movement as discussed. Despite this fact, there has been some reporting the observation of circularly symmetric depressions and protrusions associated with screened Coulomb potentials resulting from ionized dopants have been reported beneath both clean [20, 51] and hydrogen-terminated [17, 52, 53] Si(001) surfaces as shown in Fig. 2.25 (a) and 2.25 (b) respectively. These studies examined As [17] and P [20, 53] donors and B acceptors [17, 51, 52].

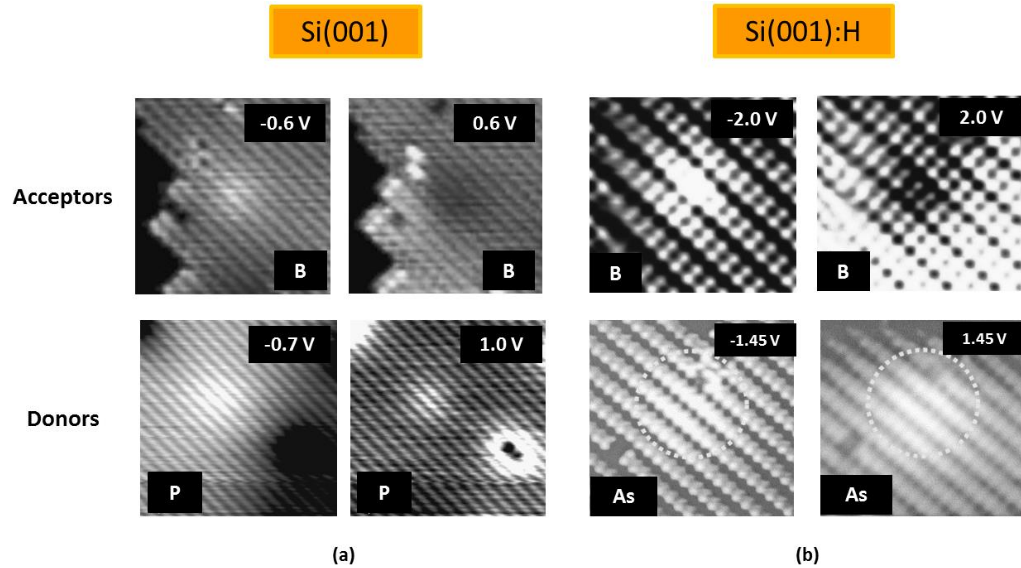

Figure 2.25 **(a)** Those subsurface donors and acceptors studies below clean Si(001) showing only circular protrusion or depression due to the charged states. **(b)** The subsurface dopants beneath Si(001):H also revealing only circular protrusion and depression inducing by the screened Coulomb potential of the charged dopants. Images are taken from Ref. [17, 51, 54].

The reason for terminating Si(001) with H atoms is to remove the π-bond surface states so that the effects of the surface states are discarded such as the pinning effect on the sample Fermi level and the tunnelling of the donor and acceptor energy levels in the semiconductor bandgap could be measured. However, all work up to the present have reported only circular protrusions and depressions induced by the ionised subsurface dopants (see Fig. 2.25 (b)). None of the studies showed the observation of neutral dopants under the Si(001):H surface at room temperature or even at low temperature such as 77 K.

In this thesis, we will present STM/STS observations of individual As dopant atoms beneath Si(001):H at 77K. We have report for the first time the observation of anisotropic protrusions for dopants atoms in silicon in low-bias filled-state imaging, consistent with the imaging of the donor wavefunctions. Our results have strong parallels like a mirror to the observations of deep acceptor states such as Mn in GaAs in that the As-induced features become isotropic circular protrusions in low-bias empty-state imaging. The controllable variation of charge states of the As atoms with the applied voltage can be described by the tunnelling mechanism using the energy-band diagrams. The work is of importance

to those pursuing the fabrication of devices from individual dopant atoms in silicon such as quantum computers that require individual dopant to be in its neutral charge state and able to be controllably and reversibly switched to an ionised charge state.

Chapter 3

Experiment Methods

In this chapter, we will review all the experimental methods we used throughout this work. We will begin with the overview of an STM system utilised for obtaining the data. Then, we will introduce the basic preparation of tips and samples, which needs to be done before the data of the sample surfaces of interest can be obtained with the atomic-scale resolution. Finally, we will end the chapter by describing gas dosing systems attached to the STM used for introducing phosphine molecules and hydrogen atoms into the chamber adsorbed onto the sample surface. For particular tools and procedures used to analyse and interpret the data, they will be mentioned in the respective chapters where they were exploited.

3.1 Low Temperature STM

All the experiments described in this thesis were performed using a commercially available low temperature scanning tunnelling microscope (LT STM) provided by Omicron, illustrated in Fig 3.1. This STM system consists of the four main parts. First is the scanning part in which the tip and the sample of interest are loaded onto the scanning stage and the measurement is performed. The second part is a system of vacuum chambers housing the tips and the samples and other electronic part of the system. Thirdly, they are the electronic controllers which control the functions of the electronic devices of the STM, including the electronic tunnelling between the tip and the sample on the scanning stage. The last part is a computer consisting of a number of programs used to give orders to those electronic controllers. Before one can start using the STM to acquire data, the one must be familiar with all of the four sub systems of the STM system.

Figure 3.1 The LT STM used in this work consisting of three main parts; the vacuum system (only the LT STM chamber and the Preparation chamber can be seen in this figure), the electronic controller instrument (stored on the shelf behind the vacuum system), and the controlling computer (adjacent to the electronic controllers but cannot be seen in the photo).

3.1.1 Ultra High Vacuum Chambers

The scanning stage of the STM system upon which a prepared tip and sample are placed such that a tunnelling current between them can flow between them operates inside an ultra-high-vacuum (UHV) system consisting of three chambers. The Load Lock chamber is used for loading tips and samples prepared ex-situ in atmosphere, into the UHV system and vice versa. The Preparation chamber, connected to the Load Lock chamber, is used to prepare the samples and the tips on the Omniax manipulator head using processes such as degassing, flashing, H termination, etc. The LT STM chamber, attached to the Preparation chamber, is where the scanning stage is housed. The scanning section is surrounded by cryogenic baths utilised to cool down the temperature of the region inside to ~ 77 K or 4 K by filling the baths with liquid nitrogen or liquid helium

respectively (the latter not used for this thesis work). Apart from the scanning operation, there is also a Tip Tool stage outside the cryogenic baths for preparation of a tip before loaded onto the scanning stage, details below. The sample is usually thermally flashed inside the STM chamber before being loaded onto the scanning stage. Although some tip and sample preparation can be done in the STM chamber, any tip or sample transferred from the Load Lock chamber must be thermally degassed in the Preparation chamber before transferred to the LT STM chamber.

The UHV condition is necessary to stop unwanted gas molecules from being adsorbed on, and chemically interacting, with the sample surface, which creates contaminating features on the surface and therefore leads to misinterpretation of the data observed. In order to achieve the UHV level inside the chambers, the chamber system must be properly baked out at 150 ℃ for 72 hours while being pumped by a turbo molecular pump. This step removes water molecules from the chambers that make the possible lowest pressure to be just in the range of 10^{-9} mbar. To further reduce the pressure, ion getter pumps and titanium sublimation pumps are exploited, resulting in the pressure that can be reduced to the range of 10^{-11} mbar.

3.1.2 Vibration Isolation System

The scanning stage of the STM system is housed inside one of the vacuum chambers. As discussed in Chapter 2, the tunnelling current between the tip and the sample is so sensitive to the distance of the tip from the surface that a change of 1 Å can alter the tunnelling current in the order of one magnitude. Therefore, vibration-isolated systems are used to isolate the scanning section from any possible vibrations so that the changes of the current are purely caused by the changes of the electronic property of the surface. For this reason, the scanning stage is mounted on a spring system inside the LT STM chamber and has an eddy current damping system to minimise mechanical vibrations. Moreover, the table upon which the chambers are placed is also isolated from the mechanical vibrations from the floor using an active damping system. Despite all the vibration isolation systems, touching the chambers or even the table is prohibited. It does

not only create noise in the STM images and spectra, but it may also cause the tip to crash with the sample and destroys the scanning performance of the tip.

3.2 Sample Preparation

There are two sample surfaces used in this work. The first is the Si(001) surface that is highly chemically active and the second is the Si(001):H surface which is chemically inert. Samples are prepared so that the surfaces are flat and clean. Before the Si(001):H surface can be obtained, a well prepared Si(001) surface is first required. The silicon wafers used in chapter 4 and chapter 5 are commercial *n*-type Si(001) wafers degenerately As-doped with the doping concentration in the range of 10^{-18} cm^{-3} while the silicon wafer used in chapter 6 are low As-doped with the doping concentration of 10^{-14} cm^{-3}.

3.2.1 Si(001) Preparation

The Si(001) wafers were cut into small pieces of about 10 mm × 3 mm in size that were mounted onto sample holders loaded into the STM vacuum system through the Load Lock chamber. During the preparation, care must be taken to prevent the sample surface from being scratched by the diamond pen apart from the cracking line. The tweezers utilised during the ex-situ preparation were made of plastic to avoid the alteration of the sample resistivity through metal contamination, while the sample was handled by the tools.

After the sample preparation in the atmosphere, the sample then was loaded into the vacuum chambers. To remove water molecules attached to the sample and the sample holder while they were in the atmosphere, the sample had to be thermally degassed at 500 ℃ for 12 hours inside the Preparation chamber. The sample was placed in the hot stage of the Omniax manipulator head. Then, a current was passed through a resistive material in the manipulator head, which increases the local temperature, including the temperature of the sample by conduction heating. However, to obtain the flat and clean Si(001) surface preferable for our measurement, the sample must be thermally flashed at a

temperature of about 1100 °C for 10 seconds by passing a current directly through the sample in order to evaporate all contaminants from the surface such as water-related or carbon-related molecules bonded to the surface. After that, the temperature of the sample is immediately decreased to about 900 °C at which the silicon atoms are sufficiently mobile across the surface to reconstruct the Si(001) surface again while the temperature was slowly cooled down to the room temperature within 200 s. This sample preparation annealing method can be repeatedly applied and it provides an atomically flat and clean Si(001) surface with large terrace suitable for the study of the surface by STM.

3.2.2 Si(001):H Preparation

The Si(001):H surface was prepared after the preparation of the Si(001) surface as discussed above. The Si(001) surface was then exposed to H atoms introduced into the Preparation chambers while the sample temperature was maintained at about 400 °C in order to obtain the H-terminated Si(001) surface. The H atoms were produced by passing H_2 gas into the Preparation chamber through a coil of tungsten (W) wire heated up to 1500 °C where the hydrogen molecules are cracked into individual hydrogen atoms. The pressure of the chamber during the H termination is typically raised to 10^{-7} mbar for 5 minutes to ensure that the surface was thoroughly terminated with the H atoms. The temperature of the sample meanwhile is also essential to mainly obtain the monohydride structure throughout the surface as discussed in Chapter 2.

3.3 Tip Preparation

In addition to the requirement of a well prepared sample, the tip or probe must be carefully prepared in order to be atomically-sharp and clean. Unlike the sample, the ex-situ preparation of the tip is as important as the in-situ preparation to generate the STM images with the atomic resolution.

3.3.1 Ex-situ

A tip can be produced by electrochemically etching a W wire in a 3 mol KOH solution. A schematic diagram of the etching process is illustrated in Fig. 3.2. A stainless steel ring with a diameter of ~ 2 cm is suspended ~ 2 mm below the surface of the solution. Then, a small piece of a polycrystalline W wire with a diameter of ~ 0.25 mm is vertically submerged ~ 4 mm below the solution surface through the centre of the ring. After that, a voltage of ~ 10 V is applied across the stainless steel ring and the W wire. According to the diagram, the wire and the ring act as an anode and cathode respectively while the solution acts as an electrolyte; thus, the wire is preferentially corroded due to the flow of electrons from the ring to the wire. The interface between the W wire and the electrolyte creates a meniscus around the wire. The current flowing through the wire induces an electrochemical reaction that occurs rapidly at the meniscus, which defines the etching area. During the etching, the current gradually decreases due to the shape of the etching area of the wire. After about 10 minutes when the wire etching is complete, the current is reduced to the level that the power supply is automatically switched off. The wire is then removed out of the solution immediately and rinsed with de-ionised water. If the etched wire is sufficiently sharp, it will be mounted onto a tip holder and loaded into the vacuum chambers. The etched tungsten wire from this point is called a metal tip. Figure 3.3 shows the tools used to produce the STM tip with the procedure mentioned above.

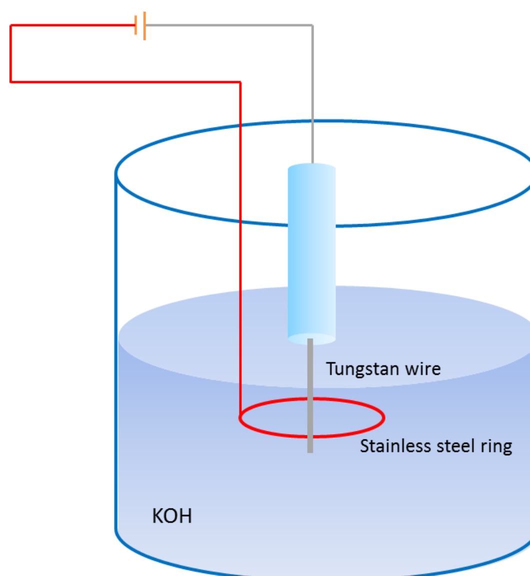

Figure 3.2 A schematic diagram of the tip-etching process. The tungsten wire and the stainless steel ring are positively and negatively biased respectively allowing the wire to be etched.

Figure 3.3 Instruments used for the tip-etching process. The beaker contains KOH solution with a stainless steel ring and a tungsten wire suspended from the micrometres, immerged into the solution and connected via a power supply.

3.3.2 In-situ

Once in UHV, the tip is initially degassed in the Preparation chamber at 150 ℃ for 12 hours so as to remove the water adsorbed to the tip and its holder with the same resistive heating method used for degassing the sample. However, the oxide layer of WO_3 coating the W tip after the etching process cannot be removed with the thermal degassing. The oxide layer causes instability in the tunnelling current leading to low-resolution STM images and can cause the shift of the energy scale involved in both topography and spectroscopy. To effectively remove the oxide layer, the tip must be treated with electron bombardment and field emission.

Electron bombardment is used to heat the tip up to 725 ℃, stimulating the tungsten trioxide (WO_3) to react with tungsten (W) and form tungsten dioxide (WO_2) which then sublimates from the tip as indicated in the reaction below.

$$2WO_3 + W \rightarrow 3WO_2 \uparrow$$

By applying a voltage of about 400 V across the tip and a tungsten filament brought very close to each other with the tip being the positive electrode, passing a current through the filament emits electrons from the filament that are accelerated towards the tip, so that the tip is bombarded by the electrons at its apex as shown in Fig. 3.4(b). This bombardment heats up the tip to the desired temperature. The current generated by the flowing of the electrons between the tip and the filament is called the emission current. The filament current is increased until the emission current reaches 20 μA and the tip is heated at this current for 5 minutes to effectively remove the oxide layer from the very end of the tip.

To check whether the tip condition is sufficiently good to load onto the scanning stage, the bias applied to the tip is switched from positive to negative compared to the filament. By appling a large negative bias to the tip, say -1100 V, electrons can be emitted from the tip and tunnel to the filament. This process is called filed emission (FE) shown in Fig. 3.4 (a). We record the emission current while we sweep the voltage from 0 to -1100 V but limit the maximum current to 1 μA to avoiding excessively heating the tip. Before the electron bombardment, the FE curves are normally very unstable as shown in Fig. 3.5(a). Nevertheless, after

the bombarding the tip by electrons, the measured FE current is found to be very stable and reproducible as seen in Fig. 3.5(b). If the tip shows successive FE curves that overlap one another, it will be loaded onto the scanning stage. This tip is usually stable and can be used for several weeks.

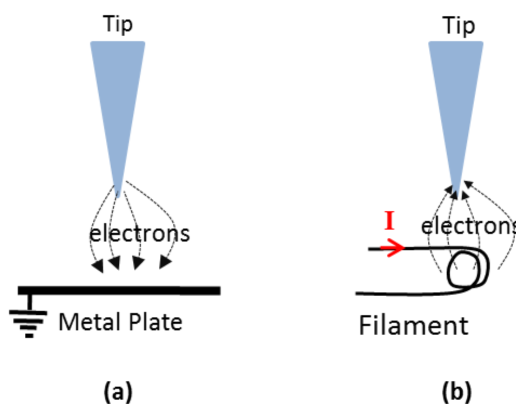

Figure 3.4 (a) Field Emission in which electrons tunnel from the negatively-biased tip to grounded filament acting as a metal plate if the tip is very sharp. **(b)** Electron bombardment in which an electron beam is accelerated from the heated filament to hit the tip apex, heating the end of the tip up significantly and removing the oxide molecules from this part of the tip.

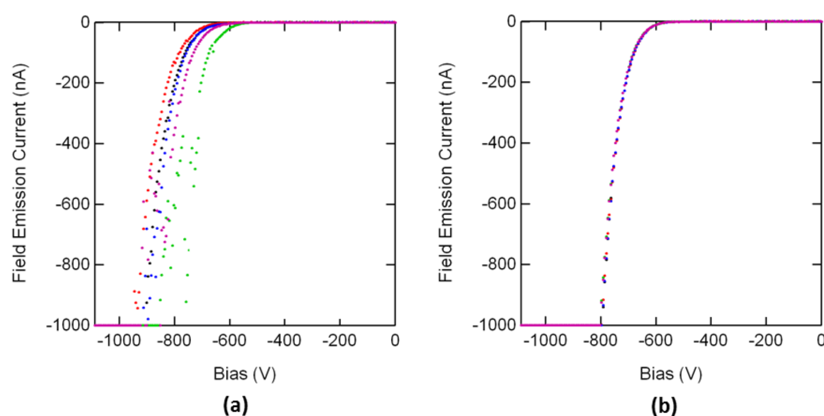

Figure 3.5 (a) Field Emission curves before the tip was heated by electron beam during the Electron Bombardment process. **(b)** Field Emission curves after the tip was thermally cleaned by the E-beam to remove the oxide from the apex of the tip, showing the tunnelling stability of the tip.

3.4 Phosphine Dosing

To dose Si(001) with phosphine molecules, a gas-dosing assembly was attached to the LT STM chamber. A capsule of 99.9996% phosphine gas was attached to the dosing assembly connected to the STM chambers. The phosphine molecules were about to be released from the capsule and stored in a small tube region of the assembly surrounded by precision leak valves on both side of the tube. Before the gas was released, the assembly was flooded by nitrogen gas and pumped out with the turbo pump until the pressure reached 10^{-7} mbar a few times to remove residual gases inside the tube. After that, the capsule was opened to the assembly and the assembly was subsequently filled by the phosphine gas, including the storage part. There are two valves surrounding the storage region with the vale between the STM chamber and the dosing assembly tightly closed. After releasing the phosphine gas out of the capsule and storing it inside the storage part of the dosing assembly, the remaining phosphine gas outside the storage part was then pumped out of the assembly by the turbo pump until the pressure reached 10^{-8} mbar. Subsequently, the capsule was detached from the assembly which was then under vacuum except for the storage part.

3.5 RGA Spectrometer

To test whether there is sufficient amount of phosphine molecules in the UHV chamber, we utilised RGA (Residual Gas Analyser) which is another type of Mass Spectrometers attached to the chamber. By releasing the phosphine gas from the storage part of the dosing assembly into the UHV chamber while operating the RGA instrument, the amount of phosphine in the chamber can be detected and displayed as an intensity peak associated with the mass of the phosphine molecule in the mass spectroscopic graph.

3.6 STM Data Processing

By using the STM tip to scan over the biased sample surface, the STM images obtained must be processed before the full interpretation can be acquired. For a quick consideration of the data, the Vernissage program can be readily used. However, to gain better quality image the Gwyddion program has been utilised to process the data throughout this PhD work. The Igor program written by our colleagues in the research group have also been exploited especially for the spectroscopic data. For the thermal drift usually occur on an STM image, Adobe Photoshop were used to remove the drift merely by aligning for example the Si dimers in different dimer rows. Apart from these programs, the Feature Tracking App program written by Adam Rahnejat was also used for tracking and counting additional features appearing on the surface after the samples were prepared.

Chapter 4

Phosphine on Si(001) at 77 K

4.1 Introduction

A phosphorous (P) dopant has been envisaged as a qubit in the Kane scheme for a silicon based quantum computer [1]. It has also be proposed as a component in quantum computing scheme shown in Fig. 4.1 in which the control atom is P and the qubit atoms both are Bi [2]. To build a quantum computer containing individual P atoms, the P atoms need to be incorporated in silicon using the method described in Ref 28. It is therefore necessary for us to understand the interaction of PH_3 with the Si(001) surface. Using low temperature STM will allow us to obtain insight into the appearance of P-containing structures on the Si(001) surface and hence to distinguish the phosphine-related structures from the commonly-observed surface defects. It may also lead us to resolve missing puzzles from the study of the PH_3-dosed Si(001) surface at room temperature [4, 35, 37] such as identifying some dissociative structures that have not been experimentally observed but proposed as important intermediates states of the dissociation mechanism.

In this chapter, firstly, the Si(001) surface dosed with PH_3 to saturation has been studied. With the aid of voltage-dependent imaging, we unveil one new feature commonly observed on the surface and propose that there are three distinct features rather than just the two features (which are PH_2+H and PH+2H) observed on the saturation-dosed Si(001) surface [37] at room temperature. Secondly, with the surface lightly dosed with PH_3, it will be shown that the measurement at 77 K reveals a number of phosphine-related structures that have never been experimentally reported. We interpret those structures as intermediate states of the PH_3 dissociation process and show that they strengthen the proposed forward thermally-driven dissociative mechanism of PH_3 on Si(001) [4, 35]. Apart from the newly-discovered dissociative structures, the measurements at 77 K also allow

us to discover a tip-induced structural transformation of the P-containing structures. We believe that the transformation happens across two different dissociative pathways for which the first pathway consists of 1 P atom and 3 H atoms [35] while the second pathway is comprised of 1 P atom and 2 H atoms [55]. However, we also propose an alternative interpretation that the transformation might be the backward process of the first dissociative pathway introduced in Ref. [4].

Since the phosphine-dosed silicon surface must be thermally annealed in order to incorporate the P atoms into the Si(001) surface layer, as another step toward the device fabrication [16] shown in Fig. 1.3, we also investigate the annealed Si(001) surface at 77 K and compare our results to the previous study investigated at room temperature [5, 38, 41]. The comparison has provided us with additional insights of the 77-K voltage-dependent appearance of the Si-P heterodimer that may lead us to a novel statement associated with the ground state of the Si-P structure for which there has been an ambiguous agreement between the room-temperature experimental STM images and the simulated STM images of the Si-P heterodimer [5].

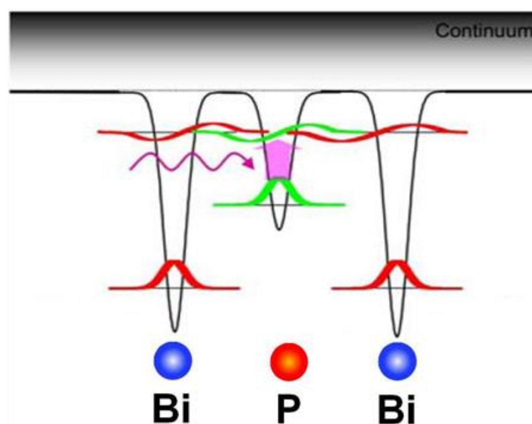

Figure 4.1 A quantum computer scheme based on Stoneham *et al.*'s proposal with P as the control atomic switch and Bi as the qubits. See the Introduction Chapter for more details of the functionality of the QIP structure. The figure is adapted from Ref. [2].

4.2 Saturation PH_3-dosed Si(001)

With the base pressure of the STM chamber about 1×10^{-11} mbar, we dosed the Si(001) surface with PH_3 gas by opening the precision leak valve of the PH_3-dosing assembly until the pressure of the STM chamber reaches 2×10^{-10} mbar and kept the pressure at this level for 30 seconds. After that, the sample was transferred onto the scanning stage at 77 K, and then the saturation-dosed Si(001) surface was imaged by the STM tip.

4.2.1 Two distinctive PH_3-related features

Fig. 4.2 (a) is a filled-state image of the saturation-dosed Si(001) surface taken at the sample bias of -2.0 V and the tunnelling current setpoint of 30 pA. Comparing this low-temperature image (Fig. 4.2 (a)) to a room-temperature image [37] shown in Fig. 4.2 (b), it is apparent that there are two distinctive features appearing for both samples. The first feature is the big circular protrusion indicated by each white arrow in Fig. 4.2 (c) and 4.2 (e). The second feature is the small circular protrusion also indicated by each white arrow in Fig. 4.2 (d) and (f). The big protrusion and the small protrusion can be assigned to the PH+2H structure and the PH_2+H structure respectively [37]. However, when the bias voltage is varied (see Fig. 4.3), the big protrusion behaves in two different ways as indicated by the white and black arrows, leading to the identification of another feature on the surface that can only be identified by performing the voltage-dependent imaging. We discuss the observation in detail in the next section.

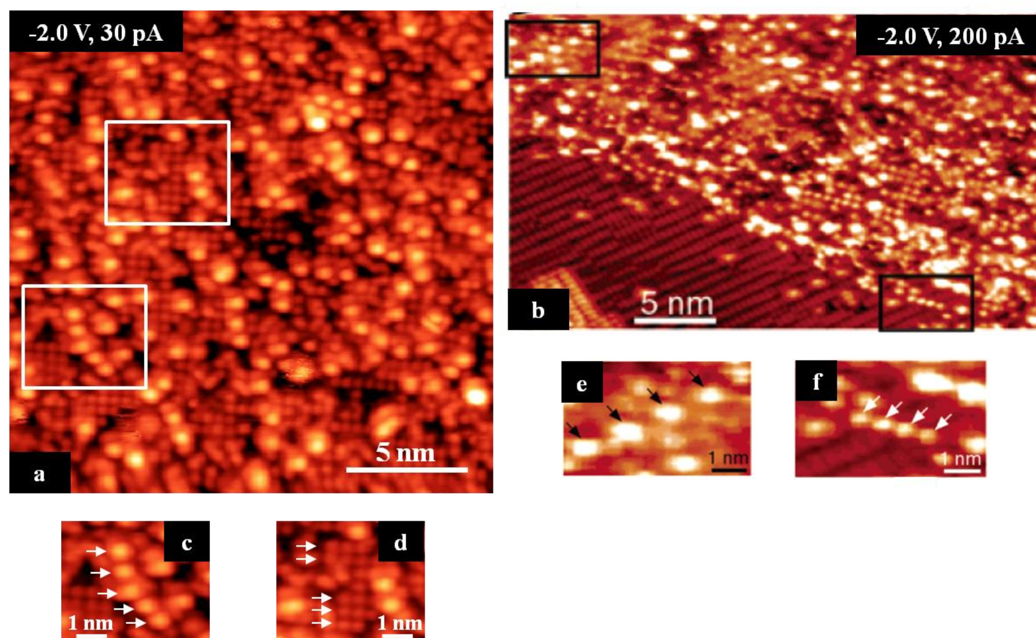

Figure 4.2 **(a)** A surface area of the saturation-dosed Si(001) surface imaged at 77 K revealing two distinct features: big protrusion **(c)** and small protrusion **(d)**. **(b)** A surface area of a saturation-dosed Si(001) surface imaged at room temperature (from Ref. [37]) revealing the same two distinct features categorised in **(e)** and **(f)**. Note that for (b) the well-reconstructed area on the left bottom corner is terminated by a single layer of H atoms which makes the surface area chemically inert; thus there is no adsorption of PH_3 molecules on the surface region [37].

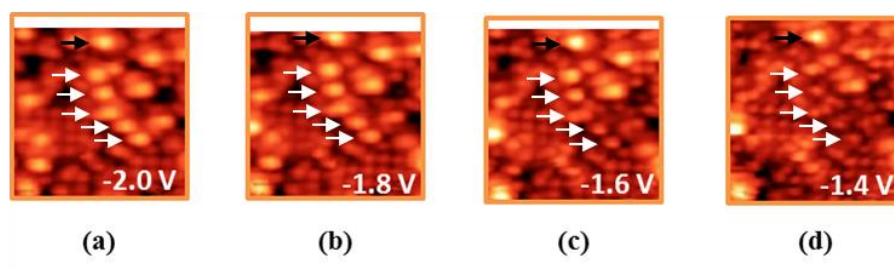

Figure 4.3 A series of STM images taken at different negative sample biases; **(a)** and **(b)** There seems to be only two distinct types of feature (big protrusion and small protrusion): **(c)** and **(d)** It is obvious that some big protrusion features do not become dimmer (black arrow) while the others do (white arrows) when the voltage magnitude decreases. The size of the box enclosing each image is 7 nm × 7 nm.

4.2.2 Voltage-dependent imaging of the saturation-dosed surface

When magnitude of the sample bias was decreased from - 2.0 V to - 1.4 V, we observed that the big protrusion features behaved in two different ways as illustrated in Fig. 4.3. Some of them still appeared with the same size and with the same intensity as indicated by the black arrows, whereas the others indicated by the white arrows became smaller in size and appeared less bright. The latter group of the big protrusion feature could not even be distinguished from the small protrusion feature (PH_2+H) at - 1.4 V. Despite the two different groups of the big protrusion features, the small protrusion features appeared the same with the bias magnitude decreasing. Therefore, with the aid of the voltage dependence of the filled-state imaging, the big protrusion features can be classified into two characteristic groups based on its voltage-dependent contrast behaviour. Both types of the big circular protrusion indicated by the black and white arrows could be the Si dangling bonds and the PH+2H structures [37]. Nevertheless, we believe that the big protrusion indicated by the black arrows should be attributed to the Si dangling bonds since the dangling bond always appears bright despite the variation of the imaging bias [30]. As a result of this assignment, the big protrusion indicated by the white arrow would be induced by the PH + 2H structures and it cannot be distinguished from the Si dangling bond without the voltage-dependent imaging.

Finally, beside the protrusion features (big protrusions and small protrusions), there are also the depression features appearing throughout the surface. The feature do not possess any P atom and can be attributed to H atoms dissociating from the adsorbing PH_3 molecules [37]. The dissociative pathway providing the separated H atoms will be discussed later in this chapter.

4.3 Low PH_3-dosed Si(001)

By significantly reducing the amount of phosphine during the dosing procedure by precisely controlling the leak valve, the Si(001) surface lightly dosed with PH_3 was obtained as shown in Fig. 4.4 (c) and 4.4 (d). The low-dosed surface allows us to investigate individual PH_3-related features appearing on the

surface after the PH_3 dosing. We dosed the Si(001) surface with PH_3 at room temperature to provide sufficient time for the thermal dissociation to proceed before transferring the sample onto the scanning stage within a few minutes. The sample temperature falls from room temperature to ~79 K immediately and became 77 K within half an hour. At this low temperature range, it has been well-known that all the thermally-driven changes on the surface cannot occur [56]; thus, any dissociative intermediate states that have not been experimentally observed at room temperature [4] might be frozen and we as a result could image them with the STM tip.

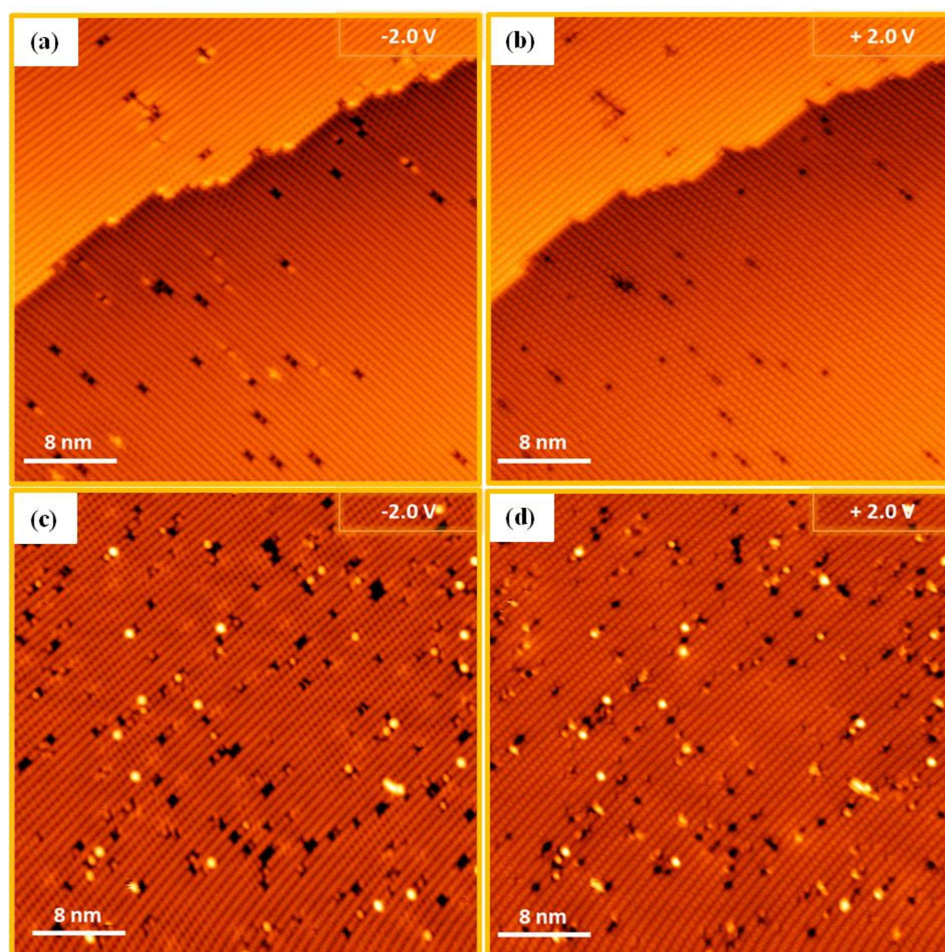

Figure 4.4 **(a)** filled-state and **(b)** empty-state images of Si(001) taken at 77 K before lightly dosing with PH_3 at room temperature. **(c)** filled-state and **(d)** empty-state images of Si(001) taken at 77 K after lightly dosing with PH_3 at room temperature.

Individual phosphine-related features

The three main phosphine-related features on Si(001) after dosing with PH_3 previously observed at room temperature have been illustrated in Fig. 4.5 (a) [4]. These three PH_3-related adsorbates have one thing in common in that each of them consists of 1 P atom and 3 H atoms in close proximity. The PH_2+H structure is the first dissociative product occurring immediately upon the adsorption of the PH_3 structure on the surface. At room temperature, in a time scale of minutes [37], the PH_2+H structure dissociates into the PH+2H structure which further dissociates into the P+3H as the last structure of the dissociation pathway. The calculated structural energy of the dissociative products are listed in the graph shown in Fig. 4.5 (b) [4]. In the energetic graph, the energy levels of the three commonly-observed PH_3-realted features are shown. It is important to note here that each dissociative structure, such as PH+H represented by PH in the diagram, can have a number of different bonding configurations possessing different energies; for example, the PH+H structure can bond to the Si(001) surface with the C1 and C4 bonding configurations which are different in energy. The insight of the phosphine dissociative products at room temperature will be exploited later in this chapter when discussing our data taken at 77 K.

In Fig. 4.6, we present high resolution images of the PH_3-related features observed on Si(001) at 77 K after dosing the PH_3 gas to the silicon substrate at room temperature. We categorised these features into three groups based on their appearance. Following Ref. [4], the features appearing one-dimer wide, with one side of the dimer being bright while the other being dark in filled-state images were classified as “asymmetric” (A1 and A2) and were assigned to the PH_2+H structure. Each of the features with a bright protrusion located symmetrically on top of the dimer row in filled-state images were categorised as “centred” (C1, C2, and C3) and were attributed to PH+2H structures. We will show later that not all the C features are associated with PH+H but they are induced by another group of PH_3-related adsorbates that consist of 1 P atom and only 2 H atoms. Finally, the features caused by the P+3H molecules were grouped as “U-shaped” (U1 and U2) based on their filled-state appearance that are three-dimer wide. Its middle dimer was bright only on one dimer end, making the feature similar to the U letter.

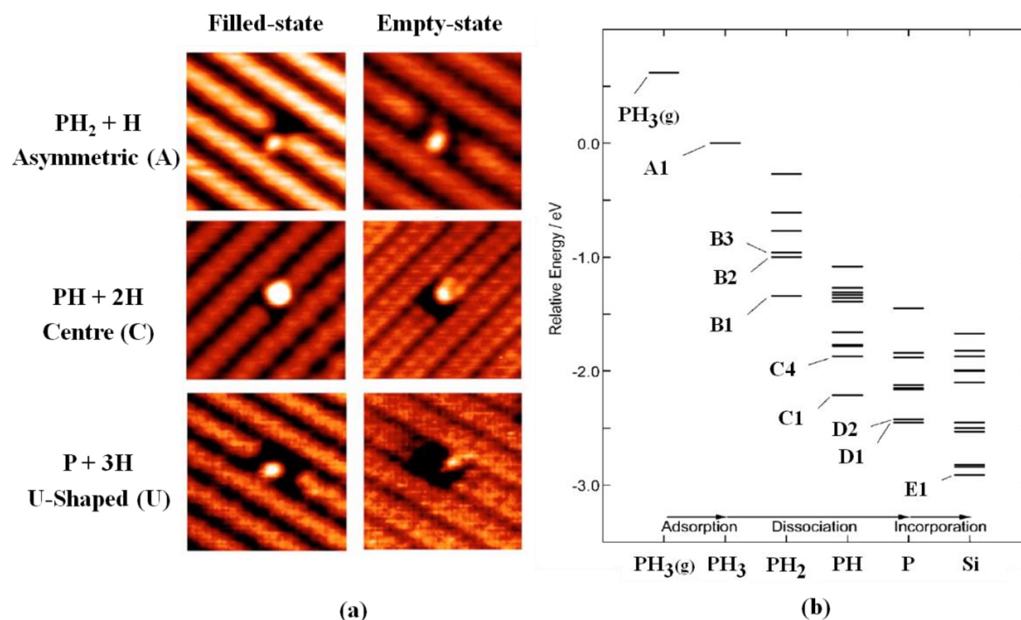

Figure 4.5 (a) High-resolution STM images of three main PH_3-related dissociative features commonly observed on Si(001) after dosing with PH_3 gas at room temperature, taken from Ref. [4]. The images were taken at room temperature with the scanning parameters of -1.6 V, 0.1 nA for the filled-state images and +1.2 V, 0.1 nA for the empty-state images. (b) A diagram showing the calculated energies associated with PH_3-related structures bonded to the Si(001) surface[4]. Each structure, such as PH+H represented by PH in the horizontal axis, can have different bonding configurations possessing different energies (see the C1 bar and the C4 bar). Note that the figures are also presented in the Introduction chapter but it is presented in this chapter again for convenience of comparison with our results.

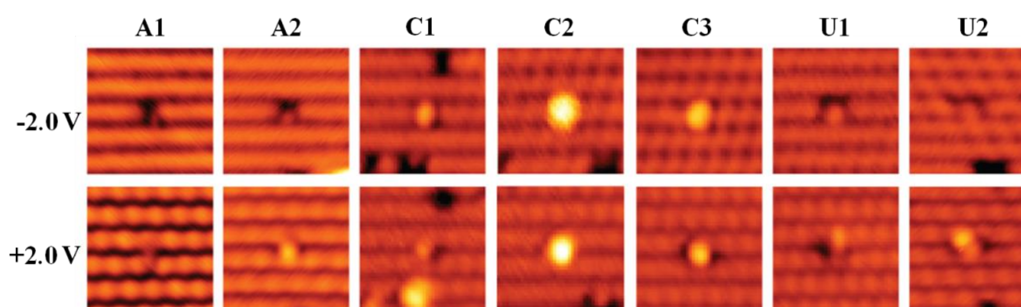

Figure 4.6 High-resolution STM images obtained by the author of all of the PH_3-related dissociative features observed on Si(001) at 77 K after dosing with PH_3 gas at room temperature. They were grouped according to the appearance with A, C, and U representing “asymmetric”, “centred”, and “U-shaped” respectively. The images were with the scanning parameters of -2.0 V and +2.0 V.

Fig. 4.7 shows the total counts of each observed phosphine-related feature as shown in Fig. 4.6. The statistic was generated by counting the number of the features observed in twenty separate 20 nm × 20 nm images. Within the associated measurement uncertainties represented by the vertical error bar of each data point, features A1, A2, C1, and U1 are the most abundant with the remaining features (C2, C3, and U2) being approximately half as common.

Error bars are defined as the square root of the feature counts, with the feature counts being the total counts in the set of the 20 images. For example, the total count of Feature A1 is 43 and thus the deviation is $\sqrt{43}$ which is about 6.5. The error bar of the A1 feature is thus ranged from 43-6.5 to 43+6.5 as shown in Fig. 4.7. For the next measurement, the total count of the A1 feature could be between 35 and 49. The error bars were added into the graph to compensate any mistake of counting such as the insufficient number of images, or simply the large separation of each image areas that allows some dissociative products related to the features in the images of consideration to be missed out.

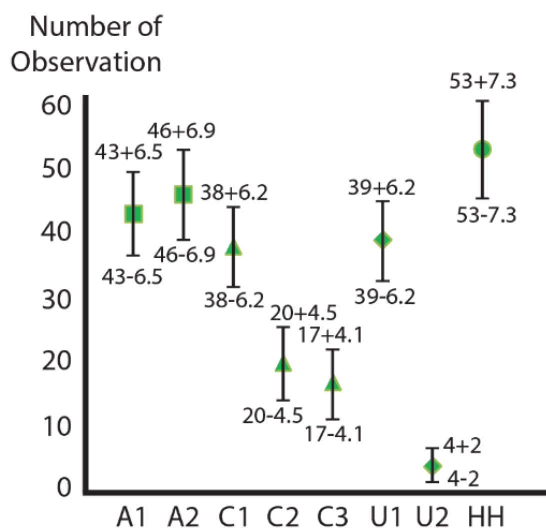

Figure 4.7 Numbers of each PH_3-related features observed in total on the phosphine-dosed sample surface by counting from 20 images of 20×20 nm^2 with the associated error bars calculated as discussed in the text. The hemidydride (HH) feature is the most commonly observed with its number relevant to a special dissociation pathway of PH_3 which will be discussed later in the text.

Apart from the A, C, and U features, there is another feature commonly observed on the PH_3-dosed surface. This feature is comprised of a single H atom bonded to one atom of a single dimer and is called the hemihydride (HH) structure. The hemihydride feature has been discussed in Ref. [37] which describes the diffusion of a PH_2 fragment away from a PH_2+H structure to subsequently attach to another hemihydride structure nearby, leaving behind the single H atom bonding to a Si dimer atom and as a result forming a new hemihydride structure. However, how the first hemihydride structure comes to being has not been discussed yet. This will be clearly discussed later in this chapter.

4.3.1 Group A features

As seen in Fig. 4.6, there are two dissociative features (A1 and A2) assigned as the asymmetric (A) structure base on their appearance. Fig. 4.8 (a)-(d) show filled- and empty-state images of a surface region where feature A1 and feature A2 are simultaneously observed. There is a buckling feature at the middle of the image that we attributed to a hemihydride dimer. Both of the A1 and A2 features are only one-dimer wide. For the imaging of the filled states (Fig. 4.8 (a) and 4.8 (c)), one dimer end of each asymmetric feature appears bright while the other end appears dark. The A1 and A2 features cannot be distinguished from each other by solely relying on the filled-state images since they look identical at low (Fig. 4.8 (a)) and high (Fig. 4.8 (c)) negative sample bias. However, in the empty-state images, the appearance of A1 is different from the appearance of A2 both at high and low positive bias for several aspects. Firstly, A1 express lower intensity than A2 at high positive bias (Fig. 4.8 (b)). Secondly, at low positive bias (Fig. 4.8 (d)) although A1 and A2 become approximately as bright as each other, the two neighbouring background Si dimers of A1 appear brighter as indicated by the white arrows.

With reference to the survey of possible stable dissociative products [4], the fact that feature A1 and A2 are 1-dimer wide provides us with only four possible bonding configurations these asymmetric features (A1 and A2) as shown in Fig. 4.9. The bonding configurations in Fig. 4.9 (c) and 4.9 (d) can be ruled out

since the PH_2 and PH fragments would be expected to appear as a feature with a protrusion at the middle of the dimer. For the PH_3 bonding configuration as represented in Fig. 4.9 (a), the simulated STM image of an adsorbed PH_3 structure does not match any of the experimentally observed A1 and A2 features. On the other hand, the simulated image of the PH_2+H bonding configuration shown in Fig. 4.9 (b) matches the observed A1 and A2 features in that one dimer end always appears bright in both bias polarity while the opposite side always appears dark. Thus, feature A1 and feature A2 should be assigned to the PH_2+H structure, consistent with the assignment made in Fig. 4.5(a) for the surface imaged at room temperature [4]. We assign the bright protrusion of the features to the PH_2 fragment of the PH_2+H structure. However, note here that the dimer end appearing as depression in the simulated STM image in Fig. 4.9 (b) is not completely dark for the empty-state image, which is consistent with the appearance of A1 and A2 in Fig. 4.8 (d).

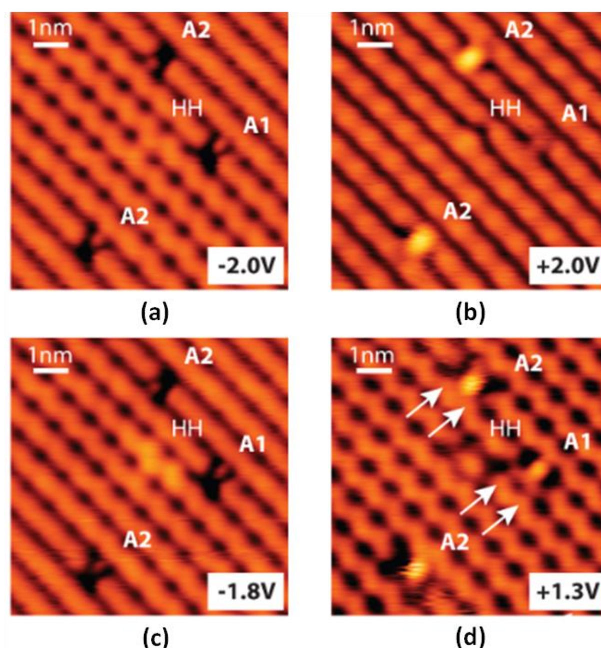

Figure 4.8 (a)-(d) Voltage-dependent images simultaneously revealing feature A1 and A2 that appear almost identical in filled-state imaging ((a) and (c)) but can be distinguished from each other in the empty-state images ((b) and (d)). The white arrows in (d) point at the neighbouring background Si dimers of the one-dimer A feature. There is one hemihydride (HH) feature at the middle of each image which will not be discussed here.

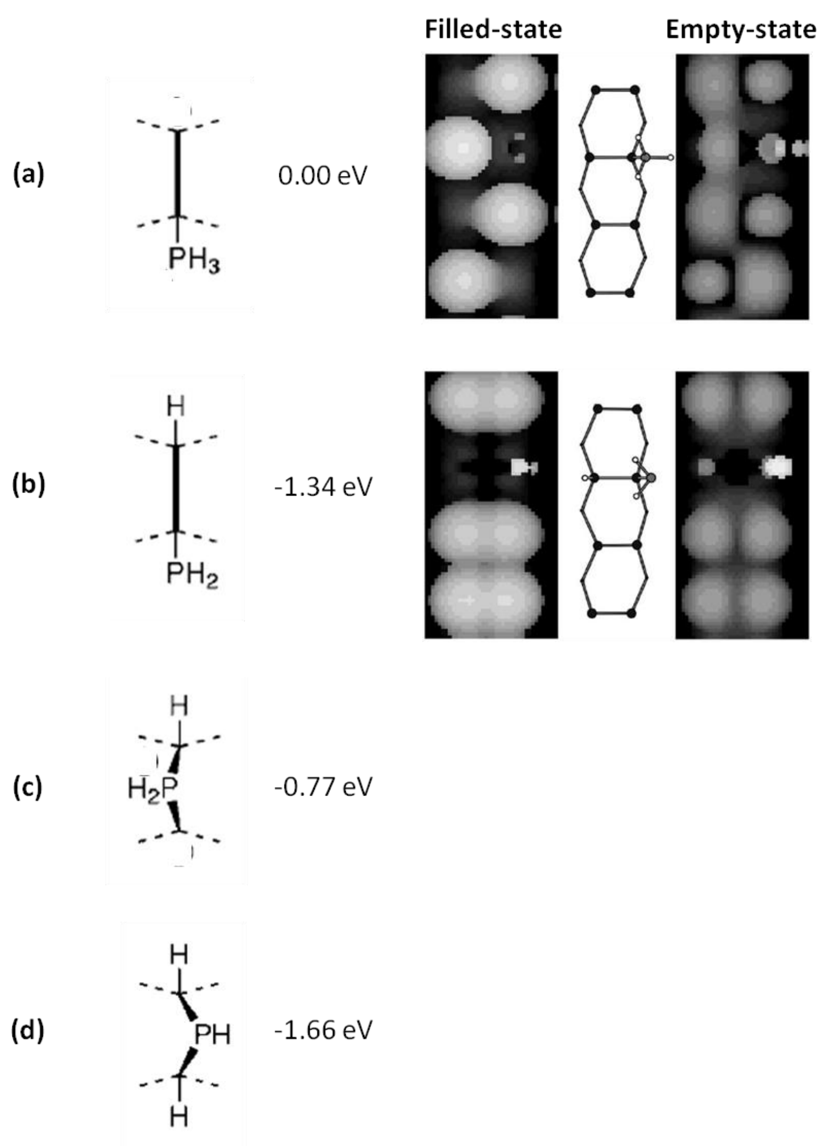

Figure 4.9 (a)-(d) Bonding configurations of the PH_3-related dissociative structures which are 1-dimer wide and the relevant calculated structural energy. The simulated STM images of some bonding configurations are provided on the right-hand side as available in Ref. [4].

Figures 4.10 (a) and 4.10 (c) show high-resolution empty-state images of feature A1 and feature A2 respectively, acquired at the very low bias of 0.8 V. Here, both features clearly appear only 1-dimer wide with the adjacent Si dimers on both sides appearing less bright than the other surrounding Si dimers, indicated by the white arrows. Moreover, both neighbouring silicon dimers of feature A1 are brighter than those of feature A2. This might be caused by the different bonding configurations of feature A1 and feature A2. Closely considering Fig. 4.10 (b) and 4.10 (d) suggests that for the A1 feature the dimer end of the silicon dimer that the PH_2 fragment is attached to is buckled down, whereas for feature A2 it is buckled up. The dual appearance of the asymmetric feature is in contrast to the room temperature measurements [4, 57, 58] in which only one type of the single-dimer asymmetric feature was observed as shown in Fig. 4.5. We interpret this as being due to the influence of the pinned buckling orientation of the silicon surface dimers. The interpretation is provided by the alignment of a green atomistic mask on top of each A feature, which leads us to the bonding configuration associated with feature A1 and A2 as illustrated in Fig. 4.10 (e) and 4.10 (f) respectively. There are two possible explanations of how there are two types of the asymmetric features appearing on the Si(001) surface. First of all, at room temperature (RT), the thermal energy is sufficient to drive the dissociation process forward and thus only the most stable bonding configuration of PH_2+H is observed. However, at 77 K, it is accepted that all the surface structures are frozen; therefore, any intermediate bonding configuration could be stopped from further dissociation to the most stable configuration. During the transfer of the sample from the room-temperature dosing stage to low-temperature scanning stage, not all of the asymmetric structures had transformed to the most stable configuration. There would be more than one types of the asymmetric feature existing on the surface once the surface was cooled down to 77 K. Secondly, it might merely be the buckling orientation of the background silicon dimers that is pinned at 77 K, which causes the asymmetric feature to split into two categories (A1 and A2). Regarding the both explanations, it informs that A2 is more energetic preferable than A1, which is confirmed by the observed number of A2 that is higher than the number of A1 (see Fig. 4.7). Moreover, A2 is the one commonly observed at RT [4] by comparing to its appearance in Fig. 4.8 (b),

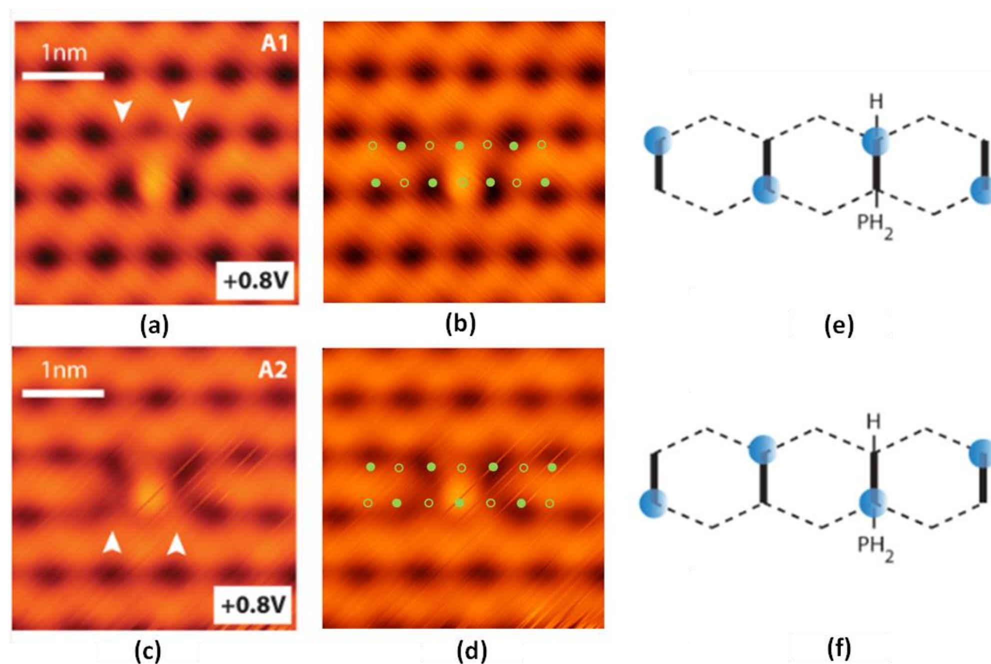

Figure 4.10 **(a)** and **(c)** empty-state images of feature A1 and A2 respectively with the white arrows indicating the down silicon atoms of neighbouring dimers. **(b)** and **(d)** are image (a) and (c) respectively with the atomistic masks showing the buckling orientation of the background silicon dimers. The alignment of the mask and the feature provides the bonding configuration associated with A1 and A2 as depicted in **(e)** and **(f)** respectively. The filled and empty green circles of the masks represent *up* and *down* Si atoms respectively. The blue circles in **(e)** and **(f)** represent the *up*-atom of the Si dimers.

4.3.2 Group U features

Due to the complexity of the assignment of the C features, which needs the clarification of the assignment of the other feature groups, it is important to discuss the assignment of the U features prior to the C features. As seen in Fig. 4.11 (a) and 4.11 (d), feature U1 and U2 both are three-dimer wide with a protrusion on the middle dimer at a dimer end, making the features look U-shaped. The appearance of the U features observed at 77 K is consistent with those observed at room temperature [4] as illustrated in Fig. 4.5 (a). As a result of this consistency, the P+3H structure is assigned to both feature U1 and feature U2. This P+3H structures is a product from further dissociation of the phosphine adsorbates at room temperature, leading to the formation of single P atoms bonded to the Si(001) surface with 3 H atoms in close proximity [35]. By solely considering the filled-state images, both U1 and U2 appear identical (Figs. 4.11 (a) and 4.11 (d)). However, they can be distinguished from each other with the empty-state images, as shown in Fig. 4.11 (b) and 4.11 (e). Like the analysis of the A features earlier discussed, by putting the atomistic masks on top of the features (see Fig. 4.11 (g) and 4.11 (h)), we found that the bonding configuration of both U features is the same except that the buckling orientation of the background Si dimers is different as shown in Fig. 4.11 (c) and 4.11 (f). However, unlike the asymmetric features, the ratio between U1 and U2 is much higher than the ratio between A1 and A2, although the reason underlying this difference is still unknown. Given the U1/U2 ratio is ~10:1, we can conclude that on the phosphine-dosed surface the U1 bonding configuration is more stable than that of U2.

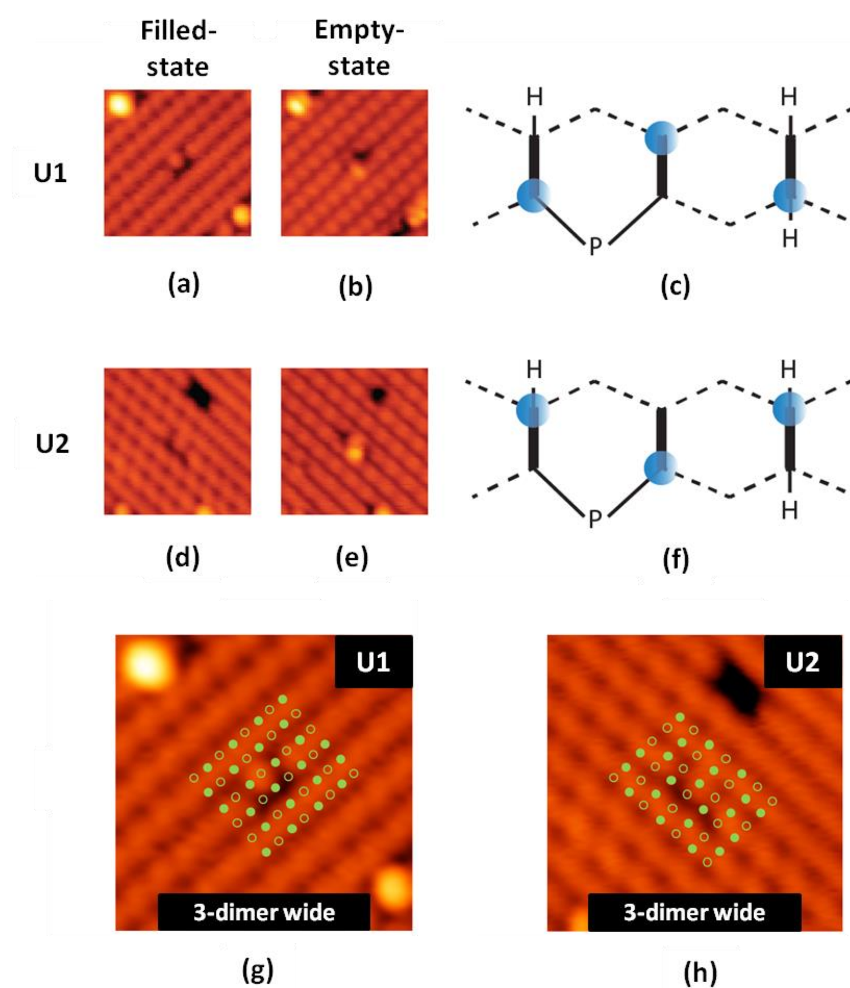

Figure 4.11 **(a)** and **(b)** show the filled- and empty-state images of the U1 features with **(c)** showing its bonding configuration. **(d)** and **(e)** show the filled- and empty-state images of the U2 features with **(f)** showing its bonding configuration for which the buckling orientation of the background Si dimer is opposed to that associated with the U1 bonding configuration. Each blue circle represents the silicon atom buckling up. **(g)** and **(h)** enlargement of (a) and (d) respectively with relevant atomic masks showing the orientation of the background silicon dimers for which the empty and filled green circle represent *down* and *up* silicon atoms respectively.

4.3.3 Group C features

We now turn our attention to the centred (C) features, each of which appears with a protrusion centred on the dimer row containing the C feature as seen in Fig 4.12. Due to their appearance being similar to the centred feature observed at room temperature (see Fig. 4.5), they can be simply thought to correspond to the PH+2H structure with different bonding configurations. Nevertheless, this assumption will be proved to be wrong and a new insight will be introduced in this section.

Before discussing the assignment of the C features, it should be noted that the assignment of the A features and the U features has been clearly made in that each of the features consist of 1 P atom and 3 H atoms in close proximity. Additionally, it should be noted that the hemihydride structure also appears on the surface after phosphine dosing; thus, this is obvious that the HH structure arises from the process of dosing the surface with PH_3. If there is a H atom on the surface, then this H atom will have been separated from any structure consisting of 1 P atom and 3 H atoms. A structure would be left with 1 P atom and 2 H atoms after losing the H atom. Based on this concept, some features in Group C would be related to the P+2H structure and the number of the C features combined would be consistent with the number of HH features.

Firstly, we consider feature C1. Illustrated in Fig. 4.12 (a), the feature is two-dimer wide. It exhibits all the same characteristics as the centred feature observed at RT [4, 57, 58]; specifically, it appears as a centred bright protrusion with an adjacent symmetric monohydride depression. We therefore assign this feature to the PH+2H structure identified in Ref. [4], with the bonding configuration shown in Fig. 4.12 (b).

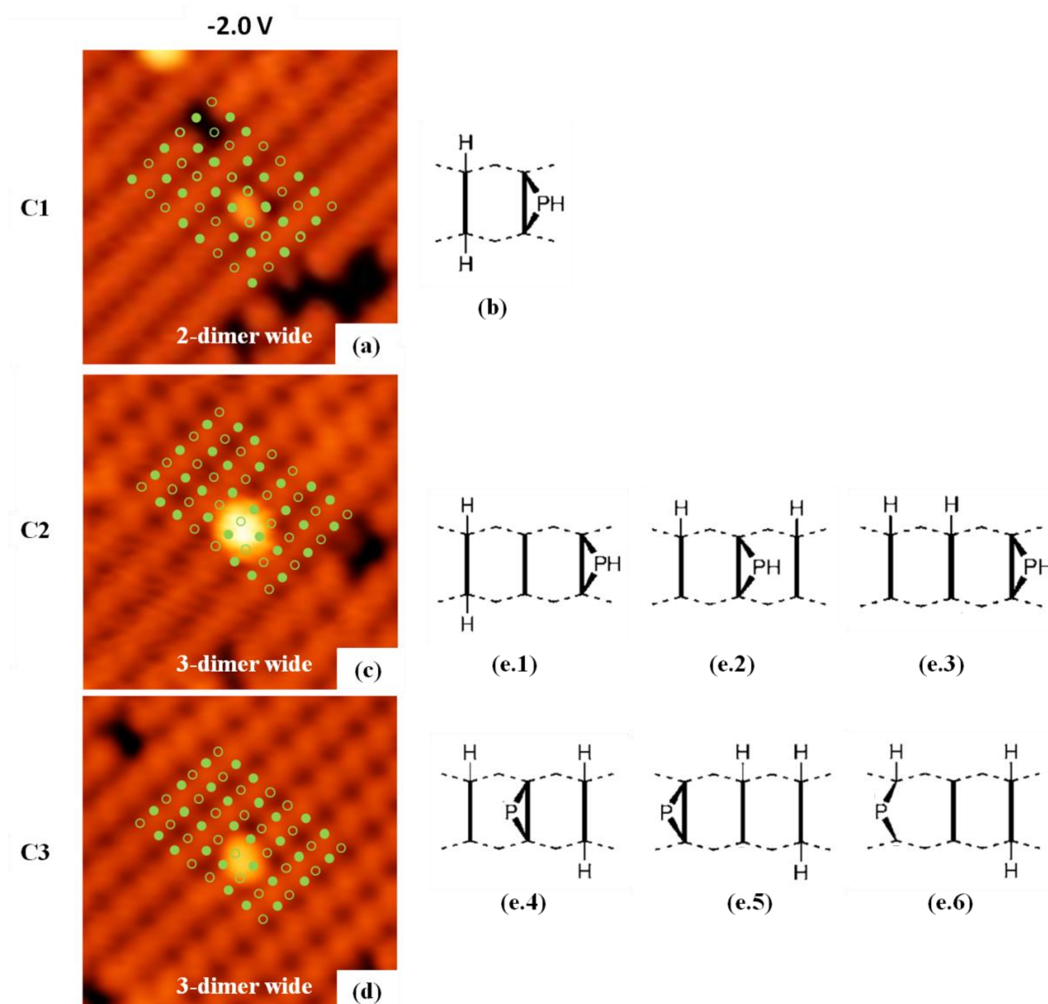

Figure 4.12 **(a)**, **(c)**, and **(d)** Filled-state images of feature C1, C2, and C3 respectively with an atomic mask on each image showing the buckling orientation of the background silicon dimers. The filled and the empty green circles represent Si atoms buckling up and down respectively. **(b)** The bonding configuration of the C1 feature. **(e.1)-(e.6)** Bonding configurations of 3-dimer width that could be assigned to the C2 and C3 features (that are 3-dimer wide).

Feature C2 and C3 are different from feature C1 in that they are three-dimer wide and they exhibit the brighter central protrusions as seen in Fig 4.12 (c) and 4.12 (d) respectively. Due to the appearance of C2 and C3, we will consider plausible bonding configuration for both features based on the energetically stable configurations proposed in Ref. [4] as listed in Fig. 4.12 (e.1) – 4.12 (e.6). According to the appearance of feature C1, the symmetric monohydride structure (one H atom bonded to each Si atom of a dimer) appears dark in both filled- and empty-state images (see Fig. 4.5 and 4.12 (a)). The bonding configurations

depicted by Fig. 4.12 (e.1), (e.4), (e.5), and (e.6) can be removed from the candidates for the C2 and C3 structural attribution. As seen in Fig. 4.8 (a), the filled-state hemihydride structure usually does not alter the appearance of the background silicon dimers except solely the intensity at low scanning bias. Moreover, by investigating the appearance of the PH fragment in Fig. 4.12 (a), the PH fragment usually appears one-dimer wide. Based on this observation, the bonding configurations shown in Fig. 4.12 (e.2) and 4.12 (e.3) cannot be assigned to feature C2 and C3 since the centred protrusion likely extends over all three dimers of the features. It is not likely that the P+3H structure can be assigned to the C2 and C3 features; as a result, we turn our attention to the P+2H structure resulting from another dissociative pathway.

Investigating the appearance of the P+2H structure depicted in Fig. 4.13 (c) and 4.13 (f) (taken from Ref. [55]), the P+2H structure appears as a protrusion of 3-dimer width for the filled-state imaging. It is still a 3-dimer feature for the empty-state image (see Fig. 4.13 (f)) but the protrusion is shrunk into 2-dimer width because the monohydride dimer appears dark. The appearance of the P+2H structure with the bonding configuration in Fig. 4.13 (i) matches the appearance of the C3 feature. Thus, it is reasonable to assign the P+2H structure to the C3 feature as shown again in Fig. 4.13 (j).

For the assignment of the C2 feature, we need to investigate the appearance of individual atoms in the P+2H structure. Firstly, we have found that the P+2H structure appears as a very bright protrusion of 3-dimer width in the filled-state image with the brightness of the P atom at the dimer-bridge position extends to the neighbouring dimers on both sides such that the dark depression of the monohydride structure cannot be seen. Secondly, for the empty-state imaging (see Fig. 4.13 (f)), the monohydride structure appears as a depression dimer but the neighbouring Si-Si dimer is still dominated by the brightness of the P atom. Since even the zig-zag appearance of the silicon dimer is overwhelmed by the brightness extension in both filled- and empty-state images, the appearance of the hemihydride structure adjacent to the P atom should also be dominated by the protrusion extension. Based on this concept, we introduce another dissociative pathway of the PH_2 fragment as illustrated in Fig. 4.14 (a), leading to another bonding configuration of the P+2H structure in which a middle P atom has the

hemihydride structure on both neighbouring dimers. As discussed, for the filled-state imaging, the brightness of the P atom extends up to 3 dimers and the zig-zag appearance of the hemihydride structure becomes invisible. In the empty-state images, the brightness of the P atom still extends and only the dark appearance of the monohydride dimer can stop the extension. Without a monohydride dimer in the structure, the resulting bonding configuration shown in Fig. 4.14 (a) should appear as a 3-dimer protrusion. Therefore, the P+2H structure with the bonding configuration depicted in Fig. 4.14 (a) will appear as a protrusion of 3-dimer width in both filled- and empty-state images. This appearance matches the contrast behaviour of the C2 feature; thus, we assign the dissociative structure in Fig. 4.14 (a) to feature C2.

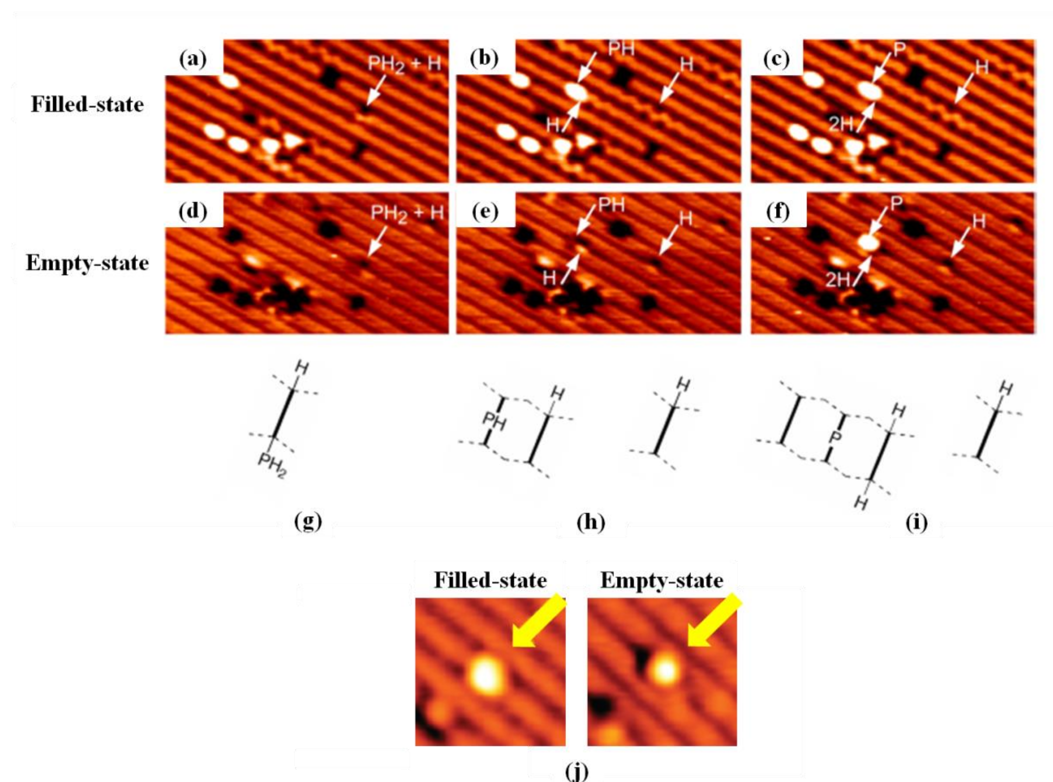

Figure 4.13 (a)-(f) STM images of the same surface area of Si(001) lightly dosed with phosphine at room temperature, revealing another species of dissociative products of phosphine on Si(001) consisting of 1 P atom and 2 H atom. **(g)-(f)** The diffusion and dissociation leading to the formation of the P+2H structure. **(j)** Another C3 feature observed in our experiment. Figure (a) – (i) are taken from Ref. [55].

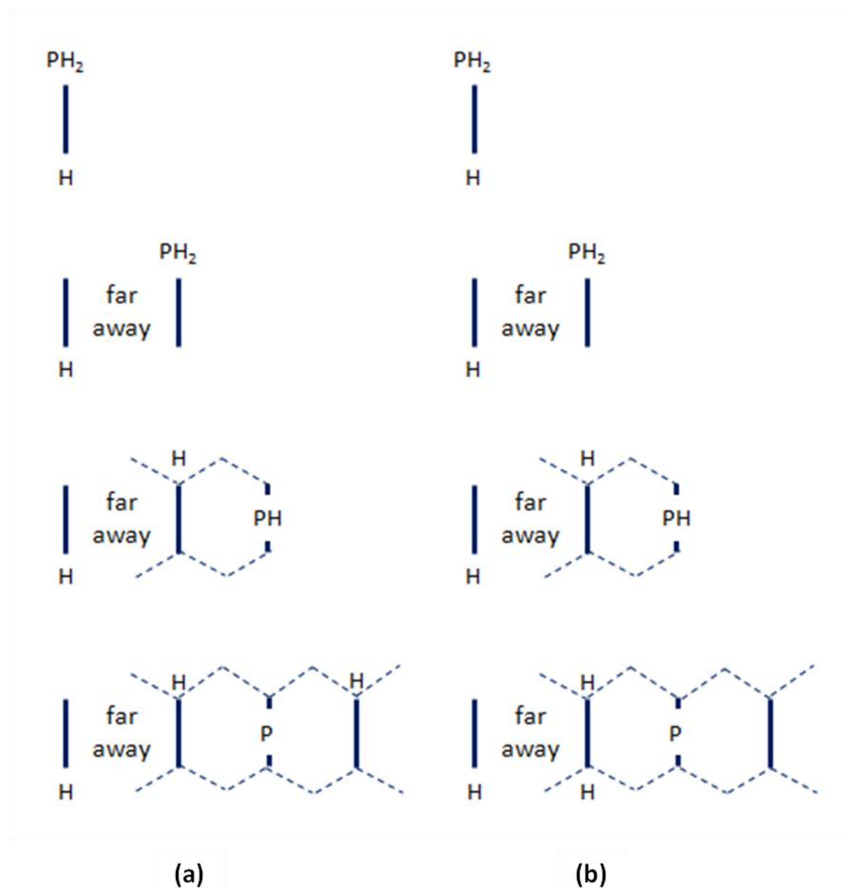

Figure 4.14 **(a)** The dissociation pathway starting from PH_2+H to P+2H and H for which the bonding configuration of the P+2H structure is associated with the appearance of the C2 feature. **(b)** The same dissociation pathway except that the bonding configuration of the P+2H structure is different by having one monohydride structure instead of two hemihydride structures, which could be assigned to the C3 feature.

4.3.4 PH_3-related hemihydride structure

Now that we have identified all the PH_3-related features observed on the Si(001) surface except for the hemihydride (HH) structure, it is appropriate at this point to further discuss the correlation between the HH structure and the remaining phosphine-related structures. The HH structure observed at room temperature (RT) and at 77 K can be seen in Fig. 2.11 and Fig. 2.16 respectively, shown again in Fig 4.15. As mentioned above, the occurrence of the HH structure arises from the diffusion of PH_2 from PH_2+H, which leaves behind a single H atom [37]. Consequently, the number of the HH structures should be equal to the dissociatively formed PH_2 structures.

Considering the relation shown in Fig. 4.15 (c), it could be stated as the following. Firstly, in line (1), a number of PH_3 adsorbed on the Si(001) surface at room temperature is N(PH_3). We assume that every PH_3 structure dissociates into PH_2+H on the surface; thus, the number of the PH_2+H structure is N(PH_2+H) which is equal to N(PH_3) as seen in line (2) of Fig. 4.15 (c). To calculate further, the total number of PH_2+H is split into two group, N1(PH_2+H) and N2(PH_2+H), with a condition that $N = N_1 + N_2$. Considering line (4), all the PH_2 fragments in the N_2 group do not diffuse from the PH_2+H structures, which results in the asymmetric feature observed on the surface as the A features discussed (A1 and A2). For the PH_2+H structures in the N1 group, every one of the PH fragments diffuses away from PH_2+H. As a result of the thermal diffusion, the number of the PH_2 fragment and the number of the H fragment are equal, $N_1(PH_2) = N_1(HH)$. Based on the dissociation of the PH_2 fragment discussed in Fig. 4.13 and Fig. 4.14, we assume that all of the PH_2 fragments dissociate into the P+2H structure as shown in line 5. Therefore, the number of the P+2H structure on the surface should be equal to the number of the HH structure, N(P+2H) = N(HH).

From our interpretation of the C2 and C3 features, both features are assigned to the P+2H structure with different bonding configurations as shown in Fig. 4.14. Hence, the number of feature C2 and feature C3 combined should be ideally equal to the number of the hemihydride (HH) features. From Fig. 4.7, the number of C2 and C3 combined is 37 while the total number of H is 53, which is not in agreement with the above-mentioned statement. However, if errors of the counting are considered and the error bars are calculated as included in Fig. 4.7, the deviation of the total counts allows us to say that the possible maximum number of C2 and C3 combined could be about 45.6 features while the possible minimum number of H could be 45.7 features. Thus, it is now more convincing to state that feature C2 and feature C3 should be assigned to the P+2H structure, and the number of both features combined is consistent with the number of the hemihydride features observed on the PH_3-dosed Si(001) surface.

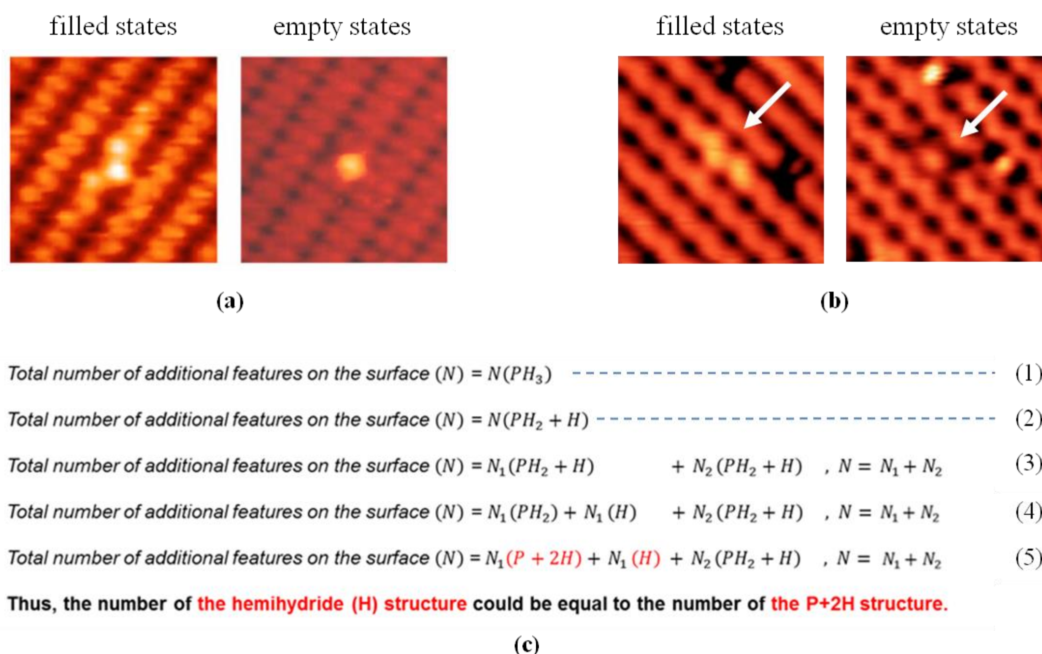

Figure 4.15 The appearance of the hemidydride feature on Si(001) at **(a)** RT **(b)** 77 K. **(c)** The relation between the number of PH_3, the number of P+3H, the number of P+2H, and the number of H on Si(001), which involves two different dissociative pathways indicating by N_1 and N_2. The images of hemihydride at RT is taken from Ref. [4].

The reason for the deviation of the counts is various. The first assumption could be the error of counting itself. While the counts are done with 20 STM images of 20 × 20 nm^2, it is possible that the occasional HH may be missed if it is in the vicinity of defect or other adsorbates, where local induced buckling of the surface dimers is strong, hence masking the zigzag appearance of the HH. It is also possible that some PH_2 could have diffused out of the frame of the 20 × 20 nm^2 images. Although the PH_2 fragment diffuses less than ~20 nm from the PH_2+H structure [37], most of the time the STM tip was laterally moved at least ~100 nm away after a surface area is scanned, potentially resulting in the missing of the diffusing PH_2 fragments associated with the HH features.

4.4 Tip-induced structural transformation

During the investigation of the phosphine-dosed Si(001) surface at 77 K, it was expected that no transformation of the phosphine-related features would be

observed due to the fact that at 77 K the thermal energy is too low to encourage any structural transformation. However, a structural transformation was unexpectedly observed on the PH_3-dosed Si(001) surface investigated at 77 K and the transition has been thought to be induced by the electrostatic influence of the STM tip. Prior to the discussion of the tip-induced transformation, it is beneficial to briefly refer to the transformation of the phosphine-related features on Si(001) occurring at RT. It has been reported in Ref. [4, 35, 37] that PH_3 dissociates into PH_2+H immediately after the adsorption on the Si(001) surface at RT, followed by the dissociation of PH_2+H to PH+H and then the dissociation of PH+H to P+3H respectively in a time scale of minutes. The dissociation is a thermally-driven forward structural transformation and is irreversible [4] as illustrated in Fig. 4.16. Since the transformation is thermally-driven, we did not expect to observe any transformation of this kind at the temperature of 77 K at which all structures are frozen. However, there is a transformation of some phosphine-related features observed on the surface as shown in Fig. 4.17.

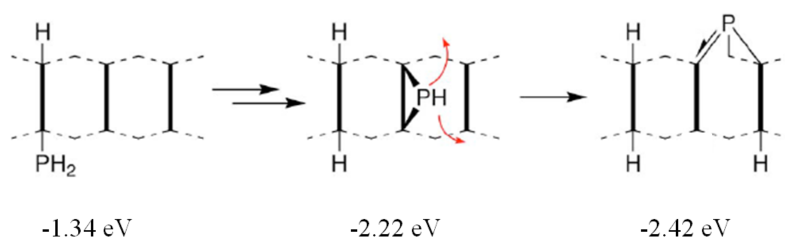

Figure 4.16 The forward transition of the dissociative products of PH_3 on Si(001) reported in [4]. The dissociation starts from the PH_2+H to P+3H which is the more energetically stable. This transformation is driven by the thermal energy and it is time dependent.

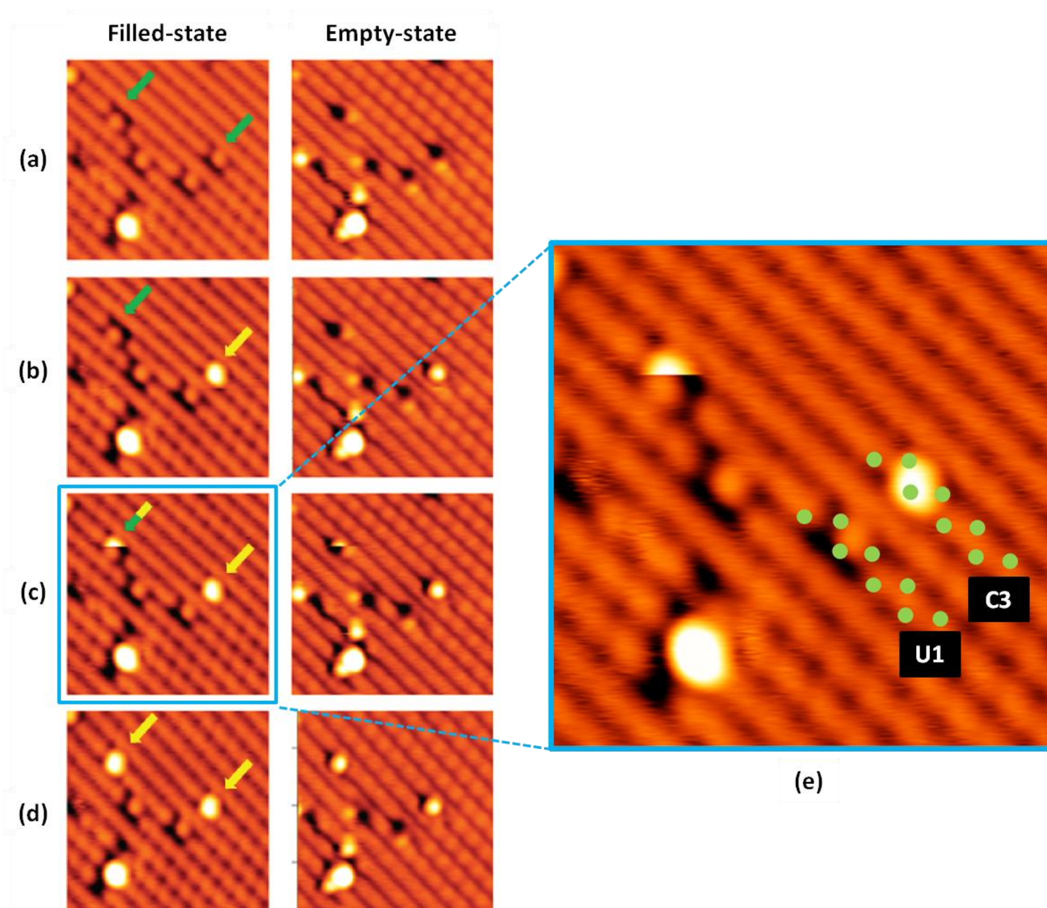

Figure 4.17 (a)-(d) time-independent sequence of imaging which shows repeatedly-observed transformation of two U1 features to two C3 features as indicated by the green arrows (starting product) and the yellow arrows (end product). **(e)** The enlargement of the filled-state image in (c) revealing the buckling orientation of background Si dimers.

In Fig. 4.17 (a), while the tip was scanning upwards, there were four phosphine-associated features simultaneously imaged with the filled states and the empty states of the sample. They are the U1 features and two of them are indicated by the green arrows. During the scanning of the tip downwards and then upwards again over the same surface region, one of the features indicated by the yellow arrow in Fig. 4.17 (b) had already changed to the C3 feature. The cause of the transformation at this point was still mysterious. In fig. 4.17 (c), after the tip scanned downwards, the tip was scanning upwards again. The transformation was observed one more time on the U1 feature indicated by the half-green half-yellow arrow. This time the structural transformation happened after the tip scanned upwards half way over the U1 feature. On the scanning way back downward, the

feature was imaged as a full C3 feature, which results in two C3 features and two U1 features in the image (see Fig. 4.17 (d)).

The transition could not be induced by thermal energy since the temperature of the sample is as low as 77 K. Thus, we have concluded that the structural transformation is associated with the electrostatic influence of the tip while the tip is scanning over feature U1. To figure out an underlying mechanism of the transition process, we have considered the transition mechanism proposed in Ref. [4] and come up with a transformation from the centred feature (PH+H) to the U-shaped feature (P+3H) as illustrated in Fig. 4.18 (a). This transformation is induced by the thermal energy at room temperature and has been reported as an irreversible process with the U0 structure being an intermediate state which has never been experimentally observed. Since the structure energy of the C1, U0, and U1 bonding configurations is -2.21 eV, -2.16 eV, and -2.42 eV respectively, the U0 structure is less stable than the C1 structure. As a result of the energy of U0 that is higher than that of C1, it is probable that the lifetime of the U0 structure is so short that it already transforms to another structure before the STM tip start scanning the surface. That is why the structure has never been experimentally observed.

For our results observed at 77 K shown in Fig. 4.17, what we have observed is the transition of feature U1 to feature C3. The transformation diagram is illustrated in Fig. 4.18 (b). Since the calculated structure energy of feature U1 (-2.42 eV [4]) is higher than the structure energy of feature C3 (-2.58 eV [55]), it might be able to say that the C3 feature should be a dissociative product of the U1 feature. However, this transition has never been reported, even at room temperature. This is because the dissociation process of the structures consisting of 1 P atom and 3 H atoms is different from the process undergone by the structures comprised of 1 P atom and 2 H atoms as illustrated in Fig. 4.13. Therefore, it can be said that the P+3H structure is the end product of a dissociation pathway of the PH_3-related structures consisting of 1 P atom and 3 H atoms or on the other hand it is the most energetically stable structure in the dissociative pathway, while the P+2H structure is the end product (the most energetically stable structure) of another dissociative pathway of the PH_3-related structures consisting of 1 P atom and 2 H atoms. Therefore the U1 to C3 structural

transformation we observe is solely caused by the presence of the electrostatic influence of the tip scanning over a surface area of interest because the 77-K thermal energy is too low to induce any structural transformation in the surface region.

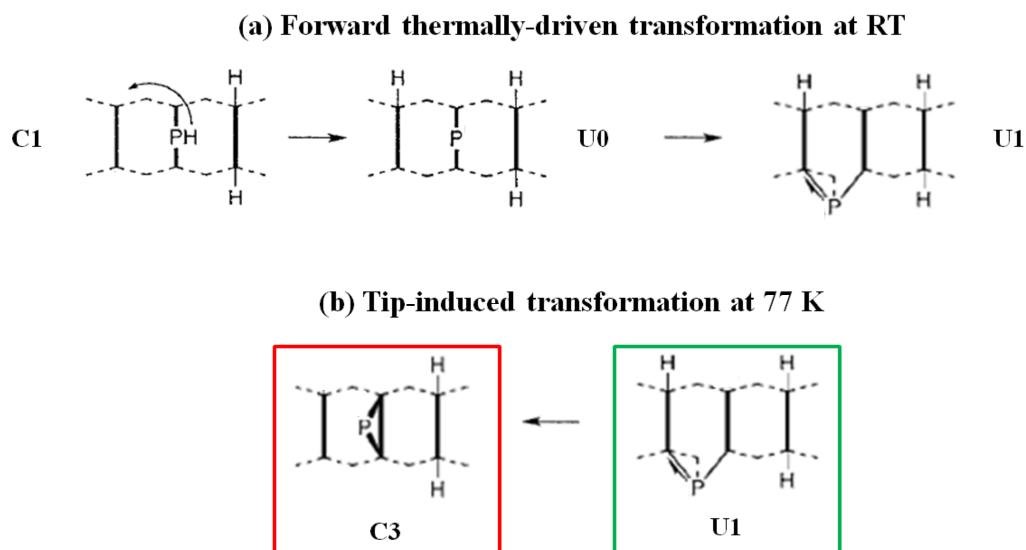

Figure 4.18 (a) The forward thermally-driven transformation of PH+2H to P+3H at room temperature. The U0 bonding configuration is the intermediate state that has never been experimentally observed. **(b)** The diagram showing the transformation we observed at 77 K, revealing the missing of one H atom and the shift of the P atom from the end-bridge site to the dimer-bridge site.

The U1 to C3 transformation is associated with the desorption of the single H atom (the hemihydride) from the U1 structure, subsequently followed by the P shift from the dimer-end bridge site to the dimer bridge position as illustrated in Fig. 4.18 (b). The desorption of the H atom has been previously reported and is even controllably exploited to precisely remove individual H atoms from a H-terminated Si(001) surface used as a resist mask – so called hydrogen lithography [15, 33, 34]. Hydrogen lithography is performed by placing the tip over a specific surface area and controlling the voltage and the current setpoint within a particular short period to be able to precisely desorb particular H atoms from the surface. The diffusion of the P atom from the end-bridge position to the dimer-bridge site

has been theoretically predicted [59] as illustrated in Fig. 4.19 but it has never been experimentally reported yet. Therefore, the transformation mechanism shown in Fig. 4.18 (b) is the first time that such a P-atom shift is experimentally observed.

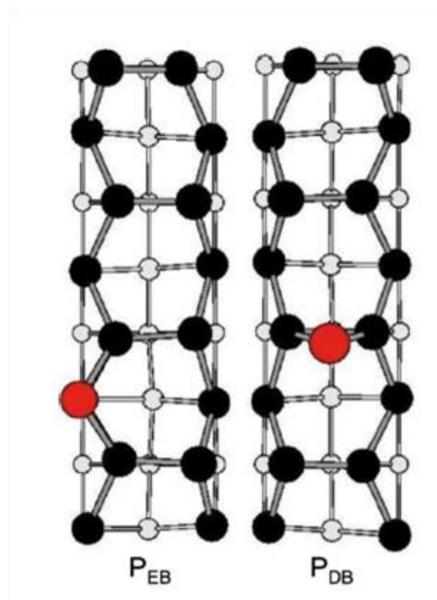

Figure 4.19 A phosphorous atom (the red circle) bonded to a Si dimer rows at the end-bridge site (P_{EB}) has been theoretically reported that it can diffuse to the dimer-bridge site (P_{DB}) which is another energetic minimum beside the end-bridge site.

According to the discussion above, the structural transformation of the U1 feature to the C3 feature is solely caused by the electrically-biased STM tip. It is a forward transition from a less energetically stable structure (U1, -2.42 eV) to a more stable structure (C3, -2.58 eV) although it is the transition across two different dissociative pathways; thus, the transformation would be irreversible.

However, there is another possible interpretation for the U1-C3 transformation. If the C3 feature is attributed to the U0 bonding configuration (see Fig. 4.18 (a)) consisting of 1 P atom and 3 H atoms with the third H atom bonded to a dimer end of the other neighbouring dimer of the P-bonded dimer, it can be straightforwardly said that the transformation is a reverse process of the thermally-driven forward dissociation illustrated in Fig. 4.18 (a). This is in contrast to the insight reported in Ref. [4] that the forward dissociation is

irreversible. Despite the fact that the number of the P+2H features combined must be consistent with the number of the hemihydride (H) feature, the appearance of the C3 feature also allows us to assign it to the P+3H structure with the U0 bonding configuration. The U0 bonding configuration is 3-dimer wide with the P atom on the dimer-bridge site of the middle dimer. The unpaired electron of the P atom provides the significant bright protrusion that extends to cover both neighbouring dimers (hemihydride and monohydride dimers) in filled-state images. In empty-state images, the monohydride dimer appears as a depression whereas the hemihydride dimer is still overwhelmed by the P-atom brightness, resulting in the feature looking 3 dimer-wide with 1-dimer depression and 2-dimer protrusion. Based on this speculation, the C3 feature can also be assigned to the P+3H structure with the U0 bonding configuration. If this is the case, then it can be stated that the transformation observed as depicted in Fig. 4.17 is a tip-induced backward structural transformation of the thermally-driven forward structural transformation illustrated in Fig. 4.18 (a).

Once the U1 feature is transformed back to the U0 bonding configuration that is less energetically stable, U0 cannot be forwardly changed to U1 again since the thermal energy is not enough to drive the forward transformation. Additionally, although the U0 configuration is a transient intermediate state with a short life time, it may be frozen from further transformation as the sample temperature is reduced immediately to ~77 K. This is the reason why we can observe the U0 bonding configuration as the C3 feature at 77 K while it has never been experimentally observed at RT. If the second interpretation of the tip-induced transformation is correct, then the observed U1-C3 transformation not only imply the possibility of using the tip to manipulate the dissociation of PH_2 on Si(001), but the transition also strengthens the forward thermally-driven transformation proposed in Ref. [4] with the U0 configuration as the intermediate state.

4.5 Si-P heterodimer at 77 K

Toward the fabrication of the atomic electronic device, the P atoms have to be incorporated into the Si(001) surface by means of thermal annealing and subsequently buried with layers of silicon, grown molecular beam epitaxy (MBE) in the vacuum chamber. We studied the Si-P heterodimer at low temperature as we thought that the low-temperature imaging may reveal different information than imaging at RT.

While heating up the silicon sample to about 400 ℃, each of the P atoms on Si(001) is incorporated into the surface layer by replacing one of the Si atoms in a Si-Si dimer. This produces Si-P heterodimers appearing randomly throughout the surface as shown in Fig. 4.20 (a). At 77 K, the Si-P heterodimer appears as a zigzag protrusion feature with its buckling direction consistent with the buckling orientation of the background Si(001) surface and its brightness extends ～2 dimers away from the Si-P dimer, agreeing with the observation at room temperature [38]. Note that the observation at RT cannot inform whether the buckling direction of the Si-P heterodimer is the same as or opposite to the buckling orientation of the silicon background dimers since the thermal energy at RT encourages the switch between the up and down silicon atoms to be so fast that the sensitivity of the STM tip cannot distinguish the up Si atoms from the down Si atoms. However, at RT it has been reported that the neighbouring silicon dimers are pinned to a buckling orientation associated with the buckling direction of the Si-P heterodimer.

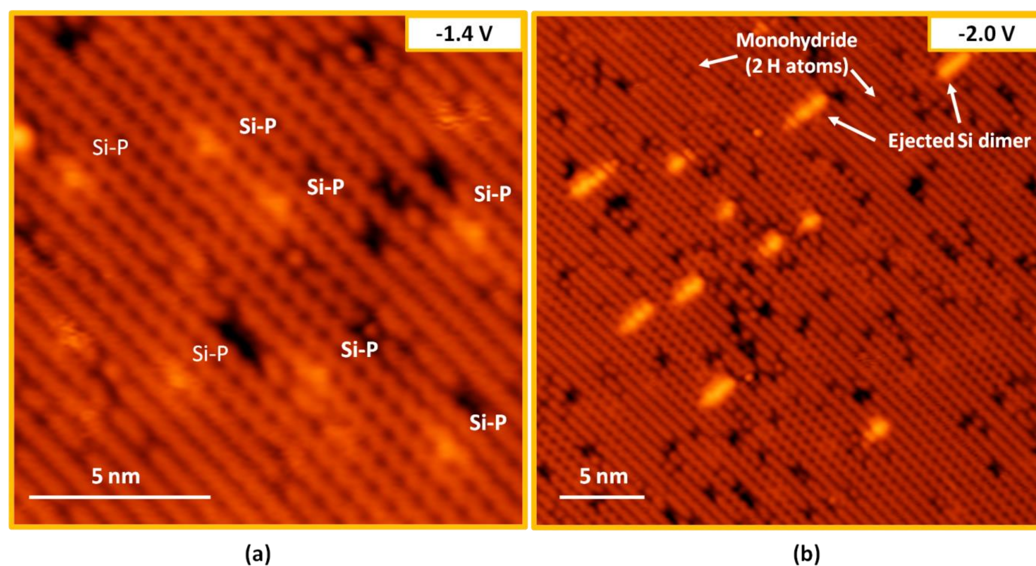

Figure 4.20 (a) A surface area of PH_3-dosed Si(001) after the thermal P incorporation scanned with low negative bias magnitude showing a number of Si-P heterodimers randomly appearing in the image. **(b)** Another surface area scanned at higher negative bias magnitude revealing other two common features (monohydride structures and ejected Si dimer rows).

4.5.1 Ejected Si dimer rows and redundant H atoms

Beside the Si-P heterodimers existing throughout the surface, there are also dimers of Si atoms ejected by the substitution of the P atoms into the surface, and H atoms in the form of monohydrides on the Si(001) surface as shown in Fig. 4.20 (b). The incorporation of the P atoms into the Si(001) layer results in the ejection of Si atoms from the surface. These ejected Si atoms diffuse on the surface before subsequently bonding together in the form of dimers. Fig. 4.21 shows close-up images of the ejected Si dimers on the surface observed at 77 K. Compared with the observation at RT [38], the appearance of the ejected Si dimer is the same except that the dimer expresses the zig-zag characteristic like the background dimers do.

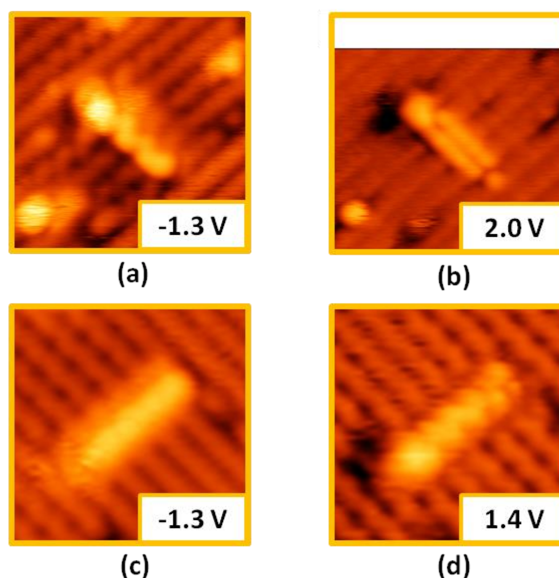

Figure 4.21 **(a)** and **(b)** filled- and empty-state images of a surface area showing a dimer row of Si atoms ejected from the Si(001) surface due to the incorporation of the P atoms into the surface layer. **(c)** and **(d)** STM images of another ejected Si dimers revealing the zig-zag characteristic of the dimer row at low positive bias.

For high empty-state bias (see Fig. 4.21 (b)), the ejected Si dimer row appears as double lines. Normally at the high positive bias, part of the Si(001) surface that appears bright is the trenches between the dimer rows. This could be used to explain why the ejected Si dimer row appears as double lines for which the dark line between the double lines could be the Si dimer. This is confirmed when the bias is reduced to a low empty-state bias as shown in Fig. 4.21 (d). In this figure, the double line of the Si dimer row changes to a single line with the zig-zag characteristic, further convincing that this feature is a Si dimer row. For filled-state bias, the ejected Si dimer row appears as a single line with the zig-zag characteristic both at high and low negative biases (see Fig. 4.21 (a) and 4.21 (c)). The appearance of the ejected Si dimer row is corresponding to the appearance of the background Si dimer rows, confirming that the feature is induced by a Si dimer row resulted from the ejection of Si atom from the Si(001) surface.

4.5.2 The ground state of Si-P heterodimer

Now, we turn our attention back to the behaviour of a Si-P heterodimer observed at 77 K by comparing with the previously reported results observed at RT [5, 38, 40, 41]. Fig. 4.22 (a) illustrates the voltage-dependent contrast behaviour of a Si-P heterodimer obtained at 77 K while Fig. 4.22 (b) depicts the voltage-dependent images of another Si-P heterodimer observed at RT [5].

Firstly, we will consider the contrast behaviour of the S-P heterodimer observed at RT shown in Fig. 4.22 (b). For the appearance of the Si-P heterodimer observed at RT, the brightness of the dimer end disappears when the bias magnitude decreases from $|-1.8\text{ V}|$ to $|-1.5\text{ V}|$. Following the interpretation in Ref. [5], at high negative bias, the tip Fermi level lies far below the sample Fermi level, resulting in the Si atom of the Si-P heterodimer possessing two electrons in its dangling bond, thereby becoming negatively-charged and buckling up as seen in Fig. 4.22 (c.1) for high negative bias. When the negative bias magnitude decreases, the Si atom loses one electron from its dangling bond and thus becomes electrically neutral, leading to the non-buckling configuration of the Si-P heterodimer as depicted in Fig. 4.22 (c.2) for the medium negative bias and associated with the appearance of the Si-P dimer at – 1.5 V in Fig. 4.22 (b). The Si atom loses the remaining electron from its dangling bond at the lower bias of – 0.9 V for which the tip Fermi level is shifted upward closer to the sample Fermi level, resulting in a positively-charged Si atom buckling down and thus appearing as a depression shown in Fig. 4.22 (b). The Si-P configuration without any electron in the dangling bond of the Si atom is interpreted as the ground state of the Si-P heterodimer (Fig. 4.22 (c.3)). When the surface is scanned with positive sample bias for which the tip Fermi level lies above the sample Fermi level, the Si-P heterodimer is always in its ground-state configuration. The Si atom buckles down, thereby appearing as protrusion in both low and high positive bias.

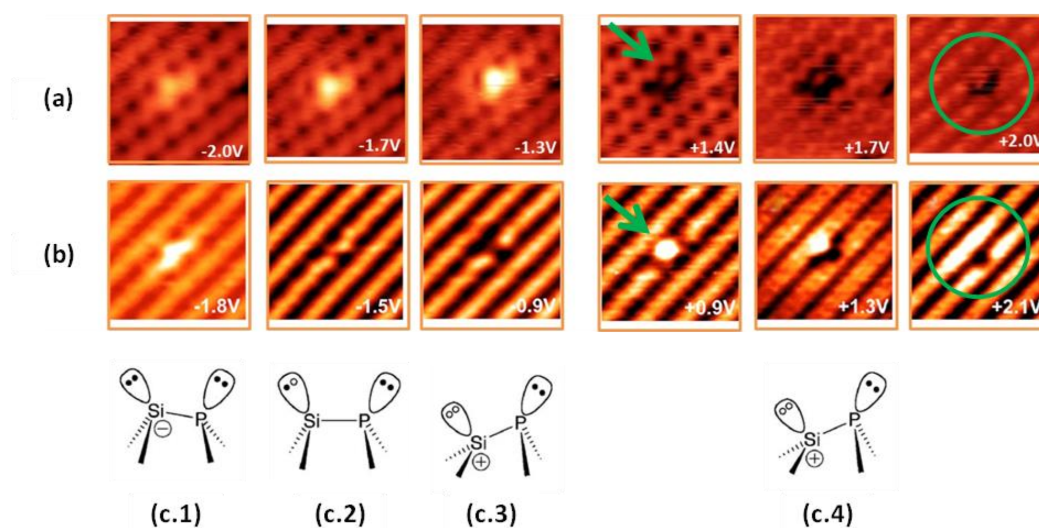

Figure 4.22 **(a)** An Si-P heterodimer observed at 77 K in our experiment showing several characteristic different from **(b)** a Si-P heterodimer observed at room temperature reported in Ref. [5] **(c)** The buckling orientation of the Si-P heterodimer with respect to various bias magnitude associated with the charge state of the Si atom proposed in Ref. [5, 41]. The green arrow points at the Si atom of the heterodimer while the green circle surrounds the area of the protrusion superimposed on the background surface reconstruction.

However, we can see that the contrast behaviour of the Si-P heterodimer at LT is not the same as the behaviour at RT. For the filled-stated images in Fig. 4.22 (a), one end of the Si-P heterodimer is brighter than the other end and also brighter than the surrounding Si up atoms for both low and high negative bias. The brightness decreases with increasing the bias magnitude and gradually disappears when the voltage magnitude is higher than $|-2.0\ \mathrm{V}|$ which is not shown in Fig. 4.22. The contrast behaviour indicates that the Si atom of the Si-P dimer buckles up with two electrons in its dangling bond. For the empty-state images, the Si atom still appears bright whereas the P atom appears dark. The brightness of this Si heterodimer atom is also approximately not different from the surrounding down Si atoms. This implies that the Si atom of the Si-P dimer buckles down as much as the Si atoms of the Si-Si dimers, each of which has two empty states (no electron) in its dangling bond.

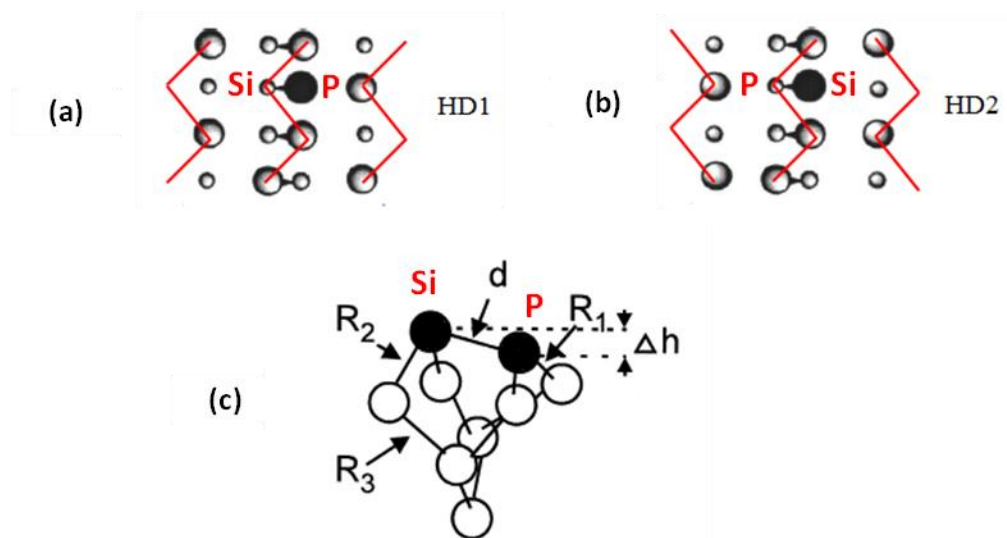

Figure 4.23 (a) Bonding configuration HD1 and **(b)** HD2 calculated and proposed in Ref. [5] as the most stable configurations of the Si-P heterodimer. For HD1 the P atom buckles up whereas for HD2 the P atom buckles down. **(c)** The Si-P structure calculated in Ref. [60] stating that the lowest dimer atom is the P atom. R1 and R2 are the bond lengths between dimerised atoms and the underlying Si layers. R3 is the bond length between Si atoms of the first and the second bulk layers.

Calculations from Ref. [5] suggest that there are two stable configurations of a Si-P heterodimer in the Si(001) surface, named HD1 (Fig. 4.23 (a)) and HD2 (Fig. 4.23 (b)), that could be the ground state of the Si-P heterodimer with the position of the P atom indicated by the red P letter. The HD2 configuration has lower energy than the HD1 reconstruction by ~ 0.14 eV; thus, the HD2 structure is in principle more stable than the HD1 structure. Despite the energetic consideration, it is stated in the publication that the HD1 configuration is observed because it matches the experimental images at RT. The authors note that it is curious that HD1 is observed instead of HD2 given that that latter is more energetic favourable.

Considering the appearance of the Si-P heterodimer in the filled-state images, the Si atom always buckles upwards. As stated in Ref. [5], the HD1 configuration is observed for the Si-P heterodimer. At low negative bias, the HD1 configuration possesses the P atom buckling up since the Si atom has no electrons in its dangling bond. However, the P atom does not appear bright in the image. When the negative bias magnitude is higher, the dangling bonds of the Si atom

can possess up to two electrons, which makes the Si atom buckle upwards compared to the P atom. Unlike the P atom, the buckling-up Si atom appears brighter in the image as seen in Fig. 4.22 (b). By making comparison with the appearance of the Si-P heterodimer at 77 K (see Fig. 4.22 (a)), it can be stated that the Si atom always buckles up. Thus, we would make a statement here that at 77 K it is the HD2 configuration that is observed instead of HD1 claimed to be observed at RT. At 77 K where the surface structures are at their ground states, it is reasonable to observe the Si-P heterodimer with the lower-energy configuration (HD2) rather than higher-energy one (HD1).

With regard to the energy-band diagram proposed for the tunnelling mechanism of S-P dimers [41], we can interpret the appearance of the S-P heterodimer observed at 77 K as the following.

For filled-state imaging, at low negative bias, the additional tunnelling contribution of the dangling-bond energy levels make the Si-P heterodimer so much brighter than the surrounding Si-Si dimers. Note that there are two electrons in the Si heterodimer atom. Moreover, the Si heterodimer is negatively charged, so the halo protrusion is observed around the Si-P heterodimer due to the negative-charged Coulomb potential reducing the downward TIBB, widening the tunnelling window of the valence band. At high negative bias, the additional tunnelling contribution of the dangling-bond energy levels and the Coulomb potential still exist. However, the valence-band tunnelling is larger such that the difference between the tunnelling current of the clean surface region and the Si-P region becomes small. As a result, the halo protrusion disappears and gradually the Si-P heterodimer becomes less bright before eventually becoming indifferent from surrounding Si-Si- dimers as previously shown in Fig. 4.20 (b).

In empty-state imaging, when the dangling-bond energy levels are pulled up by the upward TIBB until they become resonant with the edge of the conduction band, the dangling-bond electrons might be excited from the Si heterodimer atom. Both of the Si dangling-bond energy levels are empty, so they can contribute to the tunnelling current, allowing the Si atom to be bright in the empty-state images.

At 77K, it seems that the ground state is the configuration in which the Si heterodimer atom buckles upward with 2 electrons in its dangling bond which is opposed to the proposal in Ref. [5]. However, our interpretation indicates that the HD2 configuration which is energetically more stable than HD1 is experimentally observed at the temperature of 77 K. Our interpretation is also supported by a theoretical calculation done in Ref. [60] in which they found that for a Si-P heterodimer appear in the Si(001) surface, the lowest dimer atom is the P atom as shown in Fig. 4.23 (c). This makes it even more convincing that the ground state of the Si-P heterodimer is the state in which with the dangling bonds of Si dimer atom and the dangling bond of P dimer atom are fully occupied by electrons, resulting in the Si atom buckling up while the P atom buckles down.

Chapter 5

Subsurface As donors below Si(001):H at 77 K

5.1 Introduction

The basic unit of the quantum computing scheme proposed by Stoneham *et al.*[2], illustrated in Fig. 1.2, consists of a P atom as the control switch and 2 Bi atoms as qubits. Although the fabrication method for incorporating P atoms in a silicon crystal with the atomic-scale precision has been established [15, 34], the P atoms still cannot meet one of the important criteria for building the QIP device. While the donor atoms used as the control switch and the qubits need to be at their neutral (non-ionised) state at the temperature of operation, the P atom has never been reported as being electrically neutral even at the liquid-nitrogen temperature of 77 K as recently reported in Ref. [61]. Thus, a new type of donor atom has to be considered. The As donor is of interest due to its larger binding energy and consequently larger ionisation energy than the P atom (54 meV compared with 44 meV of P); suggesting an As donor will remain in a neutral state up to a higher temperature.

Like for the studies of the P atoms buried below the Si(001) surface [53, 54, 61, 62], we use bulk-doped silicon samples that allows us to study As atoms beneath Si(001) without having to deposit As-containing molecules on the surface and subsequent incorporate the As atoms into the surface before burying them with layers of silicon atoms. Our objective is to investigate the subsurface As donors randomly located in silicon below the Si(001) surface at 77 K to understand the atomic scale characteristics of the dopant. Thus, we simply use a Si(001) wafer degenerately-doped with As and use a special preparation method to enable the subsurface As atoms to be visible by STM imaging, which will discussed later in this Chapter.

So far, there are very few experimental works reported on the study of subsurface dopant-induced features observed on Si(001):H surfaces [17, 52], in

which an (*n*-type) arsenic subsurface dopant appears as delocalised circular protrusions both in the occupied-stated and unoccupied-stated images while a (*p*-type) boron atom induces a localised protrusion and depression in filled-stated and empty-stated images respectively at room temperature.

In this chapter, we will present experimental observation of the features induced by individual As donor atoms below the Si(001):H surfaces using ultra-high-vacuum scanning tunnelling microscopy (UHV-STM) at 77K. It will be shown that at the temperature of 77 K, the appearance of the features induced by subsurface As dopants is significantly different from the results at room temperature [17] in that they appear as anisotropic protrusions with different shapes, leading to an interpretation that the charge state of the dopants can be intentionally controlled by the tip bias. Moreover, it will also be shown that some of the As donors known to donate one electron to the silicon crystal surprisingly act as acceptors in that each of them accept one more electron and become negatively-charged. In addition to the imaging, the scanning tunnelling spectroscopy (STS) data of the dopant-induced feature is also explored, revealing the electronic states in the surface band gap over those feature areas. This is the first time that anisotropic protrusions for dopant atoms in silicon has been revealed and attributed to the imaging of the donor wavefunction projecting on the surface. The details of how we come across the bistable charge-state behaviour of the subsurface As atoms which results in the discovery of the As donor as a functional candidate for the QIP structure will be discussed in this chapter.

5.2 Low-temperature flash for sample preparation

The first thing that was done for obtaining the Si(001) surface suitable for the study of subsurface As donors is to find minimum flash-anneal temperature that provides a flat and clean Si(001) surface. The reason we need to flash the Si(001) sample at the lowest possible temperature is that it has been recently reported that for a bulk As-doped Si(001) sample when it is flashed with 1250 ℃ for 10 s, the density of the As donors in the subsurface region is nearly depleted

[23]. This could be attributed to the evaporation of the Si atoms in the region that allows the As dopants to also evaporate from the subsurface region.

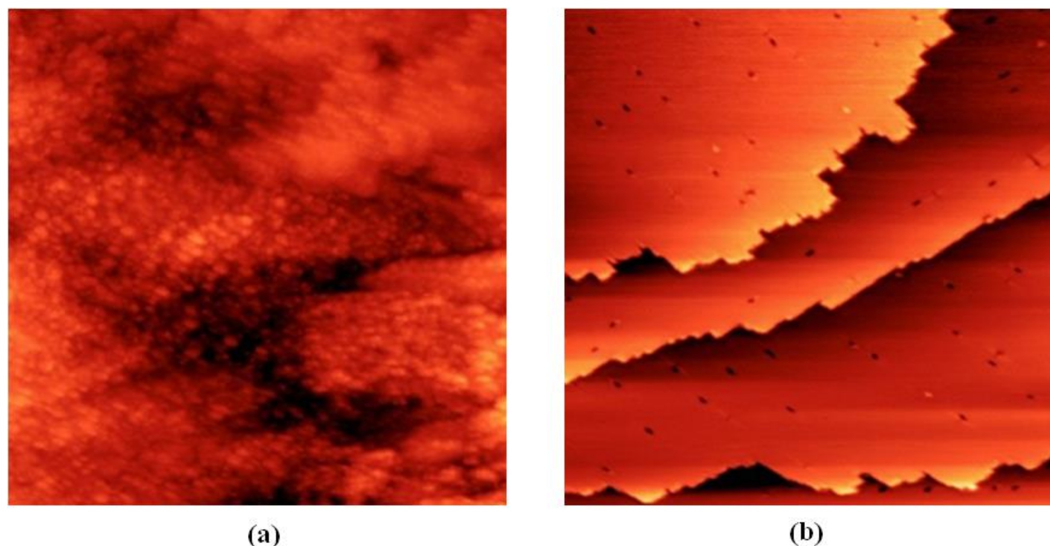

Figure 5.1 The evolution the Si(001) surface thermally flashed with the current of **(a)** 6.5 A and **(b)** 7.0 A respectively. The sample is flashed for 10 s in each case. Each image is 80 nm × 80 nm in size and was taken at -2.0 V.

We determine the lowest temperature by start flashing the silicon sample at very low current of 4.5 A, which is much lower than the current usually used for acquiring the Si(001) surface desirable for the STM measurement. At this current, the resulting Si(001) surface does not become near the flat and clean condition at all. However, it is the starting point from which after investigating the flashed sample with STM, we flash the sample again with 0.5 A more current, and continue to increase the current in 0.5 A steps until we produce a suitable surface. It appears that the lowest flashing current providing the flat and clean Si(001) surface is 7.0 A, which is associated with the sample temperature of ~1050 °C,which is lower than 1250 °C we normally utilised for this sample to obtain the flat and clean condition. Fig. 5.1 shows evolution of the Si(001) surface via the filled-stated imaging after the surface was thermally flashed with 6.5 A (see Fig. 5.1 (a)) and 7.0 A (see Fig. 5.1 (b)), respectively.

The flat and clean Si(001) surface obtained with the lowest effective flashing temperature was subsequently terminated by H atoms using the H-termination process for which the sample temperature during H-termination is only ~350 ℃. At this temperature, the dopant density in the subsurface region would not be substantially altered. Nevertheless, we have kept in mind that when the atomic structure of the QIP device is fabricated with the placement of the dopants at the atomic-scale precision, the H-termination temperature could be able to make the dopants diffuse from their desirable positions [36, 39]. Although this issue is an important problem for the device fabrication, we do not consider the factor for now since all we need to understand at this point is how individual subsurface As donors in silicon behave as we investigate them with STM via the Si(001) surface at 77 K. We do not need the subsurface dopants to be located in particular sites or as any pattern.

However, it might take at least a few cycles of H-termination before the right condition for acquiring a desirable surface are achieved for a specific silicon sample. To perform the H-termination again, it is compulsory to flash the surface in order to remove all the H atoms. It is not preferable to have the sample undergoing the thermal flash several times even with the temperature of ~1100 ℃ (equivalent to 7.0 A) since it has also been reported that flashing an As-doped Si(001) several times can lead to the depletion of the As dopants from the subsurface region [23]. Therefore, after obtaining the flat and clean Si(001) surface with the lowest flashing current of 7.0 A, we can flash the sample with lower current such as 5.0 A which still gives the flat and clean Si(001). The lower flashing temperature allows us to flash the sample more times without depleting the dopants before the desirable H-terminated Si(001) is obtained.

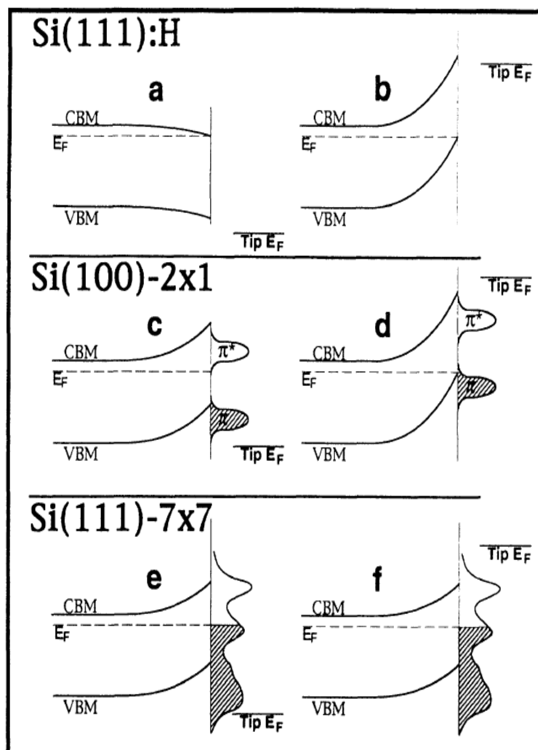

Figure 5.2 Schematic illustration taken from Ref. [63] describing tip-induced band bending of *n*-type H-terminated Si(111) (**(a)**,**(b)**), Si(001)-(2x1) (**(c)**,**(d)**), and Si(111)-7×7 (**(e)**,**(f)**), for $V_{sample} < 0$ ((a),(c),(e)) and $V_{sample} > 0$ ((b),(d), (f)). For the consideration in this thesis, only diagram (c) and (d) associated with Si(001) are taken into account.

We need to passivate the Si(001) surface in order to remove the surface π-bond states (see Fig. 5.2 (c) and 5.2 (d)). Although these states do not prevent the energy bands from being further bent due to the Coulomb potential created by the subsurface charged dopants and thus surface features induced by subsurface charged dopants can be observed, *the electron tunnelling from the dopant energy level itself cannot be observed.* By discarding the surface π-bond states, the electrons that directly tunnel out of and into the dopant energy level can be observed by STM. As a result, the surface features having characteristics associated with the wavefunction of the dopant electronic states could be visible and thus whether there any electrically neutral donors in the subsurface region could also be clarified.

5.3 Subsurface As-dopant induced features

Fig. 5.3 (a) shows a filled-state image of the Si(001):H surface of an As-doped silicon sample taken at 77 K. The background reconstruction consists of rows of paired silicon atoms called dimers, with each Si atom terminated by a single hydrogen atom. The very bright protrusions seen in the filled-state image are dangling bonds (DB) [33, 64, 65] that result whenever one of the surface Si atoms is missing its terminating H atom. In Fig. 5.3, two classes of the features induced by subsurface As dopants superimposed on the Si(001):H background surface are observed, namely As1 (see Fig. 5.3 (a)) and As2 (see Fig. 5.3 (b) and 5.3 (c)). The features on the surface other than the above-mentioned DB and As features are attributed to contaminants from the gas phase that slowly adsorb on the surface with time. We note that the dark 'shadow' below the atomic step at the top-left of the image is an artefact of the image processing and does not arise from any unexpected surface properties.

The features labelled as As1 in Fig. 5.3 (a) have not been identified before. These features have the lateral extent of a few nanometres and appear as protrusions superimposed on the background Si(001):H lattice, having a cross-like shape (i.e. "X" shaped). As Figure 5.3 (a) shows, the features labeled as As1 all have similar characteristics to one another except for the fact that some are brighter (higher intensity) than the others. This intensity difference implies that the features are associated with As donors that reside in different subsurface layers in that the features with higher intensity are believed to be induced by donors located closer to the surface [66]. We will show later that in filled-state images the As1 features can appears in different shapes other than that shown in Fig 5.2 (a). It is also essential to state here that all of the As1 features in empty-state images exhibit long-range circular protrusions. We will discuss the As1 features in full details in the next section.

Beside the Feature As1, we also commonly observe the second class of features that we label As2. Filled- and empty-state images of this feature are shown in Figure 5.3 (b) and 5.3 (c) respectively. In the filled-state image, the As2 feature appears as a circular protrusion with a diameter of a few nanometres while in the empty-state image the As2 features are seen as an isotropic depression with

the similar size to the filled-state protrusion. The observation of the As2 features forming circular protrusions in filled-state images and depressions in empty-state images makes them qualitatively different to all other dopant-related features that we have observed. The contrast behavior of the commonly-observed As2 features suggests that they are associated with negatively-charged ionised acceptors in silicon [17, 52]. However, our silicon sample is heavily doped with the As donor! The controversy will be discussed in more details after the review of As1 in the next section.

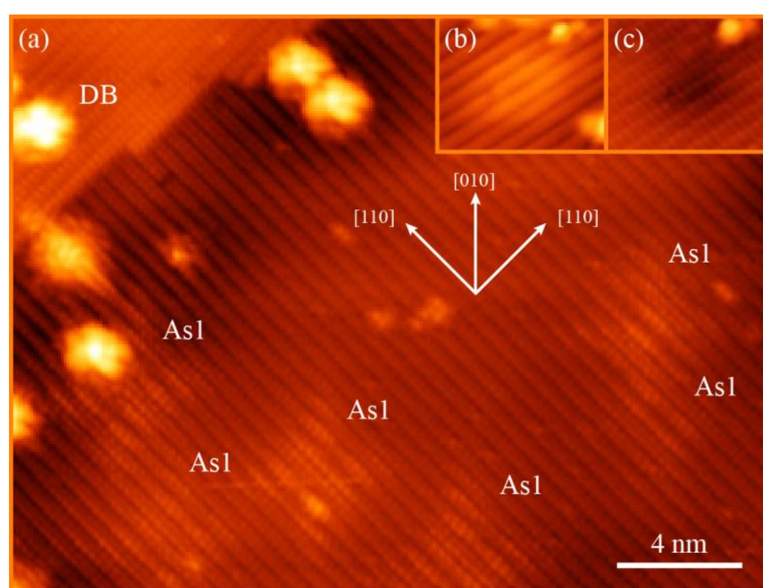

Figure 5.3 (a) A filled-state image of the Si(001):H surface observed by STM at 77 K revealing a number of the As1 features appearing as cross-like protrusions superimposed on the background surface corrugation. The image is obtained at sample bias of -1.3 V and tunnelling current of 20 pA. The size of the image is 45 nm (width) x 35 nm (height). **(b)** and **(c)** show filled- and empty-state images of an As2 feature respectively obtained at sample bias of -1.3 V and 0.8 V with tunnelling current of 20 pA.

From our experiment, we have selected 285 STM images of 50 nm × 50 nm in size taken from the Si(001):H surface to examine the appearance of the As features and by counting from these images we identified a total of 198 As1 and As2 features. Assuming that we are able to image all dopants up to 1 nm below the surface which is equivalent to 5 layers below the surface, this corresponds to

an estimated doping density of ~3×10^{17} cm^{-3} (see appendix A for details of the calculation). This is slightly lower than the bulk doping density of the wafer of 1×10^{18} cm^{-3}. However, this is not unexpected given that the surface region of silicon is known to undergo some depletion of n-type dopants during thermal treatment [23] and it is generally difficult to identify all dopants via buried dopant imaging (e.g., dopants lying directly beneath surface defects may be obscured and are therefore not counted in our statistics). Considering the surface density of dopants compared to the bulk value, we believe that the As1 and As2 features are induced by the subsurface As donors.

5.4 Feature As1

Figure 5.4 represents a more comprehensive characterization of the As1 features, showing STM images at several different negative (Fig. 5.4 (a)) and positive (Fig. 5.4 (b)) sample biases, probing filled and empty states of the sample respectively. All images were obtained with a tunnelling current of 20 pA and are displayed with the same intensity (height) scale. While all of the As1 features appear as protrusions that have a lateral extent of a few nanometres and are superimposed on the Si(001):H background lattice, their characteristic shapes in filled- and empty-state images are different. In filled state images, these features appear as a number of different shapes as seen in Fig. 5.4 (a), but with certain similarities: Every one of the As1 features exhibits maximum intensities along crystallographic directions, producing an appearance that is rectangular, cross-like, or a combination of the two. In addition, there are often structures within the features with certain surface atoms appearing brighter than their neighbours. A good example of this is feature As1.5 (see Fig. 5.5 for the enlargement) where the brightest atoms are aligned along the two dimer rows indicated by number 1 and 2. Both dimer rows are separated by the middle dimer row of the feature indicated by number 3. The adjacent bright atoms in the same row are separated by a single dimer as can be seen by considering the red and yellow arrows alternately placed to guide the eyes for each dimer in a dimer row. The intensity of the As1 protrusions is strongly dependent on magnitude of the negative sample bias with the intensity decreasing as the sample bias magnitude becomes larger. The

features gradually become almost indistinguishable from the background surface at -1.5 V.

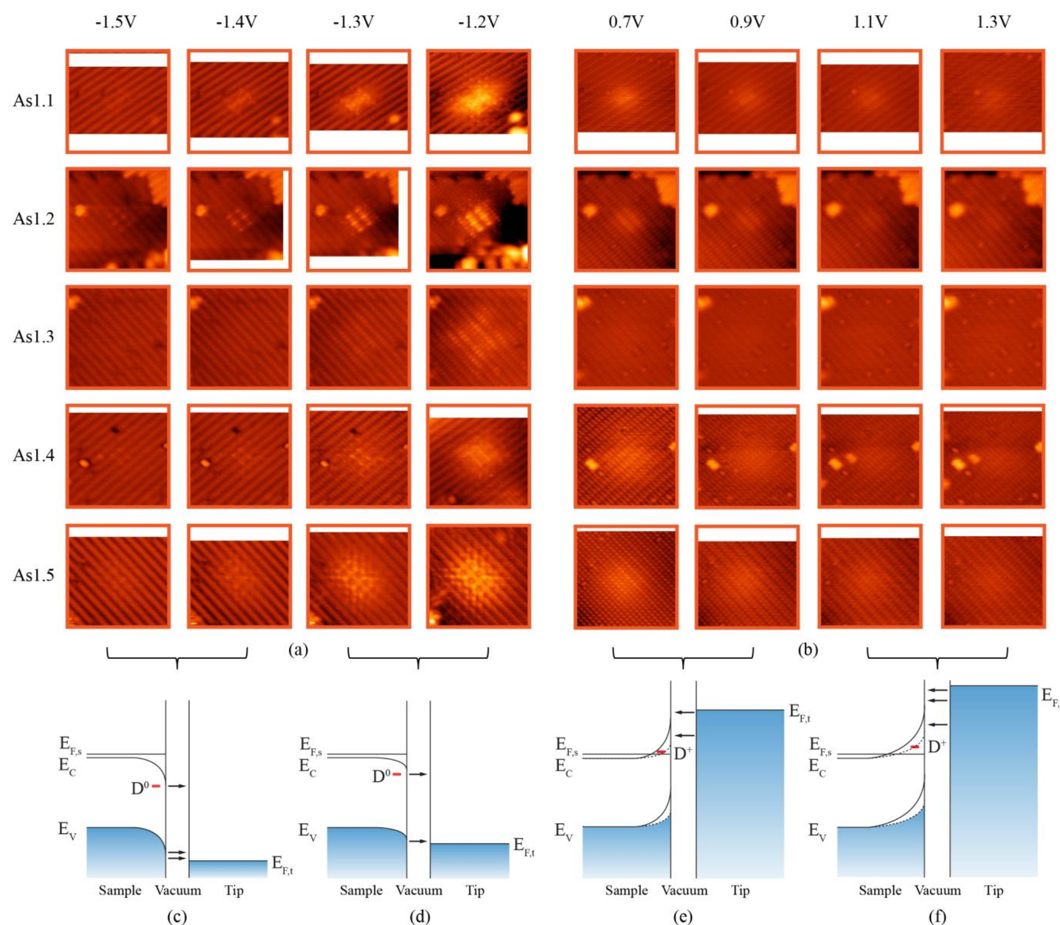

Figure 5.4 (a) Filled- and **(b)** empty-state images of different As1 features observed by STM at various sample bias with a tunnelling current of 20 pA on the Si(001):H surface at 77 K. Each of the orange boxes encloses a rectangular area of 8 nm x 8 nm. **(c-f)** Energy-band diagrams describing the tunnelling mechanism at low (d, e) and high voltages (c, f) for both filled- and empty-state imaging regimes.

The appearance of the As1 features in empty-state images (positive sample bias) differs from that of the filled-state images in a two distinct ways. Firstly, the features are more isotropic, appearing approximately circular. Secondly, the contrast is fairly uniform across the features with no atoms significantly brighter than their neighbours within the features. However, one similarity with the filled-state images is that the intensity of the empty-state features also decreases with

increasing bias magnitude. The tunnelling mechanism underlying the appearance of As1 both while the filled states and the empty states are probed will be illustrated in the next sections.

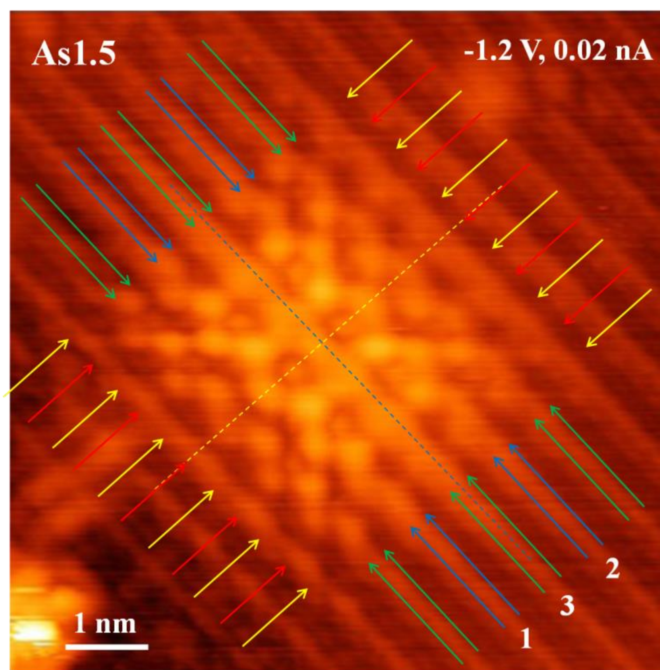

Figure 5.5 Symmetry analysis of the As1.5 feature shown in Fig. 5.4. Each couple of blue arrows and green arrows is utilised to guide the eyes for the dimer rows. The red and yellow arrows are alternately placed perpendicular to the dimer rows with each arrow indicating a dimer. Two dashed lines through the feature and crossing each other at the centre of the feature show that the As1.5 feature is symmetrical around both the axis parallel and perpendicular to the dimer rows.

5.4.1 Electrically neutral As donors (D^0)

The appearance of the As1 features as protrusions with the characteristic shapes in filled-state imaging and as circularly isotropic protrusions in empty-state imaging can be described by the aid of the energy-band model illustrated in Fig. 5.4 (c)-(f). For our case, the Si(001) samples are highly doped and thus are considered as degenerately doped, which means that the sample Fermi level must lie above the bottom of the conduction band as indicated in Fig. 5.4.

If the As donor is considered to be positively-charged ionised, the induced feature will appear as an isotropically circular protrusion [17] which does not

match the feature shapes as seen in Fig. 5.4 (a). Regarding a report in Ref. [67], when the temperature of silicon lowers, the density of electron in the conduction band is also reduced as shown in Fig. 5.6. At the room temperature (~300 K), almost all of the electrons are contributed by the ionisation of the donors, which can be noted by the equalization of the electron density and the donor concentration. However, at the temperature of about 100 K, the electron density reduces. This is because some of the donor atoms are frozen or in the other word are not ionised. Therefore, statically at the temperature of 77 K, there can also be some As donors unionised (electrically neutral donors) in the silicon sample!

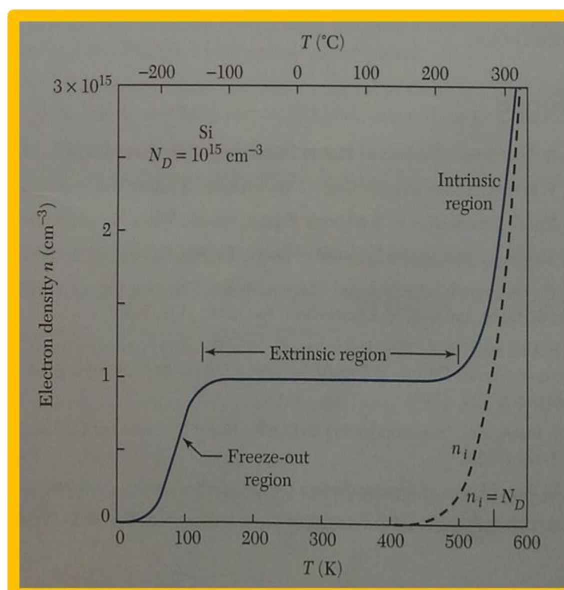

Figure 5.6 Reduction of the electron carrier in silicon for a donor concentration of 10^{15} cm^{-3} with the substrate temperature revealing three regions – the extrinsic region, the intrinsic region, and the freeze-out region. For our case, we have to compare the extrinsic and the freeze-out regions, for which the concentration of the electrons decreases due to some of the donors are not ionised at the freeze-out temperature. The graph has been taken from Ref. [67].

5.4.1.1 Voltage-dependent appearance of As^0 features

When a negative bias is applied to the sample, the Fermi energy level of the tip is shifted downward with respect to the sample Fermi level as illustrated in Fig 5.4 (c) and 5.4 (d). As a result of the misalignment of the Fermi levels, the sample energy levels near the interface are shifted downward compared to the

bulk energy levels. This effect is called tip-induced band-bending (TIBB) effect. Once the tip Fermi level become resonant with the valence-band edge at the sample surface or just a little below the edge as shown in Fig. 5.4 (d), there are two sources of tunnelling current involved. The first source contributing to the tunnelling current is tunnelling of the electrons out of the neutral donor energy level which is considered as a filled state (an electron-occupied state) of the sample. The second source of tunnelling is the filled valence-band states. Both types of the filled states of the sample provide electrons tunnelling through the vacuum gap into the empty states (the electron-unoccupied states) of the tip. Note that the energy level of the donor in Fig. 5.4 (d) is also rigidly shifted correspondingly to the conduction band edge, making the donor level becomes lower. However, the donor energy level still lies much higher than the energy levels in the valence band. Therefore, it is the tunnelling associated with the neutral donor state that dominates the tunnelling current. As a result of the dominance of the additional tunnelling current associated with the neutral As donor state, the As1 features appear on the surface as anisotropic protrusions with different characteristic shapes reflecting different projections on the surface of wavefunction of the neutral As donor.

As the magnitude of the sample negative bias becomes larger as depicted in Fig. 5.4 (c), the tip Fermi level is further moved down, causing the sample energy level near the interface to bend even more downwards. Nevertheless, this also widens the tunnelling window of the valence band, allowing more number of filled valence-band states to contribute to the tunnelling current. The increase of the valence-band tunnelling reduces the dominance of the neutral-donor tunnelling, which results in the lower intensity of the As1 features. Eventually, the tunnelling current of the undisturbed and donor-disturbed surface areas become indistinguishable, making the electronic contrast of both surface areas appears with the same intensity and the As1 features cannot be observed. Note that the amount of tunnelling current produced by the donor level is still the same but the tunnelling current of the valence band is significantly larger.

It is also interesting to note that for the filled-state imaging if the applied voltage is too low that the tip Fermi level is still above the valence-band edge (still in the band gap), the tip will not be able to scan the surface. This is because

the tunnelling current produced in the surface area without the subsurface donors is not high enough to reach the set-point current demanded by the feedback circuit, which results in the crash of the tip on the surface. This situation was realised during the experiment since we could not decrease of the negative bias magnitude to lower than about $|-1.1|$ V which is corresponding to the band gap of Si (- 1.12 eV). We have considered that the electronic states in the conduction band do not contribute to the tunnelling current for the filled-state tunnelling.

5.4.1.2 How As donors in silicon can be electrically neutral

First of all, the idea catching our attention is the electronic charge of As clusters in silicon reported in Ref. [68-70]. In that work, with the use of APT (atomic probe tomography) they reported that 60% of As in Si at room temperature are in the forms of cluster and 20% is in the interstitial sites. Both As groups are inactive, meaning that the As donors are not ionised and as a result are electrically neutral. The remaining 20% of the As population is located in the substitutional sites at which the donors are positively-charged ionised. Nevertheless, the idea of the As1 features induced by the As donors in the cluster forms or in the interstitial sites can be discarded due to the fact that it has never been reported that the donors in the cluster form and the donors in the interstitial sites can become positively-charged ionised, especially the interstitial As donors that do not couple with the silicon crystal at all.

The second theory which is sounder is as the following. Considering the concept of the enhance of donor binding energy (BE) toward semiconductor surfaces, the As donors nearer the Si(001) surface would have larger binding energy than those located in the bulk region as illustrated in Fig. 5.7 (b). Taking the BE enhancement into account, almost all of the As donors in the subsurface region would not be thermally ionised due to the fact that the thermal energy at 77 K is too small to excite the valence electrons from the donors near the interface into the conduction-band states as depicted by the red arrows shorter than the separation between the bottom of the conduction band and the varied donor energy levels. This allows the donors in the subsurface region to be electrically neutral. Moreover, for this theory, all the donors considered for the BE

enhancement are in the substitutional sites, thereby being able to be positively-charged ionised. Thus, in our opinion, this is the most possible explanation of why there are neutral substitutional As donors in the Si sample inducing the As1 features. Furthermore, with the support from DFT calculation done by our colleague [71], it will be shown later that the As donors causing the As1 features are individual As atoms residing in the subsurface layers at the substitutional sites.

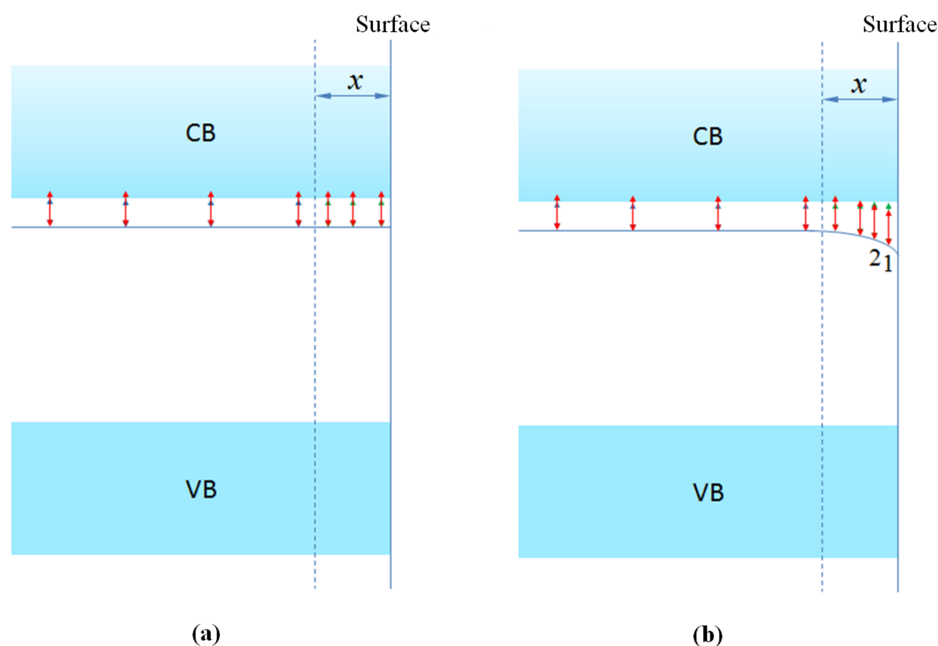

Figure 5.7 (a) Conventional energy-band diagram having the donor energy level constant throughout the sample both in the subsurface region that extends with distance x from the semiconductor surface and the bulk region that is further from the surface beyond the subsurface region. **(b)** Modern energy-band diagram expressing the donor energy level that is constant in the bulk but becomes larger towards the semiconductor surface. Donors at distance 1 and distance 2 from the surface possess different ionisation energy. In the band diagrams, the red arrows represent thermal energy while the green arrows represent the ionisation energies of donors at any depth below the sample surface.

5.4.2 Positively-Charged As donors (D^+)

If the sample bias is switched from negative to positive, the tip Fermi level is shifted upwards with respect to the sample Fermi level as seen in Fig. 5.4 (e) and 5.4 (f). Because of the TIBB effect, the energy levels of the sample near the interface are also shifted upward compared to the bulk energy levels.

If the applied positive bias is high enough that the energy level of the donor becomes resonant with or lies above the bulk level of the conduction band edge as shown in Fig. 5.4 (e), the valence electron of the donor will transfer from the donor level into the conduction band, leaving behind the fixed (immobile) positively-charged donor (D^+) with an associated Coulomb potential well. The conduction- and valence-band edges near the surface are thus pulled down due to the potential well as represented by the dashed lines in Fig. 5.4 (e) and 5.4 (f), providing more unoccupied states of the sample available for the electrons from the occupied states of the tip to tunnel into. This means that the tunnelling current of any donor-disturbed surface area is higher than the current provided by an undisturbed area. Due to the additional current generated by the ionised donor, the electronic feature induced by the donor appears as a circularly isotropic protrusion which reflects the shape of the screened Coulomb potential well at the surface.

When the sample bias become larger (see Fig. 5.4 (f)), the tip Fermi level is further shifted upwards above the sample Fermi level, resulting in more conduction-band states available for tunnelling. With the wider tunnelling window, the difference between the tunnelling current of the donor-disturbed surface area and the donor-free surface area becomes less. The intensity of the As-induced feature thus decreases compared to that of the free surface area. Eventually the additional tunnelling current of the donor-disturbed area will become insignificant. This makes the intensity of the donor surface area nearly the same as the current from the free surface area, leading to the disappearance of the circular protrusion feature on the background surface corrugation at higher bias.

5.4.3 Band-gap states related to As1

In order to learn more about the spatial profile of the local density of states (LDOS) of the As1 features, we have performed current imaging tunnelling spectroscopy (CITS) on As1.2 and As1.4 features. The process of taking the CITS data has already described in Chapter 2. Figure 5.8 (c) and 5.8 (e) show a two dimensional (2D) cut through these datasets at a constant voltage of -0.95 V over the location of the As1.2 feature, while Figure 5.8 (g) and 5.8 (i) show the equivalent cut over the location of the As1.4 feature.

Figures 5.8 (a) and 5.8 (b) show plots of conductance (dI/dV) measured as a function of sample bias acquired with the STM tip positioned over the location of an (a) As1.2 feature and (b) As1.4 feature (red traces), as compared to a measurement on a region of the hydrogen-terminated surface (black traces). For the As1.2 and As1.4 features, the appearance of the dopant spectra are qualitatively similar in that there is an enhancement in conductance in the sample voltage range between -1.3 V and -0.6 V. This indicates the presence of electronic states in the band gap that produce additional tunnelling current corresponding to the neutral donor (D^0) state discussed in Fig. 5.4 (c) for low negative bias magnitude. This is consistent with the additional intensity on the dopant surface area appearing as the As1 features with characteristic shapes. When the bias magnitude increases, the dopant and the background spectra are nearly perfectly overlapped. This informs that the additional tunnelling current contributed by the gap states does not make the total tunnelling current of the dopant surface area apparently different from the free surface area as it does in the low negative voltage range. This is associated with the decrease of the intensity of the As1 feature with increasing the negative bias magnitude as described in 5.4 (d).

In the case of positive voltages, both As1.2 and As1.4 spectra show a shift of the onset of tunnelling to lower voltages. Generally, it means that the tip Fermi level becomes resonant with the surface conduction-band edge at lower positive sample bias. Compared to the energy-band diagram in Fig. 5.4 (e), the shift of the tunnelling onset to lower bias is due to the reduction of the surface conduction-band edge resulted from the influence of the Coulomb potential of the positively-charged As donor. Once the positive bias magnitude goes up, the dopant spectra

are likely to overlap with the background spectra. This is consistent with the description of Fig. 5.4 (f) in that the difference of total tunnelling current of the dopant-disturbed and the dopant-free surface areas becomes insignificant with more empty conduction-band states being available for tunnelling due to the increase of the positive bias.

Note that the domination of gap states when taking the STS data with the negative-bias range and the shift of the tunnelling onset as the sample bias is in the positive-bias range have been observed for the Mn acceptor in GaAs system observe at room temperature [31] showing strong similarities with the As donor in Si system observed at 77 K.

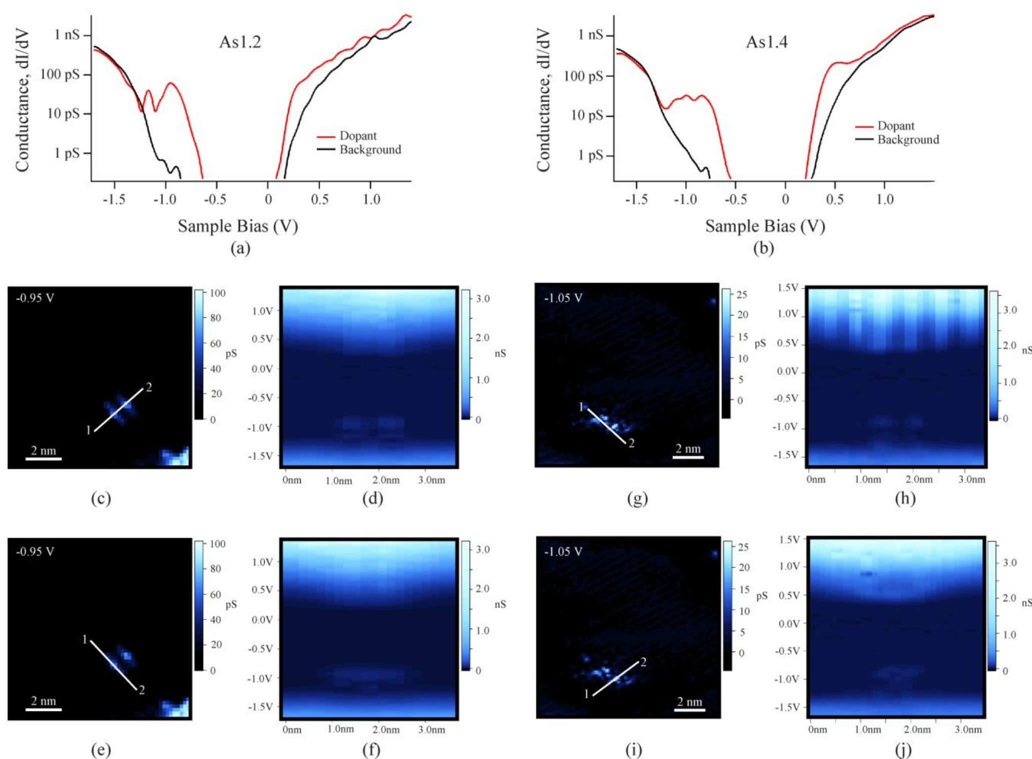

Figure 5.8 (a) and **(b)** show dI/dV spectra from As1.2 and As1.4 features (red curves) respectively compared to that of the background lattice (black curve). **(c-f)** CITS data of the As1.2 feature. **(g-j)** CITS data of the As1.4 feature. In (d), (f), (h) and (j) the colour scale corresponds to conductance plotted as a function of sample bias (vertical axis) and lateral position between the points 1 and 2 (horizontal axis) in the figures (c), (e), (g) and (i) respectively.

Fig. 5.8 (d) and 5.8 (f), show spatially resolved STS along the line between points 1 and 2 of Fig. 5.8 (c) (perpendicular to the dimer rows) and points 1 and 2 of figure 5.8 (e) (parallel to the dimer rows), respectively with the length of both lines being ~4 nm. Two notable effects related to the presence of the donor are seen in the spectra. The first is a downward curving of the spectra at positive voltage with the centre of curvature aligned with the position of the donor. This effect is caused by the screened Coulomb potential created by the positively-charged donor pulling the surface energy levels downwards, resulting in an enhanced tunnelling current and the shift of the onset of tunnelling to lower positive bias. It is the same effect that causes the circularly isotropic protrusions seen in the STM topographic images Fig. 5.4 (b). The second effect relates to the spectral aspects at negative voltage where there is no significant downward curvature, implying that there is not the long-range electrostatic effect that would be expected if the dopant were charged. Nevertheless, there is a localized region of increased conductance in the surface bandgap, in the vicinity of the neutral As atom, indicating an energetic state of the dopant inside the bandgap. The nature of the spectra shown in figure 5.8 (c)-(f) for an As1.2 feature are qualitatively reproduced in the spectra of figure 5.8 (g)-(j) for an As1.4 feature. Despite the difference in appearance in the filled-state topographic images between feature As1.2 and feature As1.4 shown in figure 5.4 (a), both of them have similar tunnelling signal in both filled- and empty-state bias – the tunnelling current in the bandgap and the shift of the tunnelling onset. This similarity implies that the As1.2 and As1.4 features should be induced by the same type of donor in the subsurface layers which is As. However, the donors would reside in different lattice positions in the silicon crystal.

5.5 Feature As2

Beside feature As1 we have also observed the second class of commonly-observed electronic feature superimposed on the surface, which indicates that they are induced by subsurface impurities. Three of the As2 features are shown again in Fig. 5.9, along with two As1 features. The As2 features differ from the As1 features in both filled and empty state images. In filled-state images, see figure 5.9

(a), the As2 features appear as circularly isotropic protrusions reminiscent of the As1 appearance in empty-state images. In contrast, when the As2 features are imaged in the empty-state tunnelling, figure 5.9 (b), they appear as circularly isotropic depressions. However, not all the As2 features appear with the same intensity and width. In Fig. 5.9 (a), the lower-intensity As2 feature on the right-hand side of the figure has its diameter wider than the other two As2 features, implying that the subsurface As dopants reside in different subsurface layers. Moreover, if we closely examine the structural details of the As2 features, it is obvious that they do not have the same structured detail. The As2 feature on the right-handed side expresses the central area dimmer than the other two As2 feature. This furthermore indicates that the As2 features are induced by As dopants in different layers and perhaps different lattice positions in a particular layer.

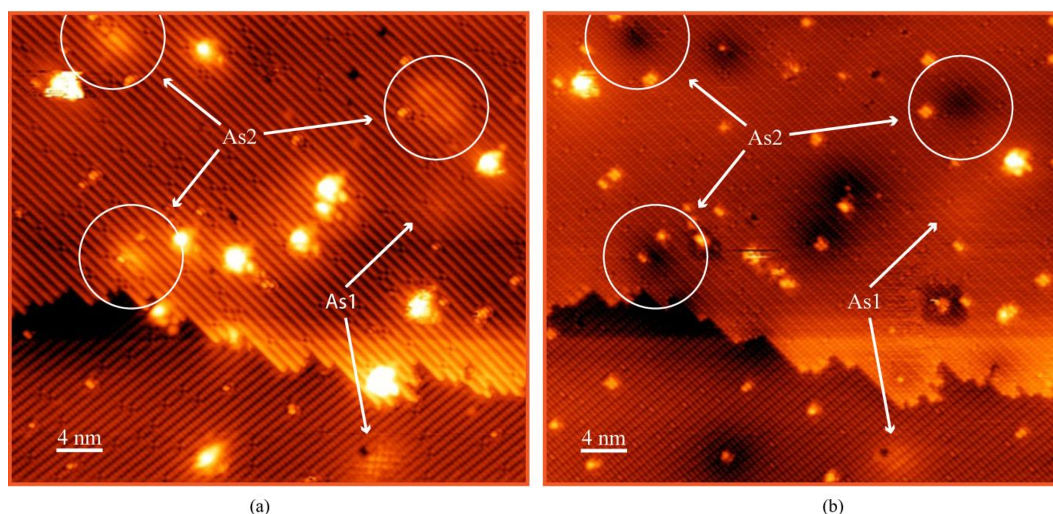

Figure 5.9 (a) Filled-state and (b) empty-state STM image of As1 and As2 features on the Si(001):H surface obtained at sample voltages of -1.3 V and 0.8 V respectively, and a tunnelling current of 20 pA. The size of each image is 40 nm x 35 nm.

The reason encouraging us to assign the subsurface As donors to the As2 feature is as the following. Statistically, we found that the density of the feature As1 and feature As2 is not significantly different. With the total number of the subsurface-impurity features observed being 198, 122 is the number of the

observed As1 features while 76 is the number of feature As2. To match the density of the subsurface As-induced feature expected to be observed on the surface by assuming that the deepest subsurface layers in which the As dopants can still be observed is the 5th layer with the Si(001) surface counted as the 1st layer, the density of feature As1 and feature As2 must be combined. This informs that the As2 features would be induced by another group of subsurface As donors different from the first group inducing the As1 features perhaps in terms of the dopant positions in the lattice, or the charge state of the dopants, or possibly both!

5.5.1 Negatively-charged As donors (D^-)

The contrast behaviour of the As2 features does not fit the energy-band model describing the appearance of the As1 features; thus the As2 donors would not be electrically neutral and positively-charged when the sample bias is negative and positive respectively [30]. The As2 appearance is also not consistent with contrast behaviour of positively-charged ionised donors for which the subsurface As-induced feature appears as a circular protrusion both in filled- and empty-state imaging [17] or recently reported the subsurface P-induced feature appears as circular depression and circular protrusion in filled- and empty-state images [61]. However, by considering the contrast behaviour of features induced by negatively-charged B acceptor below Si(001):H surface [52, 62], the appearance of the As2 feature fits well with the energy-band model used to describe the negatively-charged acceptors in silicon. Thus, we propose that the As2 features are induced by a group of negatively-charged As donors. Note that the As1 features are attributed to a group of electrically-neutral As donors.

The model proposed for B dopants in Si [52] fits well for explaining the appearance of the As2 feature. When the sample bias is negative, the tip causes downward TIBB as depicted by the solid lines in figure 5.10 (a). The Coulomb potential of a negatively-charged donor locally reduces the extension of the downward TIBB, depicted by the dashed lines in figure 5.10 (a), thereby increasing the energy window for tunnelling of the valence band. Hence, with more valence-band states available for tunnelling, the dopant-disturbed surface area appears as a circular protrusion superimposed on the lattice corrugation of the

background surface. In contrast, when the sample bias is positive, the same Coulomb potential enhances the upward TIBB illustrated in figure 5.10 (b). The energy window for tunnelling of the conduction band is narrowed; therefore, the surface area near the core of the negatively-charged donor appears as circular depression due to the local reduction of the tunnelling current compared to the dopant-free surface area. For both filled- and empty-state tunnelling, the energy-band diagrams suggest that the As2 features will become less visible when the magnitude of the applied voltage becomes larger because there will be more states of the valence or conduction band respectively available for tunnelling. The difference between the tunnelling current of the perturbed and unperturbed surface areas becomes less significant. This is confirmed by Fig. 5.10 (c) and 5.10 (d) which are bias-dependent filled- and empty-state images, respectively, of an As2 feature.

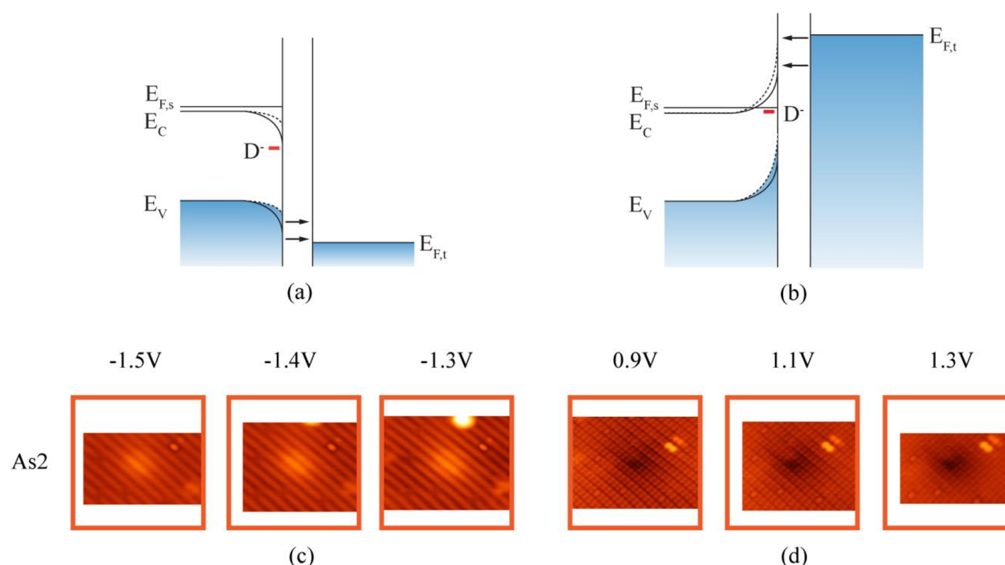

Figure 5.10 (a) and (b) The energy-band diagrams describing tip-induced band bending perturbed by a negatively charged subsurface As donor under filled-state and empty-state tunnelling conditions respectively – see main text for details. (c, d) Voltage-dependent images of an As2 feature showing that the feature become less strongly resolved with increasing bias voltage magnitude for both negative and positive bias. The size of each image is 8 x 8 nm^2.

5.5.2 Origin of the negatively-charged As donors

As a result of the similarity between the contrast behaviour of the As2 features and that of the features induced by subsurface negatively-charged ionised B acceptors in silicon, we considered the possibility that the As2 features are induced by subsurface negatively-charged ionised acceptors. Nevertheless, the idea of acceptors in the heavily-doped *n*-type silicon crystal was ruled out for two reasons. Firstly, it is extremely unlikely that a commercial degenerately As-doped silicon wafer would have such a large density of 'contaminant' acceptor atoms, and secondly it is well known that when a B-doped wafer is prepared by flash annealing, significant quantities of B segregate to the surface and are seen in STM images as pairs of protrusions perpendicular to dimer rows [72-77]. We have not seen any evidence of these features during several times of the investigation on the clean Si(001) surface. Therefore, we concluded that there was not a significant quantity of B or any other acceptor in the silicon wafer and the As2 features are not caused by negatively-charged acceptors.

There is a theoretical paper proposing that a P donor in a small Si crystal containing 100 Si atoms can express the negatively-charged properties [78]. The Si crystal in the paper contains only 100 Si atoms and thus *electronegativity* is utilised for describing charge transfer in the crystal. A group-V donor such as P and As have one more valence electron than a Si host atom, thereby having larger electronegativity. With larger electronegativity, the donor atom will attract electrons (negative charge) from the surrounding Si atoms which possess smaller electronegativity. This situation is called reversal charge transfer, which makes the donor atoms become negatively-charged. However, our sample does not have only single donor atom and the crystal size is much bigger. Therefore, the theory of the reversal charge transfer was ruled out.

Nevertheless, we have clearly explained how individual As atom in Si could be electrically neutral by taking into account the enhanced binding energy of donors towards the surface of a semiconductor. Given that all the As donors in the subsurface region are neutral, there might be some of the donors that are influenced by the imbalance of the electron tunneling rate into and out of the donor energy level. The idea of the imbalance of the input and output tunneling

rates has been proposed in Ref. [33] where the charge state of a dangling bond (DB) can be positive (0 electron), neutral (1 electron), and negative (2 electrons), depending on the number of electron bounded to the DB structure. In accordance with the concept of the unequal input/output tunneling rates, some of the neutral As donors might become stably negatively-charged and induce the As2 features. It is still controversial if this theory could be the final answer for the birth of the negatively-charged As donors in Si. However, we still have the last theory that is also promising and will be discussed below.

The region below the Si(001):H surface can be divided into two distinctive regions – *the subsurface region* in which the donor binding energy increases toward the semiconductor surface and *the bulk region* further away from the surface in which the binding energy is constant as a bulk-like value. We assume that our STM tip can observe only dopants in the subsurface region. The As donors producing the As1 and As2 features are considered to be located in the subsurface region.

Recent reports indicate that a hydrogenic donor in semiconductor crystal (the Si in GaAs(110) system) can behave as a negatively-charged dopant inducing a delocalized protrusion in filled-state images and depression when the sample bias is positive [8, 9]. That the Si donors can act as negatively-charged dopant inside GaAs is strongly supported by the enhanced binding energy of dopants towards semiconductors. We have already stated that the As donors in the subsurface layers are in the non-ionised state because of their larger ionisation energy compared to those donors located in the bulk. Considering diagram illustrated in Fig. 5.7 (b), the closer to the interface a donor is, the larger binding energy the donor possesses. Hence, if we divide the subsurface region into two parts by the dashed vertical blue line (see Fig. 5.11) with the donors in the part nearer to the semiconductor surface having larger binding energy. The As donor in this part might be able to capture one more electron from the conduction band, resulting in the donor becoming stably negatively-charged. The charge state is stable because its energy level is so deep that the range of the positive sample bias is not enough to pull the donor energy level to lie above the bottom of the conduction band.

For the donors in the subsurface region, we consider two types of the donor binding energy in a semiconductor. The first type is the binding energy of the first electron – the valence electron that makes the donor become positively charged if it is excited from the neutral donor. The second type is the binding energy of the second electron – the valence electron that makes the donor atom negatively charged if it is bound to the neutral donor. With the small thermal energy at 77 K, the first-electron binding energies could be larger than the thermal energy, making the first electron of the As atoms still bound to the donor and keeping the As dopants neutral. However, for the As donors closer to the surface as illustrated in Fig. 5.11 (a) and 5.11 (b), the second-electron binding energies are also larger than the thermal energy; therefore, the second electron that could be trapped from the conduction band is bound to the neutral As donor, which makes the donor become negatively charged.

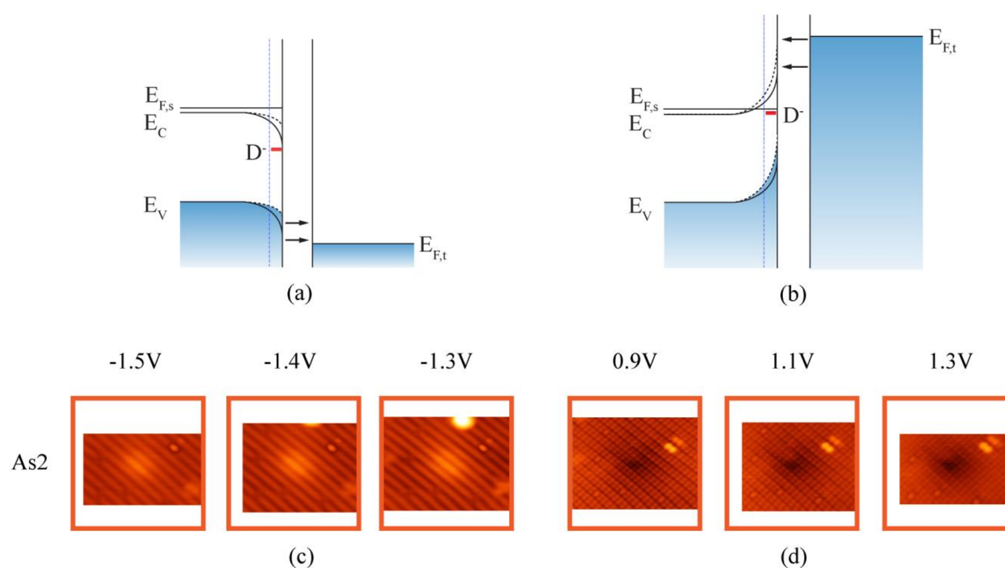

Figure 5.11 (a) and (b) The energy-band diagrams describing tip-induced band bending perturbed by a negatively charged subsurface As donor under filled-state and empty-state tunnelling conditions respectively. The vertical dashed line in each diagram represents a distance from the semiconductor surface. The donors in the region from between the line and the surface possess larger binding energies than the donors deeper than the line. Note that both donors groups are still in the subsurface region. (c) and (d) Voltage-dependent images of an As2 feature showing that the feature become less strongly resolved with increasing bias voltage magnitude. The size of each image is 8 × 8 nm^2.

5.6 DFT calculation for the neutral As features

To shed light on the nature of the neutral As donors that appear as protrusions of various characteristic shapes in filled-state images and are assigned to the projections of wavefunctions of the neutral subsurface As donors, my colleague Veronika Brazdova employed DFT calculations for estimating the energy of stable substitutional sites for the As donors in the silicon lattice. With the calculated energy of each possible substitutional site, we also generated relevant simulated STM images to compared with the experimental STM images that has led us to the assignment of the As1 features to the As donors located at particular substitutional sites below the Si(001):H surface reconstruction.

5.6.1 Calculation Methods

We have used density functional theory (DFT) with the gradient-corrected Perdew-Burke-Ernzenhof (PBE) [79] exchange-correlation functional, as implemented in the Vienna Ab-Initio Package (VASP) code [80, 81]. The core electrons were described by the projector augmented-wave (PAW) method [82, 83]. The plane-wave basis set kinetic energy cutoff was set to 200 eV. The Brillouin zone was sampled using Monkhorst-Pack grids [84]. Gaussian smearing was used for fractional occupancies, with a 0.1 eV width. The convergence criterion for forces on atoms was 0.01 eV/ Å and for total energy 10^{-6} eV.

We used the experimental lattice parameter (5.431 Å) [85, 86]. The surface unit cell was chosen so that the Si dimers on the surface were parallel to one of the cell vectors, with a lattice parameter of a = 3.86 Å. We used a (8×8) surface unit cell, resulting in eight dimers in each dimer row and four dimer rows in one computational cell. The lattice parameter perpendicular to the surface was set to 32 Å, which results in 12 Å of vacuum between the periodic images of the slab. The slab contained 14 Si atomic layers and was terminated with hydrogen atoms at the top and at the bottom, 1088 atoms in total. The bottom two Si layers were kept fixed at bulk positions, the rest of the structure was optimised for each system. We added one electron to each system to simulate the high *n*-type doping of the experimental system.

STM images were simulated using the Tersoff-Hamann approach [87]. We find agreement with experiment when we image the dopant bands, which in our simulations lie just above the Fermi level. This is in most cases achieved by setting the upper bound of the integration window to 0.086 eV or less. The lower bound, -0.7 eV, is within the band gap and therefore the simulated STM images show the lowest-lying unoccupied bands. These would be imaged experimentally in filled states due to band bending.

5.6.2 Stable substitutional sites for As

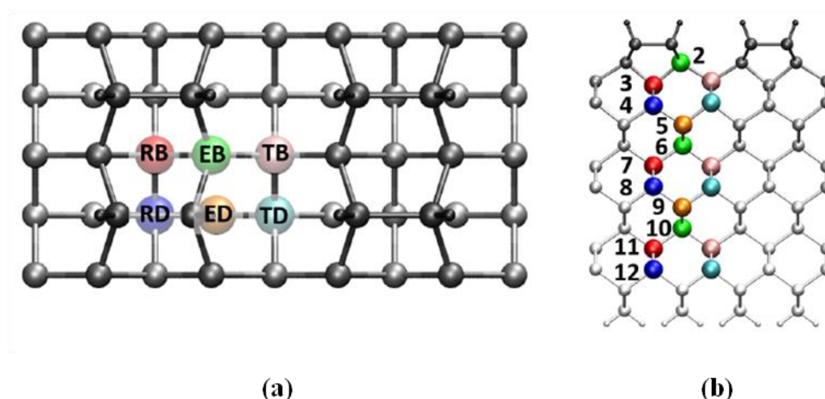

(a) (b)

Figure 5.12 (a) Six possible substitutional sites for dopants in Si according to the Si(001) surface. For more details about the labelling, please see text. **(b)** The six possible substitutional sites according to the side view of the Si(001) surface. The Si(001) surface layer is counted as layer 1.

The Si(001) surface has six possible symmetry sites for the substitution of As for the Si atoms below the surface (Fig. 5.12 (a)), which is distinguished by the position of the dopant with respect to the dimer rows and the dimers in the Si(001) surface layer. With respect to the dimer rows on the surface, an As atom can be positioned either in the middle of a dimer row (R), in the middle of a trench between two dimer rows (T), or at the edge of a dimer row and a trench (E). In either of these locations an As atom can be positioned in line with a dimer (D) or in between two dimers (B). The possible combinations of these locations give the six symmetry sites as shown in Fig. 5.12 (a). We also notate the sites by the layer they are in with the Si(001) surface layer numbered as 1. For instance, TD4 denotes a dopant atom located in the middle of a trench between two dimer rows,

in line with a dimer, in layer 4. Sites of the same symmetry repeat every four layers. This is associated with the light-blue circle in layer 4 in Fig. 5.12 (b).

Donor Site	ΔE (eV)
RB3	0.00
TB3	0.14
TD4	0.11
RD4	0.04
ED5	0.04
EB6	0.04
RB7	0.01
TB7	0.07
TD8	0.08
RD8	0.03
ED9	0.04
EB10	0.07
RB11	0.07
TB11	0.05
TD12	0.16
RB12	0.16

Table 5.1 Energies of As donors substituting for each lattice site shown in Fig. 5.12 (b). All energy values are in the eV unit.

The energies of the dopants located at the substitutional sites illustrated in Fig. 5.12 (b) are calculated and shown in Table 5.1. The most stable dopant site is RB3; dopants in layers 3 and 4 are up to 0.14 eV less stable than RB3, dopants in layers 5 to 11 up to only 0.08 eV less stable. Dopants in layer 12 are 0.16 eV less stable, however, that may be due to layer 12 being very close to the artificial surface and the fixed atoms at the bottom of the slab. Even though the dopants energies substituting for different sites are varied, these energy differences are too small to make a practical difference in the number of dopants observed in the various sites. In the other word, we cannot estimate from the calculated energies which site should be the most commonly observed as features superimposed on the surface. However, simulated STM images corresponding to particular dopant

sites are generated and the images are compared with the experimental STM images of the As1 feature to match them, leading to the assignment of particular As1 features to relevant subsurface As dopants in particular substitutional sites.

5.6.3 Simulated STM images

Fig. 5.13 shows the simulated filled-state images of features induced by the As donors located at some of the substitutional site as seen in Fig. 5.12 (b) along with the As1 features that match them. The comparison between the simulated and the experimental images suggests that the shallowest As donors inducing the As1 features lies in layer 7. We speculate that the As dopants located in the layers above layer 7 are not electrically neutral but they are negatively charged, thereby causing the As2 features as previously discussed. The DFT simulation in general struggles to simulate Coulomb potentials which extend over several atoms; thus, the effect of tip-induced band bending (TIBB) was not included in the calcualation. As a result of the TIBB exclusion, the features caused by any charged As donor are not displayed in the simulated STM images – the As1 features in empty-states images, and the As2 features in both filled- and empty-state images.

Considering Fig. 5.13 (a), any substitutional As dopant located at the RB lattice position in layer 7 (RB7) induces a single As1.1 feature superimposed on the Si(001):H surface. The charge state of this dopant is electrically neutral as earlier mentioned; therefore, the shape of the As1.1 feature is related to the projection on the surface of the wavefunction of the As dopant. Like the assignment done for the As1.1 feature, the simulated image associated with the As dopant in the TD8 substitutional position matches the appearance of feature As1.2 as depicted in Fig. 5.13 (b). The As1.3 feature is attributed to the projection of the wavefunction of the As dopant in the TB11 lattice position as depicted in Fig. 5.13 (c) while the simulated image corresponding to the As dopant at the TB7 matches the appearance of the As1.4 feature (see Fig. 5.13 (d)). Since the calculation work is still an ongoing project although it is giving out very promising result, we still cannot find any simulated image that could be assigned to the As1.5 feature.

The detail of the propagation of the wavefunction from the dopant site to the surface is unknown, but it could be stated that the surface has influence on the wavefunction of the dopants [7]. It would not be just the dopant positions that determine the shapes of the wavefunction projections on the surface. It could also be the interaction between the surface and the wavefunction of the dopants at different sites. Hence, it should be emphasised that the surface providing the As1 features for our investigation is the Si(001):H surface. The appearance of the wavefunction projection of the subsurface As donors residing in the same lattice positions could be different if the scanned surface is not Si(001):H.

Fig. 5.14 shows all the As1 features observed with arrows and lines highlighting the symmetry of the features. Considering the dimer row at the middle of each feature, we can say that each feature is symmetric around the dimer-row axis. Similarly, every feature also expresses symmetry around the axis cutting through the feature at the middle and perpendicular to the dimer-row axis. Due to the symmetry of the wavefunction projection on the surface, the subsurface As donors would be located right below the centre of the features. This is also supported by positions of the subsurface As dopants associated with the simulated STM images assigned to the As1 features [71].

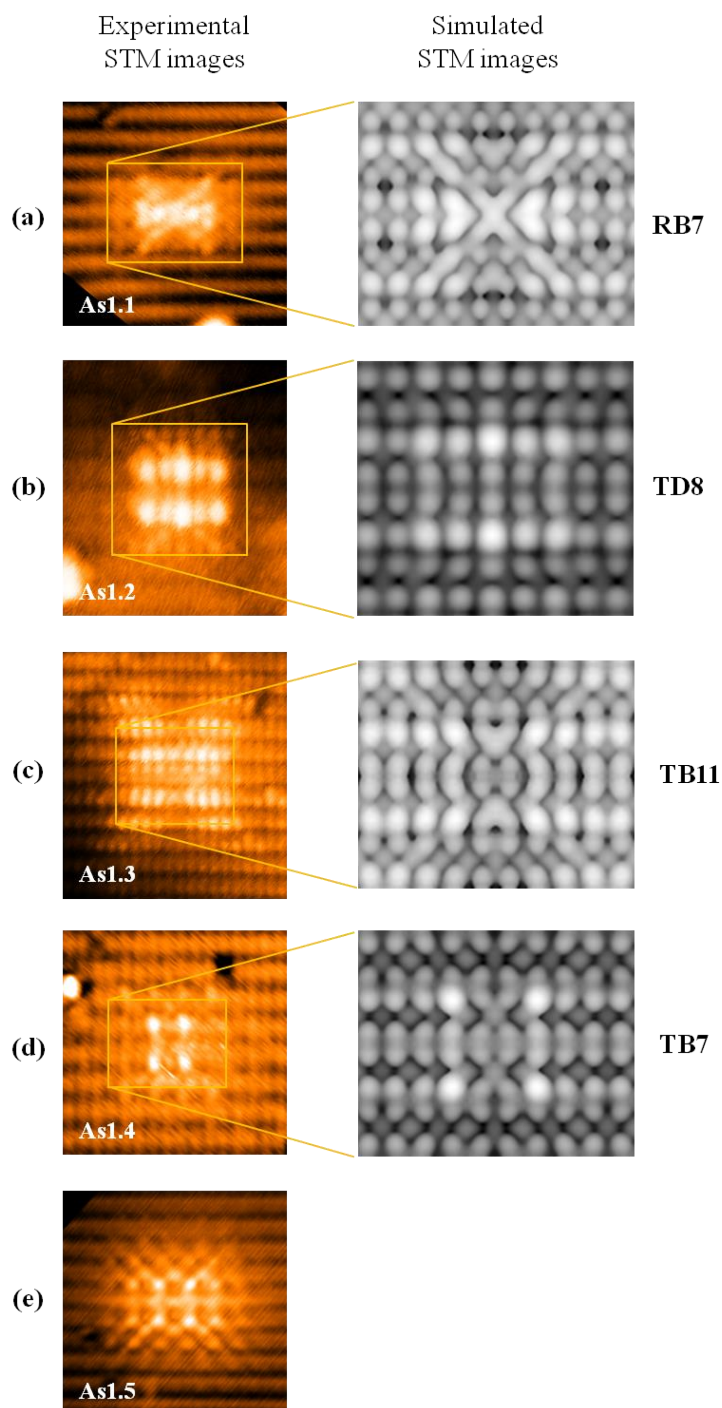

Figure 5.13 Pairs of experimental and simulated STM filled-state images that match each other for feature **(a)** As1.1 **(b)** As1.2 **(c)** As1.3 **(d)** As1.4 and **(e)** As1.5. Since the separated theoretical work is still being done, a simulated image matching the image of feature As1.5 has not been found yet. The theoretical work is expected to be submitted and published soon [71].

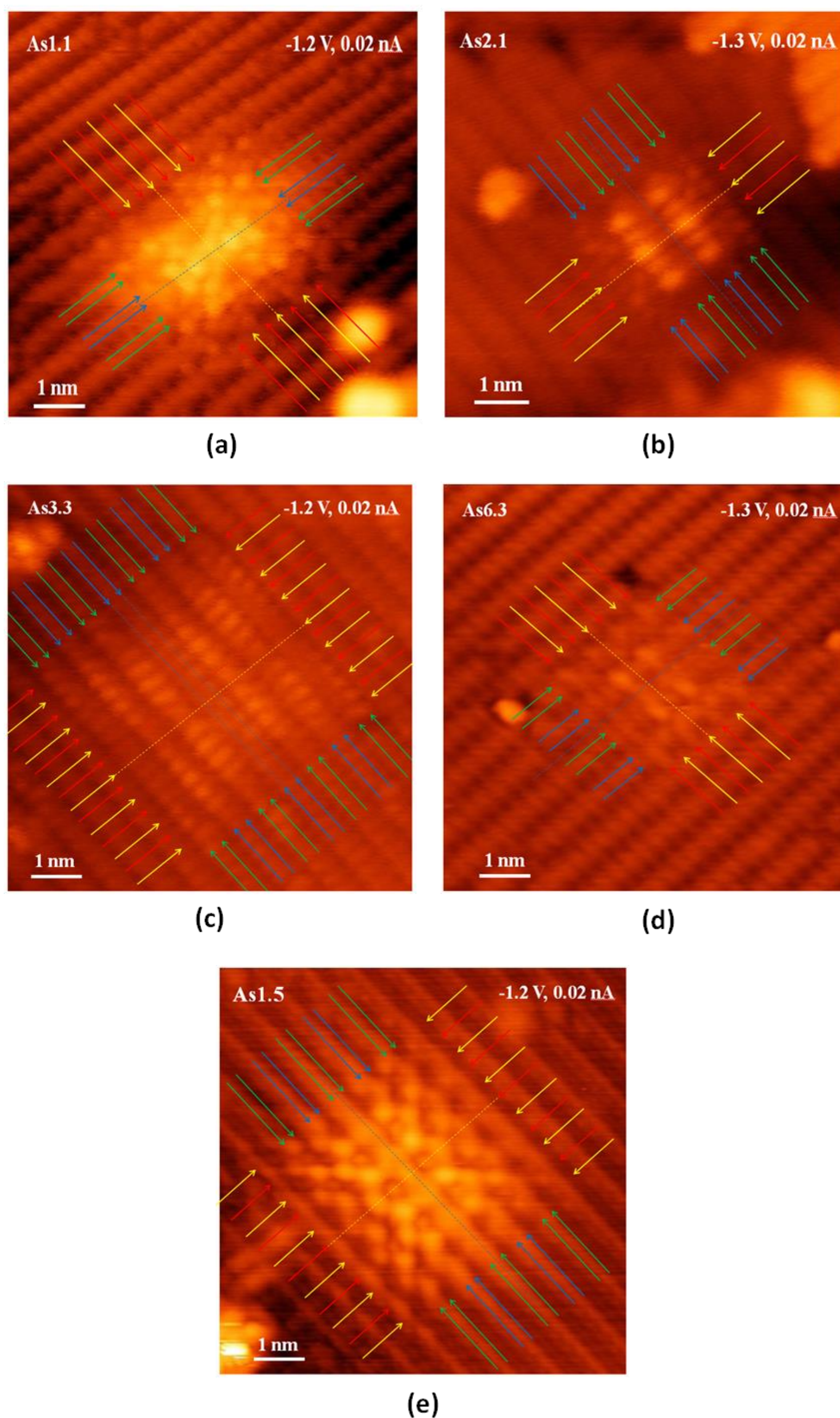

Figure 5.14 (a)-(e) Close-up images of feature As1.1-As1.5 respectively with the coloured arrows guiding the eyes to the dimer rows and individual dimer axis. With the dashed lines crossing at the centre of each feature, it is obvious that all the As1 features have symmetry around the axis parallel to the dimer row and the axis perpendicular to the dimer row.

5.7 Dimer-row shift of the Si(001):H surface

Since we needed to scan the surface with as low bias magnitude as possible to allow the tunnelling current associated with the subsurface As dopants to be visible, the tip Fermi level had to lie just below the top of the valence for the filled-state imaging and this is corresponding to the bias of -1.2 V. By closely examining the appearance of the As1.5 feature when the bias changes from -1.2 V to -1.3 V, apart from the reduction of the feature intensity, we also observed the shift of the dimer rows of the background surface as shown in Fig. 5.15 (a) and 5.15 (b). From the figure, the purple dashed lines are drawn through the middle of the dimer rows in Fig. 5.15 (b), extending to Fig. 5.15 (a). In Fig. 5.15 (a), we can see that the dashed lines are no longer aligned with the axis of each dimer row. However, each atomic protrusion of the As1.5 feature is stable with respect to the dashed lines. The dimer rows of the background Si surface are shifted! For the time being, we have not known what causes the dimer-row shift when the negative bias is so low (-1.2 V) that the tip Fermi level lies just below the top of the valence band. Nevertheless, there are some theories that might explain the underlying mechanism of the dimer-row shift.

One theory is that when the tunnelling current contributed by the valence-band filled states becomes very small, the tunnelling current contributed by the donor filled states become dominating. With the coupling interaction between the wavefunction projection of the feature and the tunnelling current of the valence band which in principle provides the background surface appearance and is very small in this case, the appearance of the background surface is visibly altered as seen by the shift of the dimer row. However, this theory is ruled out once we zoomed out the surface area as shown in Fig. 5.15 (c). Even on the free surface areas which are far away from the dopant-disturbed surface area, the shift still exists as can be seen from the consistency of the dimer-row separation. Therefore, we believe it is not the subsurface As dopant that causes the shift of the dimer row when the scanning bias magnitude decrease from -1.3 V to -1.2 V, which shifts the tip Fermi level even closer to the band gap.

Another theory is that the conduction-band filled states might also contribute to the tunnelling current when the sample bias is negative. As shown in

Fig. 5.6, at 77 K some of the dopants are not ionised while some are ionised donating valence electrons to the conduction band. For scanning the surface with negative bias, the energy levels near the surface are bent downwards, causing the electron carrier accumulation in the conduction band near the surface. When the bias is so low such as -1.2 V, the tunnelling window of the valence band is very small and as a result this allows the tunnelling current of the filled states in the conduction band to dominate the background surface, causing the shift of the dimer rows.

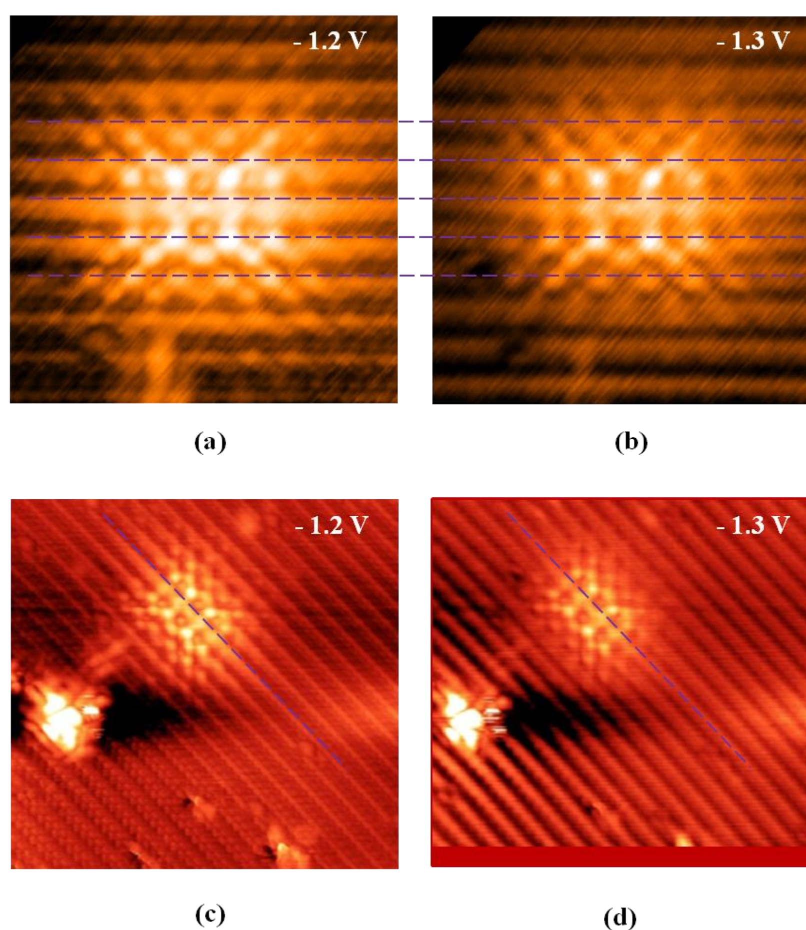

Figure 5.15 (a) and **(b)** filled-state images of feature As1.5 taken with the bias of -1.2 V and -1.3 V as labelled in the figure. The purple dashed lines are drawn through the middle of each dimer rows in (b), extending into (a) and revealing the shift of dimer rows. **(c)** and **(d)** are the wider-view images of (a) and (b) indicating that the dimer-row shift occurs throughout the surface, not just about the feature area. The purple arrows in (c) and (d) cutting through the feature at the same axis reveal that the dimer rows actually shift even on the surface area far from the feature.

Chapter 6

Subsurface Bi donors below Si(001):H at 77 K

6.1 Introduction

We have already revealed in Chapter 5 that arsenic (As) atoms in a silicon crystal exhibit the neutral charged state at the temperature of 77 K when scanned with STM at negative sample bias. This suggests that at 77 K the neutral As donor, rather than the P donor (which has not been observed in the neutral state at this temperature), could play the role of the control atom of the fundamental three donor atom building block of the *Stoneham et al.* QIP scheme [2], shown in Fig. 4.1. Bi donors seem ideal candidates for the qubit atoms of the scheme as they fulfil the requirement of having a significantly larger binding energy than the control atom, 71 meV compared to 54 meV that is the binding energy of an As atom [88]. This larger ionisation energy could allow the novel atomic device to operate at higher temperature [2, 89-91]. Beside the large ionisation energy, Bismuth also possesses long spin-lattice relaxation time which is a favourable property for the QIP device. Like the study of subsurface As donors in silicon, the objective of investigating subsurface Bi dopants buried in silicon is to understand the atomic-scale characteristics of this type of dopant, including the surface features induced by the subsurface Bi donors, and ultimately to find out whether the Bi atoms can be electrically neutral.

Even though STM has been widely used to characterise shallow donors below the Si surfaces [51, 52, 62, 92, 93], little work has been done on deep group V donors such as As [17]. In the case of Bi there has not been any report on the observation of subsurface Bi dopants inside silicon although there are some recent publications revealing individual Bi atoms located in the Si(001) and Si(111) surface layers at 77 K [94, 95]. This gap must be filled if Bi is to be exploited as a key dopant in atomic-scale electronic devices such as a single-atom transistor [43] and the quantum computer [1-3].

In this chapter, the observation of Bi dopant atoms in the subsurface layers below the H-terminated Si(001) surface at 77 K will be discussed. A multi-step thermal procedure for sample preparation in order to obtain the desirable characteristics of the sample surface and also to acquire a sufficient amount of Bi in the subsurface layers will be revealed. We have observed three distinctive types of features superimposed on the background Si(001):H surface that we believe are induced by subsurface Bi atoms. All of the observed subsurface Bi-induced features do not show the sign of the positively-charged ionised donor atom [92] which appears as a circular depression and a circular protrusion features superimposed on the surface at the negative and positive sample bias respectively due to the associated Coulomb potential. Hence, we believe that this could be the first observation of individual non-ionised subsurface Bi atoms in silicon that could be in their neutral charged state or else we might observe the negatively-charged Bi donors. If this is the case, our results could enhance the practical possibility for fabricating the atomic electronic device such as that QIP structure. Toward the end of this chapter, we discussed possible interpretations of the underlying tunnelling mechanism that provides the Bi features.

6.2 Sample preparation

The silicon samples used for the study of individual Bi donors in the subsurface layer were cut from a silicon wafer doped with five layers of Bi using ion implantation. Each layer has the doping density in the range of 10^{19} cm^{-3}. In this section, we will discuss the necessity of employing such that method to introduce Bi into Si through the Si(001) surface. Each Si(001) sample also underwent a multi-flashing procedure so as to obtain the flat and clean surface reconstruction together with a sufficient amount of Bi in the subsurface layers suitable for the STM study. The special thermal treatment of the samples will also be reviewed in this section.

6.2.1 Ion implantation

To introduce Bi atoms into a silicon wafer suitable for the STM study, there are four technique commonly used including thermal evaporation, chemical vapour deposition (CVD), molecular beam epitaxy(MBE), and ion implantation. Other than managing to incorporate dopants in the silicon crystal, the doped wafer must not be contaminated during the impurity doping process and it must still be possible to prepare flat and clean surface for the STM measurement of the individual dopants. However there is one serious problem with the thermal evaporation and CVD methods that deposit dopants onto the sample Si(001) surface which is subsequently annealed to incorporate the dopants into the surface layer and then buried by overgrowing silicon layers on top of the surface layer. The problem is that the Bi dopants form clusters of Bi dopants in the form of nanolines nearly immediately after landing on the Si(001) surface [96, 97] preventing the study of properties of individual Bi donors in Si with STM. Molecular Beam Epitaxy (MBE) suffers similar issues. However, with the ion implantation method, the Bi dopant atoms not only can be introduced into the silicon single crystal through the Si(001) surface with well-known depth and precisely-controlled concentration but the Si(001) surface can also be thermally prepared to obtain flat and clean quality suitable for characterising individual single dopant atoms by STM [94].

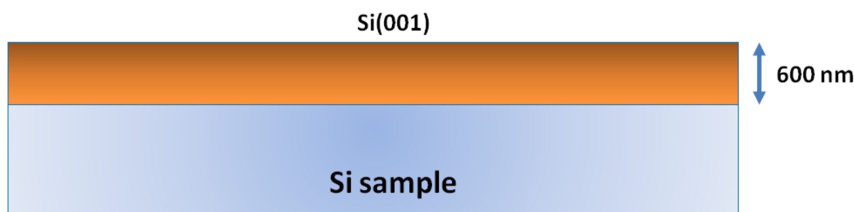

Figure 6.1 A representation of the Si wafer doped with Bi in five layers that can be imagined as a doping band represented by the brown-coloured region. The first implanted layer is just beneath the surface while the fifth implanted layer is 600 nm below the Si(001) surface.

Unlike the silicon samples used in the study of subsurface As donors which is highly As-doped throughout the Si wafer with the doping concentration

in the order of 10^{19} cm^{-3} samples, the silicon samples used in the study of subsurface Bi donors are lightly As-doped throughout the Si wafer with the doping concentration of just 10^{14} cm^{-3}. Subsequently, five layers of Bi donors were implanted into this Si wafer using the ion implantation method with the 1st layer lying just below the Si(001) surface and the fifth layer lying approximately 600 nm deep inside the silicon crystal (see Fig. 6.1). The depth of each Bi-implanted layer is comparable with an Bi ion beam shot at the acceleration energy of 250, 500, 850, 1350, and 2000 KeV respectively as shown in Table 6.1. Each Bi-implanted layer has doping concentration in the order of 10^{19} cm^{-3}. The high density of Bi donors in each implantation layer would increase our chance for the observation of any surface feature induced by subsurface Bi dopants. The low background concentration of As dopants (10^{14} cm^{-3}) approximately correspond to less than one dopant within the surface area of 1000 nm^2 of a silicon layer thereby being nearly impossible to accidently find one during the STM observation. The high concentration of the Bi dopants is equal to ~8 dopants in the surface area of 50 nm^2. Regarding the dopant density, any feature appeared and superimposed on the surface corrugation beside the commonly-observed defects such as dimer vacancies and dangling bonds of the Si(001):H surface was assigned to being induced by Bi dopants in the subsurface layers of the silicon crystal.

Bi ion energy (KeV)	Dose (cm^{-2})
2000	1.09×10^{15}
1350	1.70×10^{15}
850	0.90×10^{15}
500	0.64×10^{15}
250	0.41×10^{15}

Table 6.1 Parameters used for Bi implantation.

6.2.2 Two-step flashing procedure

To prepare a Si(001) sample for the STM measurement, the sample is degassed at 500 ℃ for 12 hours in the UHV chamber and subsequently flashed

with ~1250 ℃ for 10 s to obtain the well-reconstructed flat and clean surface corrugation. Although the desirable surface condition can be achieved with the 1250 ℃ flash, this flashing temperature is too high, resulting in the depletion of dopants in the surface layers of the Si(001) sample [23], due to evaporation of dopant atoms from the surface region. Thus, we would not be able to observe any surface feature induced by the subsurface dopants when performing the STM measurement. Nevertheless, it has been reported that flashing the Si(001) sample at ~1050 ℃ for 10 s also provides well-reconstructed flat and clean Si(001) surface with the density of the dopants nearly unchanged compared to the initial condition [23]. Following the flashing procedure in that work, we found out that our Si(001) surface is not even flat and clean at the flashing temperature of ~1050 ℃. Thus, we turned our attempt back to the method we used to find the lowest flashing temperature for the degenerately As-doped Si(001) sample studied in the previous chapter. We eventually found that the lowest flashing temperature for obtaining the flat and clean reconstruction of the Si(001) surface is ~1300 ℃ for 10 s. However, at this high temperature, it seemed that the Bi donors were depleted from the subsurface layers convinced by the STS curve on the empty-state tunnelling range. We will discuss the way we used to check whether there are sufficient amount of Bi dopants in the subsurface layers later in this section.

To overcome the Bi depletion issue we developed a two-step flashing method. We first flash the sample to ~1300 ℃ to obtain a flat and clean surface. After the first flash, which depletes the Bi dopants from the subsurface layers, the sample then was flashed again with the temperature of ~1100 ℃ for 10 s. With the low temperature flash, most of the Bi dopants in the subsurface layers did not evaporate from the surface and the dopant density was sufficiently high while the surface was still flat and clean, suitable for the STM characterisation. We also found that the number of Bi dopants remains significant after several flashes at ~1100 ℃ for 10 s. This was also reported by J. L. Pitters [23] and K. Iwaya [94]. It has been estimated that Bi diffusion constant at 1380 ℃ is about 250 nm for a time period of 10 seconds. This drops to about 42 nm if the temperature is kept at 1220 ℃ for 10 seconds; thus, at 1100 ℃ the diffusion constant would be less than 42 nm [98]. Regarding this estimation, the first flash with ~1300 ℃ for 10 s may lead to the diffusion of Bi dopants to about 250 nm toward (and outward) the

surface but the deepest layer of Bi is 600 nm below the Si(001) surface; thus, there are still plenty of Bi dopants not diffusing far enough into the dopant depletion region [23]. Subsequently, the second flash with ~1100 ℃ for 10 s would provides energy for Bi dopants to diffuse less than 42 nm without a significant evaporation of the dopants from the subsurface layers; therefore, uniformly high density of Bi dopants in the subsurface region could be achieved. Note that whether the Bi concentration is depleted, or it is not depleted but not sufficiently high and not uniform, or it is uniformly high enough for the STM characterisation can be checked by considering STS curves obtained from the surface.

6.2.3 Checking subsurface Bi concentration using STS curves

To check whether there is abundant amount of Bi dopants in the subsurface layers, the secondary ion mass spectroscopy (SIMS) measurement technique can be utilised. Nevertheless, this technique requires the sample to be removed from the UHV chamber, which costs time and may bring contamination to the sample surface. Luckily, the SIMS measurement is not the only way to check the density of subsurface Bi donors, as described below.

6.2.3.1 Checking Bi concentration below Si(211) with X-STM

Another method to check whether there is abundant amount of Bi dopants in the subsurface layers of a Si crystal is to perform the STS measurement on Si(111) exposed by cleaving Si(211) undergone Bi implantation as shown in Fig. 6.2 (a) and 6.2 (b). This technique is known as X-STM [99]. Simply taking STS curves of several areas of the Si(111) surface, the Bi concentration at several depth with respect to Si(211) could be examined by considering the empty-state tunnelling current. By cleaving the sample and approaching the STM tip to the exposed Si(111) surface (Fig. 6.2 (b)), the STS curves can be taken both in the implanted region and in the bulk region away from the Si(211) surface.

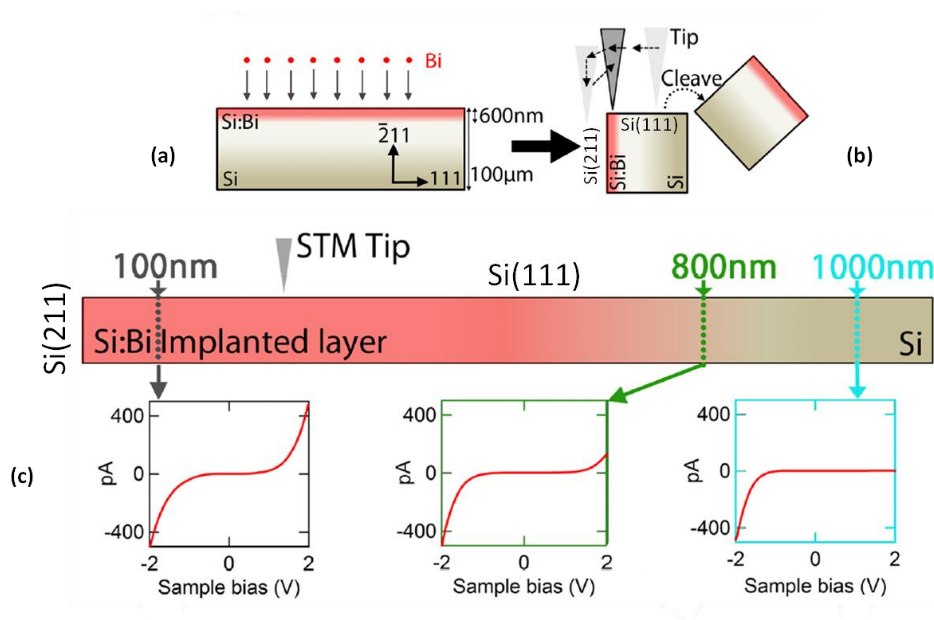

Figure 6.2 Dependence of empty-state tunnelling current on the density of Bi dopants in the silicon sample, adapted from Ref. [99].

Fig. 6.2 (c) shows the STS curves taken over three different areas of the Si(111) surface away from the S(211) layer. While the filled-state tunnelling current exhibits the same characteristic in all three regions, the empty-state tunnelling current exhibit variation which corresponds to the Bi concentration in the particular regions. At 1000 nm away from the Si(211) surface, there is no Bi dopants in the region. The very low background P doping concentration (about 10^{15} cm^{-3}) resulting in low density of electron carriers largely induces the upward band bending of the conduction band and thus increases the offset bias of the empty-state tunnelling. Consequently, electrons cannot tunnel from the tip to the sample, seen as zero empty-state tunnelling current. For the areas 800 nm away from Si(211), the Bi concentration is higher indicated by the red shade. The region is more conducting (having more electron carriers), resulting in the reduction of the upward band bending. This decreases the offset of the empty-state tunnelling current. This reduction of the upward band bending becomes even stronger for the STS curve taken at the distance of just 100 nm from the Si(001). In this region, the Bi concentration is as high as 10^{19} cm^{-3}. The offset of the empty-state tunnelling current is shifted to ~1 V.

6.2.3.2 Checking Bi concentration below Si(001) without X-STM

For our Si sample doped with As (10^{14} cm^{-3}) and implanted with 5 layers of Bi (10^{19} cm^{-3} for each layer) from just below the surface down to 600 nm, we also checked the density of the Bi atoms in the Si(001) surface region after the thermal preparation using STS curves. If there is abundance of Bi implanted dopants in the subsurface region, the STS curve taken over the Si(001) surface will show approximately the same characteristic as the STS curve taken over the Si(111) surface at the region of 100 nm away from the Si(001) layer shown in Fig. 6.2 (c) in which the bandgap is ~2 eV and the offset off the empty-state tunnelling is ~1 V.

Fig. 6.3 (a) – Fig. 6.3 (c) show three STS curves taken on the H-terminated Si(001) sample undergone the thermal flash at three different temperatures (1100 ℃, 1200 ℃, and 1300 ℃). The silicon sample flashed up to 1300 ℃ provided the STS curve with the offset of the empty-state tunnelling current higher than 2 V (see Fig .6.3 (c)). This is because of the depletion of the Bi dopants from the subsurface region due to the evaporation. We then tested the sample flashed with 1200 ℃ by performing STS on several surface areas. It revealed the empty-state tunnelling current offset being at low voltage of only 1 V. This indicates that the Bi concentration in the subsurface region was higher (see the light-blue line No. 1 in Fig. 6.3 (b)). Nonetheless, the increase of the current has a low saturation limit. This might be due to that the Bi concentration in the subsurface layers is still low although it is sufficient to contribute to the tunnelling. The Bi concentration also seems not to be uniform, which is observed by the blue I-V curves in Fig. 6.3 (b) representing STS taken on other surface areas. Considering this blue curve, it looks like that the Bi concentrations are higher than the concentration in the former areas. We thought that it might be the poor performance of the tip that caused such the variation of the STS curves taken over different areas of a surface. The spectroscopy had been expected to be uniform throughout the Si(001) sample surface.

To test whether the tip worked properly when it gave the STS curve with the saturation limit after flashing the sample to 1200 ℃, we used that same tip to take STS curves on a *p*-type Si(111) sample surface. The STS curve of the Si(111)

surface reveals the bandgap of about 1.2 eV (see Fig. 6.3 (d)); therefore, this tip performed properly at the time of measurement and the STS curve with the saturation limit is a real effect from the sample characteristic, not from the poor functionality of the tip. However, the characteristic of the empty-state tunnelling current of this Si(001) surface is not what is expected. Therefore, we used lower flashing temperature (1100 ℃). From Fig. 6.3 (a), the STS curve is a representation of a number of STS curves taken over the Si(001):H surface with the Si(001) surface prepared by flashing with 1100 °C. The empty-state tunnelling current does not show the saturation limit at all, which is consistent with the result in Ref. [99]. It indicates that the Bi concentration in the subsurface region is uniformly high enough for the STM observation. Additionally, the sample is now sufficiently conducting for the measurement of the empty states of the sample.

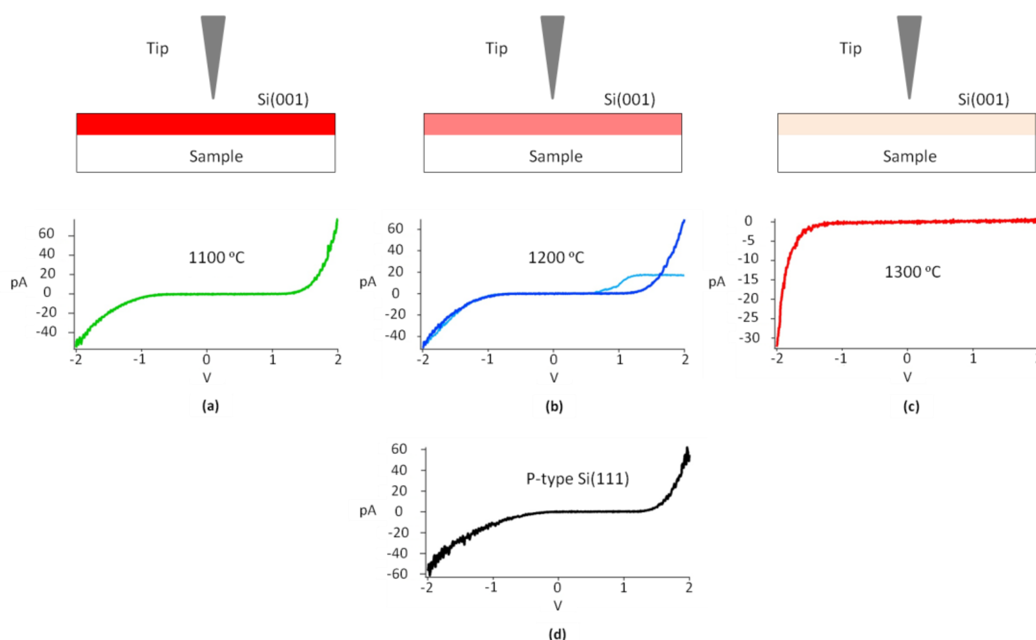

Figure 6.3 (a) (b) and (c) STS curves obtained from the *n*-type Si(001):H surface earlier undergone thermal flash at 1100 °C, 1200 °C, and 1300 ℃ respectively. (d) The STS curve of the cleaved *p*-type Si(111) surface. The intensity of the horizontal coloured bar in each STM schematic diagram above its relevant STS curve indicates the density of Bi in the subsurface layers of Si(001). The more intensive the bar is, the more concentrated the Bi density is represented.

6.2.4 Removing the surface states of Si(001) with H-termination

Like the subsurface As experiment discussed in the last chapter, the sample surface used for the study of subsurface Bi donors is also the Si(001) orientation terminated by a single layer of hydrogen to allow the tunnelling current of any electronic states in the band gap of the semiconductor samples to be visible in STM images. After the two-step flash process the sample surface is H-terminated with the sample temperature kept around 330 ℃ for 5 minutes during which minimal dopant diffusion will occur [34]. For our characterisation of individual subsurface Bi donor, we did not care about the specific location of the donors as long as they induced feature superimposed on the sample surface corrugation. Moreover, the sample temperature during the termination process could not significantly disturb the Bi concentration in the subsurface region.

However, a crucial point is that it is nearly impossible to obtain an excellent H-terminated surface within the first H-termination. By flashing the sample at only 1100 ℃ each time before performing the H-termination, the Bi dopants diffuse less than 40 nm [98] and this allows us to perform H-termination several times (and of course several flash times) until we obtain an excellent H-terminated surface for STM measurement without substantially reducing Bi dopant concentration in the silicon sample [94]. Despite that fact, we still have to bear in mind that flashing the sample too many times even at 1100 ℃ can also reduce the concentration of Bi dopants in the subsurface region down to the level that the Bi dopants cannot significantly contribute to the tunnelling [23].

6.3 Subsurface Bi-induced features at 77 K

There has been a publication reported an experimental observation of features induced by Bi donors in the Si(001) surface layer [94]. A feature caused by a dopant in the surface and a dopant in a subsurface layer are in principle different from each other in that the subsurface dopant-induced features are delocalised and superimposed on the surface corrugation while the surface dopant-induced features are usually localised. An example of the appearance difference is shown in Fig.6.4 where subsurface Sb-induced features are observed

in the same surface are as surface Sb-induced features [95], in this case for a Si(111) with H-termination. According to this hint and the STM images of surface Bi-induced features, we were able to identify features that are likely to be induced by Bi in the subsurface layers as described in the next sections.

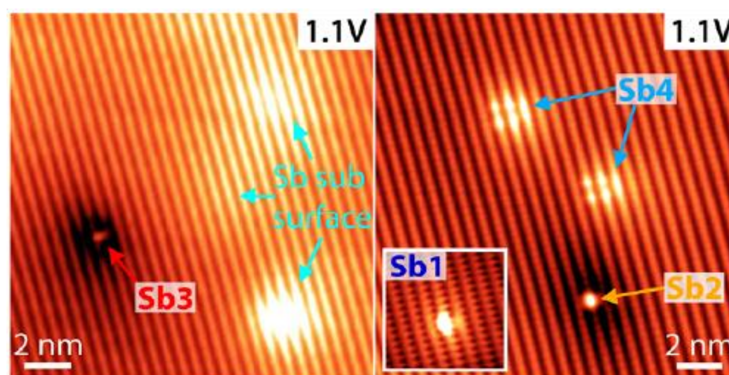

Figure 6.4 Empty-state STM images of a cleaved Si(111) surface revealing electronic features induced by subsurface and surface Sb donors. The subsurface dopant-induced features are always delocalised and superimposed on the surface corrugation. The images are taken from Ref. [95].

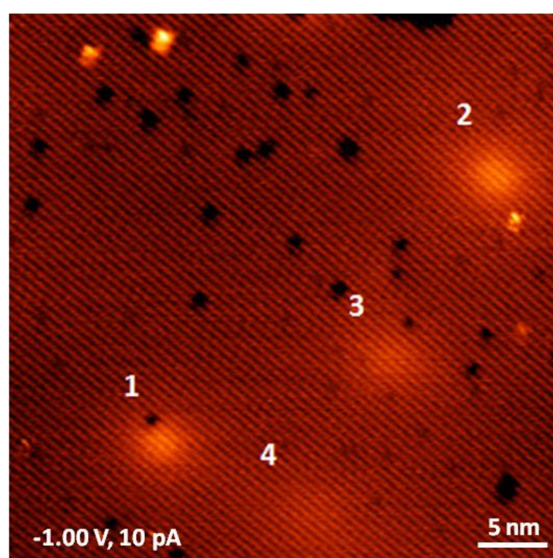

Figure 6.5 A filled-state image of a Si(001):H surface taken at 77 K with the sample voltage bias of -1.00 V and the tunnelling current setpoint of 10 pA showing four delocalised protrusions superimposed on the Si(001):H surface corrugation.

6.3.1 Many Bi features in the same image

Fig. 6.5 is a filled-state image of a Si(001):H surface area taken at 77 K with the sample bias and the tunnelling current setpoint of -1 V and 10 pA respectively. The image reveals 4 delocalised circular protrusions superimposed on the Si(001):H background lattice, which indicates that these features are induced by charged impurities in the subsurface layers [100]. Considering different intensities of these features, the features could be induced by charged impurities located in different subsurface layers [52] or different lattice positions in case they are in the same layer [30]. These features were commonly observed throughout the surface and are attributed to subsurface Bi atoms as previously discussed in section 6.2.1. The frequency of the observation of the subsurface Bi-induced features during the investigation is about a few features in a surface area of 50×50 nm^2. The frequent observation of the subsurface Bi features also confirms our assertion that STS curves can be used for judging whether the density of Bi in the subsurface layer is sufficient for the STM measurement or not as discussed in section 6.2.3.

6.3.2 Three classes of subsurface Bi-induced features

By imaging a number of Si(001):H surface areas at 77 K, we have found that there are "three" distinctive subsurface Bi-induced features named Bi1, Bi2, and Bi3. Every one of the subsurface Bi features is delocalised and superimposed on the background surface corrugation as shown in Fig. 6.6.

Feature Bi1 appears as a circular protrusion for all the negative bias with its intensity decreasing with increasing the magnitude of the applied voltage. In empty-state images, at 1.3 V, Feature Bi1 appears rectangle-like with one of the diagonal axes which runs from the top left corner to the lower right corner expresses higher brightness than the other. At the middle of the feature, there is a small depression surrounding by the delocalised protrusion characteristic of the Bi1 feature. When the voltage rises from 1.3 V to 1.5 V, the intensity of the delocalised protrusion becomes lower and instead the central depression appears more obvious with its relatively larger size. At the sample bias higher than 1.5 V,

the delocalised protrusion completely disappears but the central depression still remains and becomes even more obvious.

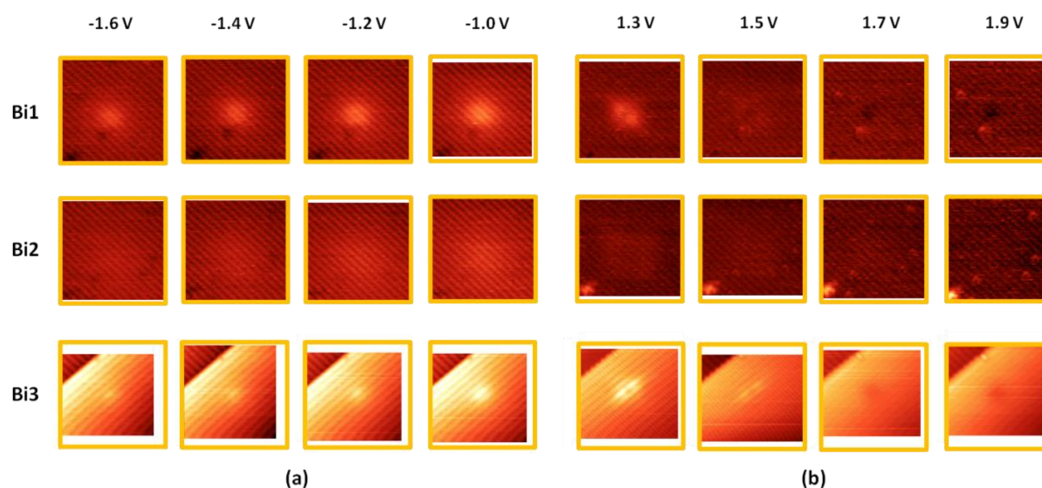

Figure 6.6 (a) filled-state and (b) empty-state images of three different subsurface Bi-induced features superimposed on the Si(001):H surface observed at 77 K. Each feature appears as a delocalised protrusion in filled-state images and a rectangle-like protrusion with a small depression at the feature centre in empty-state images. The box enclosing each image is 10 × 10 nm^2 in size.

Feature Bi2 also appears as a circular protrusion in the filled-state images however with apparently lower intensity than Bi1. Like the Bi1 feature, the intensity of Bi2 decreases with respect to the negative bias magnitude. Considering the appearance of Bi2 in the empty-state images, at 1.3 V the feature shape is apparently rectangle-like with a depression at the centre of the feature. The characteristics are the same as what have been noted for feature Bi1 except that the rectangular protrusion and the central depression of the Bi2 feature are larger in size (more delocalised). Moreover, the rectangular protrusion of the Bi2 feature expresses consistent intensity in all directions, unlike the rectangular protrusion of the Bi1 feature that has one diagonal axis much brighter than the other. Another crucial different point is that the depression at the middle of the Bi2 feature completely disappears once the positive bias increases to a certain voltage (~1.5 V). However, similar to Bi1, the protrusion of Bi2 also has its intensity decreasing when the positive bias magnitude increases and also disappears at higher positive bias. Although the Bi 2 feature shown in Fig. 6.6 has

very low intensity compared to Bi1, which might indicates that the Bi2 donor is located in a deeper subsurface layer than the layer the Bi1 donor, other Bi2 features does not show the same intensity such as the Bi2 feature shown in Fig. 6.7. For the Bi2 feature in Fig. 6.7, the contrast behaviour described can be clearly seen.

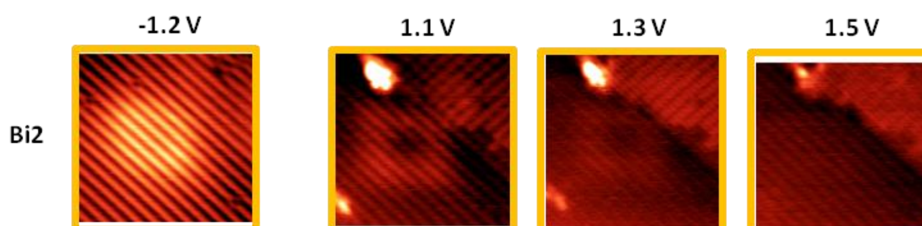

Figure 6.7 Another Bi2 feature shown in both filled-state and empty-state images, expressing higher intensity in both bias polarities and thus allowing the characteristic described in the text to be more easily observed.

The final class of the subsurface Bi features is named Bi3 (see Fig. 6.6). Unlike the first two subsurface Bi-induced features, feature Bi3 in the filled-state images consists of one outstanding bight line on the middle dimer row which becomes more obvious at higher bias magnitudes. The Bi3 feature also expresses the circular protrusion characteristic surrounding the central bight line. When the negative bias magnitude increases, the intensity of the bright line and the circular protrusion is reduced and eventually disappear as seen in Fig. 6.6 (a). Considering the empty-state images, feature Bi3 still appears as circular protrusion with the middle dimer row being distinctively brighter. Nevertheless, there is a very small depression at the centre of the feature, similar to feature Bi1 and Bi2. As the positive bias magnitude increases, the circular protrusion gradually disappears and the central depression expands and becomes more obvious as seen in Fig. 6.6 (b). Once the imaging voltage goes up from 1.5 V to 1.7 V, there is no longer the protrusion characteristic but the feature is replaced with a apparently delocalised depression.

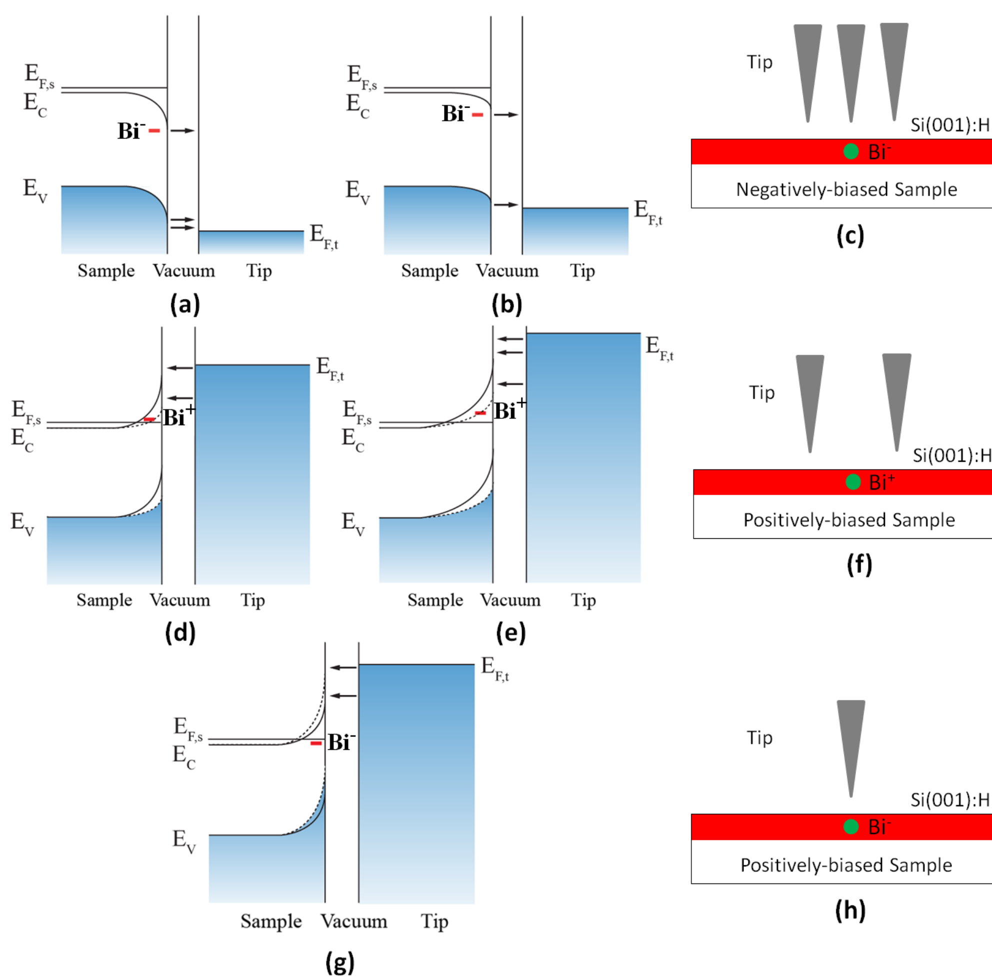

Figure 6.8 Schematic illustration of the energy-band diagram for the tunnelling mechanism associated with subsurface Bi-disturbed surface area of **(a)** high negative sample bias **(b)** low negative sample bias despite the tip position (see **(c)**). **(d)** and **(e)** Low and high positive sample bias respectively with the tip not over the donor position (see **(f)**). **(g)** Any positive sample bias with the tip over the donor position (see **(h)**).

6.3.3 Mechanism inducing the subsurface Bi features

As discussed in chapter 5 about the charge states of the subsurface As donors below Si(001) that cause such the stunning appearance of the subsurface As feature, in this chapter we will make use of the energy-band diagram and the consideration of the band movement to figure out the mechanism underlying the appearance of the subsurface Bi feature shown in Fig. 6.6. While further experiments, and ideally theory support, are required to provide conclusive explanations to the origins of our data, we suggest phenomenological explanations for our findings.

6.3.3.1 Filled-stated appearance

For every Bi feature – Bi1, Bi2, and Bi3 – their common characteristic in imaging the filled states of the sample is the circular delocalised protrusion that has intensity reduced with increasing the negative bias magnitude and disappears at a certain high voltage magnitude. The circular protrusion can be interpreted as a result of the Coulomb potential created by the Bi donor that is negatively charged.

At low negative sample bias (such as -1.0 V) combined with the fact that the sample Fermi level is further away from the conduction-band edge due to the low bulk-doping concentration, the tip Fermi level is shifted downwards into the valence-band range as shown in Fig 6.8 (a). Similar to the consideration of the negatively-charged As donor, with the Bi donor becoming negatively-charged, an associated Coulomb potential is created. This potential well reduces the downward band bending and as a result makes the tunnelling window of the valence band wider, which allows more filled states in the valence band to contribute electrons that tunnel to the empty states of the tip. Thus, the donor-disturbed surface area appears as a circular protrusion and the circular characteristic reflects the shape of the Coulomb potential projected on the background sample surface.

As the negative bias magnitude is changed to a higher value as depicted in Fig. 6.8 (b), the tip Fermi level is moved further downwards. This allows more valence-band states to participate in the tunnelling current both in the donor-

disturbed the donor-free surface areas. Consequently, the additional tunnelling window opened up by the negatively-charged Coulomb potential becomes insignificant, which makes the tunnelling current of the donor-free and the donor-disturbed surface areas approximately the same. Therefore, the intensity of both surface areas appears the same, equivalent to the decrease of the intensity of the subsurface Bi features until the feature disappear from the filled-stated images at high negative sample bias as seen in Fig.6.6 (a).

Dopant	Atomic Number	Ionisation Energy	Size [$\Delta V/V_{Si}$]
Phosphorous (P)	15	44 meV	-8 %
Arsenic (As)	33	54 meV	+4 %
Antimony (Sb)	51	39 meV	+17 %
Bismuth (Bi)	83	71 meV	+30 %

Table 6.2 Size and ionisation energy of all group V donors [2].

However, apart from the delocalised circular protrusion appearing in the filled-states images, there is actually also the central bright part of the Bi features that are not likely to disappear at high negative bias magnitude. This phenomenon occurs with the Bi1 and Bi3 features. Since the feature induced by Bi in the Si(001) surface layer has already been reported [94] and it is not similar to our Bi features, we discarded the idea of attributing the Bi1 and Bi3 features to negatively-charged Bi donors in the Si(001) surface although the appearance of both of the features was similar to the appearance of P in the Si(111) surface [101, 102] in that there was some brightness extended from the central small depression of the positively-charged P features. Considering the brightness of feature Bi1 and Bi2, it can be said that the underlying Bi donors could be located in the subsurface layers very closed to the Si(001) surface; for example, a few layer below Si(001). Since the size of a Bi dopant is much larger than the Si host atom [2] as show in Table 6.2, it could be that the strain created by the substitution of the Bi donor for the Si atom causes the stable localised protrusion on the sample surface as seen in Fig. 6.6 (a) for feature Bi1 and feature Bi3. Since the Bi donor is negatively-

charged, this is probably why the donor-disturbed surface area appears as stably localised small protrusion surrounding by a delocalised larger protrusion. For the Bi2 feature, the reason there is no localised protrusion at the middle part of the feature could be that the underlying Bi donor resided in a deeper subsurface layer such that the lattice strain resulted from the dopant substitution cannot be alter the sample surface corrugation. This is also supported by the much less intensity of the Bi2 feature compared to the Bi1 and Bi3 features.

6.3.3.2 Empty-state appearance

Their common characteristic for the empty-state imaging is the delocalised protrusion which has the intensity reduced and eventually disappears with increasing the positive sample bias. By closely examining all three Bi features at +1.3 V in Fig. 6.6 (b), it can be stated that the shape of the delocalised protrusion is rectangle with a small depression at its centre. The intensity of the protrusion decreases with increasing positive bias magnitude and eventually disappears at a certain high bias for all three Bi features (see Fig. 6.6 (b)). Considering the energy band diagrams illustrated in Fig. 6.8 (c) and (d), it has to be said that the subsurface Bi donor must be positively-charged. The Coulomb potential of the positively-charged Bi donor reduces the upward band bending, thereby making the tunnelling window of the donor-disturbed surface area wider than the donor-free region. However, the surprising scenario is the depression at the centre of each Bi feature which implies that the donor is negatively-charged. This is a weird charge-state behaviour that cannot be easily explained. However, interestingly there is a publication partly reporting the observation of a single dangling bond (DB) in filled-state and empty-state imaging [33] that can be compared to our Bi features.

In that reference, the dangling bond is created by the desorption of a single H atom from a Si dimer on a Si(001):H surface. In filled-state images, the DB is negatively charged but their charged state changes when the bias is switched to the opposite polarity. Under the empty-state tunnelling condition (positive sample bias), while the tip is scanned close to the DB, the defect is positively-charged; thus, there is a delocalised circular protrusion observed. The DB becomes

positively-charged because the tip influence raising the DB energy level above the bottom of the conduction band and thus the DB is ionised. An interesting situation happens when the tip scanned closer to the DB. With the shorter tip-donor distance, the tip electrostatic influence induces the DB to become negatively charged again! This is confirmed by delocalised depression surrounding the DB position which is caused by that fact that the tunnelling rate of electrons into the DB energy level is higher than the tunnelling rate of electrons out; thus, the defect becomes negatively-charged again. To make the comparison of the DB appearance with the appearance of our Bi features easier for keeping track of, we put the DB feature from the reference in Fig 6.9 below.

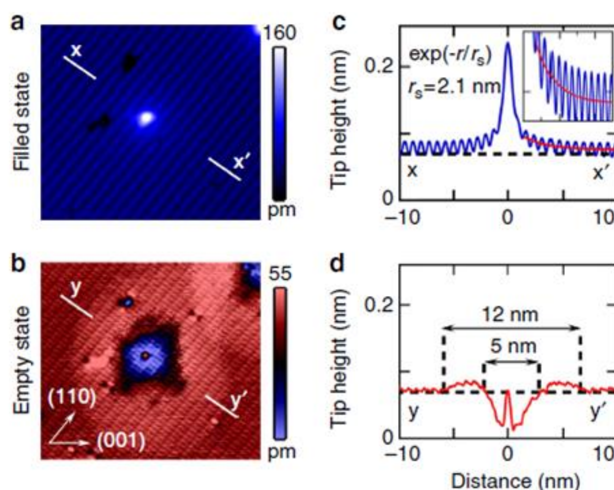

Figure 6.9 (a) and **(b)** Filled and empty-state images of a single DB taken at 77 K with +1.7 V and -1.7 V respectively. The tunnelling current setpoint for scanning is 25 pA. The size of each image is 16×14 nm^2. Intensity of the feature corresponding is shown in **(c)** and **(d)** as a high profile analysis. The screening length of 2.1nm calculated from the filled-state image is in agreement with a Thomas–Fermi estimate [103]. In the empty-state image, the DB exhibits 12-nm enhancement disc due to positively-charged ionization surrounding a 5-nm depression of the DB becoming negatively-charged again due to non-equilibrium tunnelling in/off rate. The figure is taken from Ref. [33].

The contrast behaviour of the DB feature has distinct similarities to the contrast behaviour of the Bi features except that the Bi donors in our consideration are all in the subsurface layers. Firstly, in filled-state images, all three types of Bi features appear as protrusions indicating that the subsurface Bi donors are negatively charged. Secondly, in empty-state images, each Bi feature appears as a delocalised protrusion (actually rectangular) informing that the Bi donor is positively charged as schematically shown in Fig. 6.8. (e). We would say that this is due to the raising of the donor energy level to lie above the bottom of the conduction band, making the Bi donor becomes positively-charged ionised. Thirdly we might speculate that similar to the DB case, when the tip scans over the central part of the feature, the tunnelling rate of electrons in and off the donor is not equal. The input rate is higher than the output, meaning the Bi donor becomes negatively-charged again as illustrated in Fig. 6.8 (f). As a result of the negatively-charged Bi donor, the central part of each Bi feature appears as a small delocalised depression in the empty-state images.

When the positive bias increases, the intensity of surrounding protrusion decreases and finally disappears at a certain high positive bias for all three Bi features in the empty-state images (see Fig. 6.6 (b)). Nonetheless, the central depression of feature Bi1 and feature Bi3 does not disappear even at the 1.9 V where it is not there in the case of feature Bi2. This could be attributed to the distance of the subsurface Bi donors from the surface. Similar to the central localised small protrusion in the filled-state images that does not disappear at high negative bias, the Bi donors associated with the Bi1 and Bi3 features are located closer to the Si(001) surface (probably just a few layers beneath the surface) than the Bi donor related to the Bi2 feature; thus, the central depressions of feature Bi2 and feature Bi3 do not disappear at high positive bias. The reason the Bi can accumulate the negative charge and become negative again from being positively-charged ionised might be due to its large binding energy.

Even though we have already ruled out the possibility of the Bi donors inducing the Bi1 and Bi3 features from being located in the Si(001) surface layer in our assignment above, we still open for that possible scenario. Since the intensity of the central part of Bi1 and Bi3 does not completely disappear at high

negative and high positive polarities, it might be that the Bi dopants inducing both features actually reside in the Si(001) surface layer [104].

The last but not least for the discussion of the three types of subsurface Bi features observed in our experiment, the reason that the delocalised protrusions in empty-state images are rectangular-like is still a mystery. However, we would propose that the tunnelling mechanism in empty-state images providing the appearance of the rectangular protrusion is associated with the tunnelling of electrons from the filled states of the tip to the empty states of the sample. If we reconsider the appearance of the subsurface As1 feature shown in Fig. 5.4, especially the As1.2 feature, it is obvious that there are some characteristics of the filled-state appearance in the empty-state appearance. In empty-state images, the As donor is also positively-charged (an empty state), thereby being able to have electrons tunnelling to its electronic state according to the energy-band diagram. In filled-state images, the As donor is neutral (a filled-state), so it can provides electrons tunnelling to the tip and create the relevant wavefunction projection as a As1 feature on the surface. Hence, in the empty-state images, the tunnelling of electrons into the As empty state can also provide the projection on the surface although the intensity is not as obvious. For the Bi case, since one of the empty states of the sample when the sample is positively-biased is the Bi donor state which is positively-charged due to the ionisation. Thus, electrons from the tip can tunnel into the electronic state of the Bi donor. Based on the case of the As1 features, we state that the rectangle-like protrusion of the Bi features when imaged with positive sample bias is associated with the wavefunction projection of the subsurface Bi donor. Therefore, if the Bi donor is electrically neutral in when the sample is negatively biased, a rectangle-like feature superimposed on the Si(001):H surface with varied atomistic details in the feature area similar to the As1 features could be observed.

Chapter 7

Conclusion and future work

7.1 Conclusion

The aim of this PhD work was to investigate donors in silicon using scanning tunnelling microscopy (STM) and spectroscopy (STS) with partial support from DFT calculations, performed by our colleagues where necessary. Knowledge acquired from the characterisation of the individual donors with atomic-scale resolution contributes to efforts to fabricate devices in silicon for quantum information processing (QIP) applications. Three different experimental systems were studied, each relevant to QIP applications in different ways. The key conclusions from these studies are summarised below.

7.1.1 The study of phosphine on Si(001) at 77 K

This PhD work began with the study of PH_3 molecules deposited on the Si(001) surface at room temperature that was transferred to the 77-K scanning stage for STM measurement within a few minutes. For the project on the investigation of PH_3 on Si(001), we divided the work into three main tasks. The first was the study of saturation-dosed Si(001), the second was the investigation of lightly-dosed Si(001), and the last was the investigation of the lightly-dosed Si(001) after being thermally annealed to incorporate the adsorbed P atoms into the surface layer.

Firstly, we studied Si(001) with STM at 77 K after being dosed with phosphine to the saturation level at room temperature. The results had shown nothing distinctively different from the previous work in which the saturation-dosed Si(001) surface was investigated with STM at room temperature [37] until we performed the voltage-dependent imaging. With the sample bias decreasing, we found that there were three protrusion features commonly appearing on the

Si(001) surface instead of only two as reported in Ref [37]. We attributed small protrusions to PH_2+H while the big protrusions were assigned to PH+H and Si dangling bond (Si DB), depending on its voltage-dependent contrast behaviour. When the magnitude of negative bias decreased, the big protrusions assigned to PH+H became smaller in size and less in terms of intensity while the other type of the big protrusion assigned to Si DB remained nearly the same. Without the voltage-dependent imaging, the PH+H and Si DB features would not be able to be distinguished from each other at the sample temperature of 77 K.

After the saturation-dosed surface, we turned our attention to the study of Si(001) lightly dosed with PH_3 at room temperature and subsequently, after a few minutes, measured at 77 K. With the surface and adsorbate states frozen, we discovered a number of different PH_3-associated features individually appearing on the surface beside those PH_3-related features commonly observed at room temperature. We also categorised them into three groups, depending on their characteristic appearance – asymmetric (A), centred (C), U-shaped (U). Unlike the room-temperature observation, there is more than one type of features in each group. In group A, there are feature A1 and A2 with the A2 feature having the same appearance as the asymmetric feature observed at room temperature. Each one of the A features was assigned to the PH_2+H structure. Although all of them have the same bonding configuration on the Si(001) surface, they do not have the same appearance. Feature A1 and A2 can only be distinguished from each other using the empty-state images. For the filled-state images, both of them appear the same at low and high bias magnitudes. The difference of the appearance of A1 and A2 is attributed to the variation of the buckling orientation of the background Si dimers. Like the features in group A, the PH_3-related dissociative adsorbates in group U also have different buckling orientations with respect to the background Si dimers as the underlying mechanism that makes them appear different. Feature U1 and U2 can are also identical in all filled-state images but can be distinguished with the empty-state images. For the phosphine-related features in group C which consists of feature C1, C2, and C3, we assigned the C1 feature to the PH+2H structure with the same bonding configuration as that assigned to the centred feature observed at room temperature. More puzzling were the assignments of features C2 and C3, neither of which could be assigned to any bonding

configuration consisting of 1 P atom and 3 H atoms. However, by our survey of another PH_3-on-Si(001) work of our colleagues measured at room temperature [55], we explored another dissociative pathway in which a PH_3 molecule dissociates into two fragment; PH_2 and H. We proposed that each PH_2 fragment would further dissociate into a structure consisting of 1 P atom and 2 H atom, however, with two possible bonding configurations. One of the bonding configurations was attributed to the C2 feature while the other was assigned to feature C3. The number of hemihydride features counted on the surface is consistent with the number of feature C2 and feature C3 combined, providing supporting evidence that the P+2H structures could be attributed to the C2 and C3 features.

Although no structural transformation at 77 K was expected, we still observed a transformation of feature C3 to feature U1. The transformation is not time dependent. Since the thermal energy at 77 K is not enough to cause such a transition, we believe that the transformation of the PH_3-related structures is driven by the electrostatic influence of the STM tip. The transformation happens with 1 H atom out of 3 being desorbed and the P atom shifting from the end-bridge site to the dimer-bridge position. This leaves behind a P+2H structure with the bonding configuration associated with feature C3 which is more energetically preferable than feature U1. Unlike the transformation previously reported at room temperature, this transition crosses between two different dissociative pathways, from the most energetically stable structure of the first path to the most stable structure of the other path. However, if the C3 feature was interpreted as an intermediate state of the dissociation from the centred feature (C1) to the U-shaped feature (U1) at room temperature, then it could be that the transformation we observed at 77 K is the backward and tip-induced process of the forward thermally-driven dissociative transformation at room temperature that has been thought to be an irreversible process.

The last of our studies on the phosphine-dosed Si(001) surface is the investigation of the Si-P heterodimer occurring due to the P incorporation into the Si(001) surface by heating up the sample and keeping it at the temperature of ~350 °C for 10 seconds. In this process, P atoms were incorporated into the Si(001) layer by substituting for Si atoms in the surface forming a Si-P

heterodimers, with the ejected Si atoms forming chains of dimers, as previously observed [38]. Monohydride dimers were also present on the surface. For the Si-P heterodimer. In filled states, the feature appeared as a zigzag feature with the buckling orientation consistent with the background surface except that the feature area was brighter. The bright side of the Si-P dimer was attributed to the Si atom with its dangling bond fully occupied by two electrons. In empty-state images, the Si atom lost both electrons, making the Si atom appears as bright as the surrounding Si dimer atoms. At 77K, it seems that the ground state is the configuration in which the Si heterodimer atom buckles upward with 2 electrons in its dangling bond which is opposed to the proposal in Ref. [5]

7.1.2 Subsurface As donors in Si

For the study of As donors below the Si(001):H surface, careful choice of sample preparation parameters was crucial in enabling us to image the buried dopants. In order to have sufficient amount of As in the subsurface layers below the Si(001):H surface, we had to flash the sample at the temperature as low as 1050 °C to obtain a flat and clean Si(001) surface and prevent subsurface As donors from evaporating out of the Si sample. Then, the surface was terminated with a single layer of H atom to remove the surface π states. We observed two classes of subsurface As-induced features – As1 and As2.

The As1 features appear as protrusions in both filled- and empty-state imaging. However, in filled-state images, the features appear as a protrusion with characteristic cross-like shape, with symmetry both around the axis parallel to the dimer rows and the axis perpendicular to the dimer rows. For the empty-state images, the As1 features interestingly changes from the anisotropic shape to circularly isotropic protrusions. In both filled- and empty- state images, the intensity of the feature decreases with increasing magnitude of sample bias.

We employed the energy-band diagram with tip induced band bending (TIBB) to explain the underlying tunnelling mechanism of the appearance of the As1 features. For the imaging of the filled states, assuming that the As donor is electrically neutral perfectly explains the appearance of all the As1 features in that

the cross-like shapes are associated with the projection of the wavefunction of the neutral subsurface As donor on the Si(001):H surface. In empty state images, the circular protrusion is induced by Coulomb potential created by positively-charged ionised As donors. The circular shape reflects the shape of the potential well below the surface. For both bias polarities, negative and positive, the increase of the bias magnitude enhances the tunnelling current associated with the valence band and conduction band respectively, causing the influence of the As donor on the total tunnelling current to be smaller and resulting in the suppression of the intensity of the As features. STS data obtained over As1.2 and As1.4 features confirmed the similarity of their electronic properties, supporting the conclusion that they are both neutral As dopants.

Beside the As1 features, caused by subsurface As donors which were either in a neutral or ionised state, we also observed another other class of feature named As2. The contrast behaviour of the As2 features is very similar to the contrast of negatively-charged ionised acceptors in silicon. Since the density of the As2 features is so high that the As2 features cannot be induced by ionised acceptor contaminating in this *n*-type silicon, we need to consider negatively-charged subsurface As donors.

We suggest that the subsurface As donor can be electrically neutral due to the enhancement of the donor binding energy as the donors are located in the substitutional sites closer to the surface. With the larger ionisation energy, the thermal energy at 77 K is not enough to excite the excessive valence electrons from the As donors. In the surface region, the donors within a few layers away from the surface possess larger ionisation energy; thus, they would act like a trap capturing additional electrons to be lightly bound to the As atoms and thus makes the donor atom negatively-charged. For the donors further away from the surface but still inside the subsurface region, they still have larger binding energy than those in the bulk such that they are electrically neutral at 77 K.

Our interpretation for the As1 features have been confirmed by DFT calculations and simulated STM images, by one of our colleagues. With the energy calculation of possible substitutional sites for the As donors in the subsurface layers together with the relevant simulated STM images, we found out

that the shallowest As donor that can be compared with the As1 feature resides in the 7th layer (we counted the Si(001) surface as the 1st layer). This indicates that the As donors in the subsurface layers closer to the Si(001) surface are not neutral so that they cannot produce the feature with characteristic shapes corresponding to their wavefunction projection superimposed on the surface. With the combination of our earlier qualitative interpretation, we suggest that the shallower As donors are negatively-charged.

The last phenomena we observed, a by-product of the attempt to see the As-induced features, is the shift of the Si dimer rows of the background surface, as the scanning bias was changed from -1.3 V to -1.2 V. This means that the tip Fermi level is aligned very close to the top of the valence band by taking TIBB into account. Under this condition, we think that the tunnelling current produced by the valence-band states is very small and that the tunnelling current contributed by the filled conduction-band states cannot be ignored.

7.1.3 Subsurface Bi donors in Si

For the the QIP structure proposed by Stoneham *et al.*, the As donor in Si reported in chapter 5 could play the role of the control switch. However, the donor suitable as a qubit must have larger binding energy than As and that led us to focus on the Bi donor.

Since we could not find any commercial bulk Bi-doped Si wafer, we employed ion implantation technique to introduce Bi atoms into a Si(001) wafer with the controllable doping density and depth of the implanted layer. To study the Si(001) surface with STM, the surface must be thermally flashed to $\sim 1300\ ℃$ for 10 s to obtain the flat and clean condition of the surface reconstruction. However, we found that at this high temperature there were not a sufficient amount of Bi dopants in the subsurface layer as determined by the fact that the onset of empty-state tunnelling is higher than 2 V in STS data. This issue was overcome with a with the two-step flashing procedure. Firstly flash the sample to obtain the flat and clean condition with $\sim 1300\ ℃$ for 10 s, and then flash again to drive the Bi donors into the subsurface layers from the bulk of the

sample, with ~1100 ℃ for 10 s. Subsequent imaging after H-termination, revealed a surface band gap of approximately 2 eV, from about -1eV to around 1 eV, confirming the density of Bi donors in the subsurface layers is sufficiently high to image buried Bi dopants.

We observed three classes of subsurface Bi-induced features superimposed on the Si(001) surface corrugation at 77 K – Bi1, Bi2, and Bi3. Each of the three features appeared as a delocalised protrusion in filled-state images. Its intensity decreases with increasing negative bias magnitude. The central small localised protrusion of feature Bi1 and feature Bi3 was dedicated to surface strain induced by the substitution of a Bi donor for a Si atom in a subsurface layer very close to the surface based on the fact that a Bi atom is 30% larger than a Si atom; thus, the central small protrusion did not disappear at higher negative bias. With the aid of the energy-band diagram, all three Bi features were believed to be induced by negatively-charged Bi donors in the subsurface layers with the Bi1 and Bi3 donors residing very close to the surface.

For empty-state images, each subsurface Bi feature appeared as a rectangle-like delocalised protrusion with a small depression at the middle of the feature. For feature Bi2 both characteristics gradually disappeared at higher positive bias. For feature Bi1 and feature Bi3, the depression became more obvious with increasing positive bias and it did not disappeared at higher positive bias. The rectangular protrusion was attributed to the induction of positively-charged ionised Bi donors while the central depression was associated with the Bi donors becoming negatively-charged again due to the tunnelling rate into the donor energy level was higher than the output rate.

The rectangular shape was attributed to the tunnelling of electrons from the filled states of the tip to the energy level of the positively-charged Bi donor which was considered as another empty state of the sample. Thus, the rectangle-like protrusion would be associated with the wavefunction projection of the Bi donor on the Si(001):H surface reconstruction. If the charge state of the Bi donor is filled-state imaging is neutral, a feature with the rectangular shape would be observed on the surface.

7.2 Possible future work

Although the three main experiments done in this PhD work have discovered several novel results, with publications ensuing, the work has also opened- up the opportunity for new experiments with the potential to contribute toward the fabrication and characterisation of future QIP devices.

7.2.1 Possible future work for PH_3 on Si(001)

With the discovery of several phosphine-related features on the Si(001) surface with the sample cooled down to 77 K a few minutes after phosphine dosing at room temperature, it could be interesting to try phosphine dosing at 77 K. This might provide novel adsorbate structures that have been theoretically predicted but has never been experimentally observed. However, running another experiment with the same condition could also be intriguing but with an emphasis on investigation of any structural transformation happening on the surface. It has been speculated that the tip-induced transformation is induced when the imaging area is reduced. If the area is reduced to just a few nanometres square so that the tip always scans over the feature, a successive transformation further beyond what we reported in chapter 4 might be observed.

7.2.2 Possible future work for subsurface As and Bi donors in Si

The negatively-charged subsurface As donor is a real surprise from the experiment reported in chapter 5. We think that this is allowed to exist due to the low sample temperature. The experiment could be examined at room temperature to see whether the features induced by the negatively-charged As donors that are speculated to reside in the subsurface layers above the 7th layer are still observed. If not, and there are only neutral As-induced features observed, then the enhanced binding energy concept will become more convincing. Additionally, this result will inform that the *Stoneham et al.*, QIP device can operate at room temperature.

Appendix A

The density of subsurface As donors

The simplest way to do estimate the doping density from the STM images we have taken is to assume that we can image 1 nm below the surface (this is equivalent to 5 layers below the surface). If we count N dopants in a (100 nm × 100 nm) area, then we have measured N dopants per $100 \times 100 \times 1$ nm^{-3}, (the 1 nm is the depth). This is N dopants per 10^4 nm^{-3} or in the other word we have measured $N \times 10^{-4}$ dopants per nm^{-3}. To convert from nm^{-3} to cm^{-3}, we need to multiple by $(10^7)^3$. Thus, we have

$$N \times 10^{-4} \times 10^{21} \text{ dopants per cm}^{-3}$$

$$= N \times 10^{17} \text{ dopants per cm}^{-3}$$

What we need now from our data is the value of N. For our STM images, there are 198 dopants in 285 images of 50 nm by 50 nm. This means statistically that there are 198/285 = 0.7 dopants per 50 by 50 nm^2. Thus, the number of dopants (N) is

$$100/50 \times 100/50 \times 0.7 \text{ dopants per } 100 \text{ nm} \times 100 \text{ nm}$$

$$= 2.8$$

This means that statistically the measured doping density is ~ 2.8×10^{17} cm^{-3}, which is slightly lower than the bulk doping density of the wafer of 1×10^{18} cm^{-3}. However, this is not unexpected given that the surface region of silicon is known to undergo some depletion of n-type dopants during thermal treatment [23] and it is generally difficult to identify all dopants via buried dopant imaging (e.g., dopants lying directly beneath surface defects may be obscured and are therefore not counted in our statistics).

The uncertainty of the measured doping density is the total counts (N) of the As features observed. Thus, for a new set of 285 STM images of 50 nm by 50

nm obtained with the same experimental criteria, N should be in the range of $198 \pm \sqrt{198}$. Hence, the number of dopants becomes

$$100/50 \times 100/50 \times (198 \pm \sqrt{198})/285 \text{ dopants per } 100 \text{ nm} \times 100 \text{ nm}$$

$$= 2.80 \pm 0.19$$

This means that by taking into account the uncertainty of our data, the measured doping density can be expressed as ~ $(2.8 \pm 0.19) \times 10^{17}$ cm^{-3}.

Lists of Figures

Fig. 1.1 Variation of the Mn wavefunction of below GaAs(110) at 5 K 13

Fig. 1.2 The Quantum Computer schemes 16

Fig. 1.3 Atomic-scale device in Si fabricated using STM 17

Fig. 1.4 STM images of Si below GaAs(110) and As below Si(001):H 18

Fig. 2.1 A diagram illustrating an STM structure 22

Fig. 2.2 One-dimensional tunnelling through a rectangular potential 24

Fig. 2.3 Energy-band diagrams of an STM system 25

Fig. 2.4 Energy-band diagrams for both filled- and empty-state imaging 26

Fig. 2.5 Modes of STM imaging 28

Fig. 2.6 Dependence of the appearance of Si(001) on the bias polarity 29

Fig. 2.7 A schematic illustrating the CITS measurement 32

Fig. 2.8 An energy-band model with the TIBB effect 33

Fig. 2.9 The mechanism causing the double-tip effect 34

Fig. 2.10 Reconstructions of the Si(001) surface 36

Fig. 2.11 Filled- and empty-state images of a hemihydride feature 37

Fig. 2.12 Surface reconstruction of degenerately-doped Si(001) at 77 K 38

Fig. 2.13 The surface states of an *n*-type Si(001) sample 41

Fig. 2.14 Intrinsic surface defects of Si(001) 43

Fig. 2.15 Structure of hemidydride, monohydride, and dihydride 44

Fig. 2.16 A hemihydride dimer appearing on the (001) surface 46

Fig. 2.17 Monohydride and dihydride dimers on the (001) surface 47

Fig. 2.18 Energy-band models of Si(001) and Si(001):H 48

Fig. 2.19 Common PH_3-related features on Si(001) at RT 50

Fig. 2.20 Energies for bonding configurations of PH_3 dissociative products 51

Fig. 2.21 The time-dependent transformation of PH_3 on Si(001) at RT 52

Fig. 2.22 Saturation-doped Si(001) with PH_3 measured at RT 53

Fig. 2.23 Appearance of a Si-P heterodimer at RT 54

Fig. 2.24 Features induced by some subsurface dopants below GaAs(110) 56

Fig. 2.25 Features induced by B, P, and As below Si(001) and Si(001):H 57

Fig. 3.1 The LT STM used in this PhD work 60

Fig. 3.2 A schematic diagram of the tip-etching process 65

Fig. 3.3 Instruments used for the tip-etching process 65

Fig. 3.4 Field Emission and Electron bombardment 67

Fig. 3.5 Field emission curves before and after the electron bombardment 67

Fig. 4.1 Quantum computer scheme based on the Stoneham's proposal 71

Fig. 4.2 Saturation-dosed Si(001) surface at 77 K and at RT 73

Fig. 4.3 Images of saturation-dosed Si(001) at different negative biases 73

Fig. 4.4 Si(001) at 77 K before lightly dosing with PH_3 at RT 75

Fig. 4.5 High-resolution images of the PH_3-related features at RT 77

Fig. 4.6 High-resolution images of the PH_3-related features at 77 K 77

Fig. 4.7 Numbers of each PH_3-related features observed in total at 77 K 78

Fig. 4.8 Voltage-dependent images of feature A1 and A2 80

Fig. 4.9 1-dimer-wide Bonding configurations of the PH_3-related structures 81

Fig. 4.10 Close-up images of feature A1 and A2 83

Fig. 4.11 Images of U1 and U2 with bonding configuration (BD) 85

Fig. 4.12 Images of the C1, C2, and C3 features with BD 87

Fig. 4.13 A series of STM images showing dissociation pathway of P+2H 89

Fig. 4.14 Dissociation pathway of P+2H 90

Fig. 4.15 Hemidydride feature on Si(001) at RT and at 77 K 92

Fig. 4.16 Forward transition of phosphine dissociation on Si(001) at RT 93

Fig. 4.17 Time-independent transformation of U1 to C3 at 77 K 94

Fig. 4.18 Dissociative diagram of the transformation at 77 K 96

Fig. 4.19 Diffusion of P from the end-bridge site to the dimer-bridge site 97

Fig. 4.20 PH_3-dosed Si(001) after the thermal P incorporation 100

Fig. 4.21 Dimer rows of ejected Si atoms on the Si(001) surface 101

Fig. 4.22 Si-P heterodimer observed at 77 K and RT and its charge states 103

Fig. 4.23 Possible stable bonding configurations of Si-P heterodimer 104

Fig. 5.1 Si(001) surface thermally flashed with different current 109

Fig. 5.2 Schematic illustration describing tip-induced band bending 111

Fig. 5.3 Filled-state image of Si(001):H at 77 K showing As1 and As2 113

Fig. 5.4 Voltage-dependent images of different As1 115

Fig. 5.5 Symmetry analysis of the As1.5 feature 116

Fig. 5.6 The electron carrier in silicon and sample temperature 117

Fig. 5.7 Constant and enhanced dopant binding energy 120

Fig. 5.8 CITS data of As1.2 and As1.4 123

Fig. 5.9 Filled-state image of Si(001):H at 77 K showing several As2 125

Fig. 5.10 Band diagrams of a negatively charged subsurface As donor 127

Fig. 5.11 Subsurface region of Si(001):H divided into two region 130

Fig. 5.12 Possible substitutional sites for As dopants in Si 132

Fig. 5.13 Pairs of experimental and simulated STM filled-state images 136

Fig. 5.14 Close-up images of As1.1-As1.5 showing their symmetry 137

Fig. 5.15 Dimer-row shift at very low negative bias 139

Fig. 6.1 Si wafer doped with Bi in five implantation layers 142

Fig. 6.2 Dependence of tunnelling current on Bi dopant density 146

Fig. 6.3 STS curves of *n*-type Si(001):H with various flash temperatures 148

Fig. 6.4 Features induced by subsurface and surface Sb donors 150

Fig. 6.5 Image of Si(001):H at 77 K revealing subsurface Bi features 150

Fig. 6.6 Voltage-dependent images of Bi1, Bi2, and Bi3 features 152

Fig. 6.7 Another Bi2 feature 153

Fig. 6.8 Tunnelling mechanism of subsurface Bi features 154

Fig. 6.9 Filled and empty-state images of a single DB taken at 77 K 158

List of Tables

Table 6.1 Used parameters for Bi implantation 143

Table 6.2 Size and ionisation energy of all group V donors 156

Bibliography

1. Kane, B.E., *A silicon-based nuclear spin quantum computer.* Nature, 1998. **393**(5).
2. Stoneham, A.M. *et. al.*, *Optically driven silicon-based quantum gates with potential for high-temperature operation.* Journal of Physics: Condensed Matter, 2003. **15**(27).
3. Morton, B.E. *et. al.*, *Embracing the quantum limit in silicon computing.* Nature, 2011. **479**: p. 345.
4. Warschkow, O. *et. al.*, Physical Review B, 2005. **72**(125328).
5. Randy, M.W. *et. al.*, *Importance of charging in atomic resolution scanning tunnelling microscopy: Study of a single phosphorous atom in a Si(001) surface.* Physical Review B, 2006. **74**(113311).
6. Feynmann, R.P. *et. al.*, *There's plenty of room at the bottom.* Engineering and Science, 1960. **23**(22).
7. Celebi, C. *et. al.*, *Surface Induced Asymmetry of Acceptor Wave Functions.* Physical Review Letters, 2010. **104**(086404).
8. Wijnheijmer, A.P. *et. al.*, *Enhanced donor binding energy close to a semiconductor surface.* Physical Review Letters, 2009. **102**(16).
9. Garleff, J.K. *et. al.*, *Bistable behavior of silicon atoms in the (110) surface of gallium arsenide.* Physical Review B, 2011. **84**(075459).
10. Wijnheijmer, A.P. *et. al.*, *Single Si dopants in GaAs studied by scanning tunnelling microscopy and spectroscopy.* Physical Review B 84, 2011. **125310**.
11. Teichmann, K. *et. al.*, *Controlled charge switching on a single donor with a scanning tunnelling microscopy.* Physical Review Letters, 2008. **101**(076103).
12. Teichmann, K. *et. al.*, *Bistable charge configuration of donor systems near the GaAs(110).* Nano Letters, 2011. **11**.
13. ITRS, *International technology roadmap for semiconductors.* 2009.
14. Shinada, T. *et. al.*, *Enhancing semiconductor device performance using ordered dopant arrays.* Nature, 2005. **437**(7062): p. 1128-1131.

15. Schofield, S.R. *et. al.*, *Atomically precise placement of single dopants in Si.* Physical Review Letters, 2003. **91**(13).
16. Ruess, F.J. *et. al.*, *Toward atomic-scale device fabrication in silicon using scanning probe microscopy.* Nano Letters, 2004. **4**(10).
17. Liu, L. *et. al.*, *Subsurface Dopant-Induced Features on the Si(100)2x1:H Surface: Fundamental Study and Applications.* IEEE Transactions on Nanotechnology, 2002. **1**(4).
18. Loth, S. *et. al.*, *Band structure related wave-function symmetry of amphoteric Si dopants in GaAs.* Solid State Communications, 2008. **145**: p. 551-555.
19. Depuydt, A. *et. al.*, *Scanning tunneling microscopy and spectroscopy at low temperatures of the (110)...surface of Te-doped GaAs single crystals.* Physical Review B, 1999. **60**(4).
20. Brown, G.W. *et. al.*, *Observation of buried phosphorus dopants near clean Si(100)-(2x1)...surfaces with scanning tunneling microscopy.* Physical Review B, 2004. **70**(121301).
21. Hamers, R.J. *et. al.*, *Scanning tunneling microscopy of Si(001).* Physical Reveiew B, 1986. **34**(5343).
22. Hata, K. *et. al.*, *How to fabricate a defect free Si(001) surface.* Journal of Vacuum Science and Technology A, 2000. **18**(1933).
23. Pitters, J.L. *et. al.*, *Dopant depletion in the near surface region of thermally prepared silicon(100) in UHV.* JVSTB, 2012. **30**(021806).
24. Bining, G. *et. al.*, *Tunneling through a controllable vacuum gap.* Applied Physics Letters, 1982. **40**(2): p. 178-180.
25. Bining, G. *et. al.*, *Surface studies by scanning tunneling microscpy* Physical Review Letters, 1982. **49**(1): p. 57.
26. Li, M.Q. *et. al.*, *Scanning probe microscopy (STM/AFM) and applications in biology.* Applied Physics A, 1999. **68**(2): p. 255-258.
27. Meier, J. *et. al.*, *Nano-scale effects in electrochemistry.* Chemical Physics Letters, 2004. **390**(4-6): p. 440-444.
28. Cyr, D.M. *et. al.*, *STM investigations of organic molecules physisorbed at the liquid-solid interface.* Chemicstry of Materials, 1996. **8**(8): p. 1600-1615.

29. Eigler, D.M. *et. al.*, *Positioning single atoms with a scanning tunneling microscope.* Nature, 1990. **344**: p. 3.

30. Sinthiptharakoon, K. *et. al.*, *Investigating Individual Arsenic Dopant Atoms in Silicon using Low-Temperature Scanning Tunnelling Microsopy.* Journal of Physics: Condensed Matter, 2014. **25**.

31. Yakunin, A.M. *et. al.*, *Spatial structure of an individual Mn acceptor in GaAs.* Physical Review Letters 2004. **92**(21).

32. Studer, P. *et. al.*, *Model system for controlling strain in silicon at the atomic scale.* Physical Reveiew B, 2011. **84**(4): p. 041306.

33. Schofield, S.R. *et. al.*, *Quantum engineering at the silicon surface using dangling bonds.* Nature Communications, 2013.

34. Simmons, M.Y. *et. al.*, *Towards the atomic-scale fabrication of a silicon-based solid state quantum computer.* Surface Science, 2003. **532**: p. 2109-1218.

35. Wilson, H.F. *et. al.*, *Phosphine dissociation on the Si(001) surface.* Physical Review Letters, 2004. **93**(226102).

36. Oberbeck, L. *et. al.*, *Challenges in surface science for a P in Si quantum computer - phosphorous adsorbtion/incorporation and epitaxial Si encapsulation.* Surface Review and Letters, 2003. **10**: p. 415.

37. Schofield, S.R. *et. al.*, *Phosphine dissociation and diffusion on Si(001) observed at the atomic scale.* Journal of Physical Chemistry B, 2006. **110**: p. 3173-3179.

38. Curson, N.J. *et. al.*, *STM characterisation of the Si-P heterodimer.* Physical Review B, 2004. **69**(195303).

39. Curson, N.J. *et. al.*, *Critical issues in the formation of atomic arrays of phosphorus in silicons for fabrication of a solid-state quntum computer.* Surface Science 2003. **532**: p. 678-684.

40. Reusch, T.C.G. *et. al.*, *Phosphorus and hydrogen atoms on the (001) surface of silicon: A comparative scanning tunnelling microscopy study of surface species with a single dangling bond.* Surface Science, 2006. **600**: p. 318-324.

41. Reusch, T.C.G. *et. al.*, *Single phosphorus atoms in Si(001): Doping-induced charge transfer into isolated Si dangling bonds.* Journal of Physical Chemistry C, 2007. **111**: p. 6428-6433.

42. O'Brien, J.L. *et. al.*, *Towards the fabrication of phosphorus qubits for a silicon quantum computer.* Physical Review B, 2001. **64**(161401).
43. Fuechsle, M. *et. al.*, *A single-atom transistor.* Nature Nanotechnology, 2012. **7**: p. 242-246.
44. Zheng, Z.F. *et. al.*, *Empty state and filled state image of ZnGa acceptor in GaAs studied by scanning tunneling microscopy* Applied Physics Letterss, 1994. **64**(1836).
45. Kort, R.d. *et. al.*, *Zn- and Cd-induced features at the GaAs(110) and InP(110) surfaces studied by low-temperature scanning tunneling microscopy.* Physical Review B, 2001. **63**(125336).
46. Mahieu, G. *et. al.*, *Direct evidence for shallow acceptor states with nonspherical symmetry in GaAs.* Physical Review Letters, 2005. **94**(026407).
47. Loth, S. *et. al.*, *Depth Resolved Scanning Tunneling Spectroscopy of Shallow Acceptors in Gallium Arsenide.* Japanese Journal of Applied Physics, 2006. **45**(3B).
48. Loth, S. *et. al.*, *Connection of anisotropic conductivity to tip-induced space-charge layers in scanning tunneling spectroscopy of p-doped GaAs.* Physical Review B, 2007. **76**(235318).
49. Loth, S. *et. al.*, *Probing semiconductor Gap states with Resonant Tunneling.* Physical Review Letters, 2006. **96**(066403).
50. Wijnheijmer, A.P. *et. al.*, *Influence of the tip work function on scanning tunneling microscopy and spectroscopy on zinc doped GaAs.* Journal of Vacuum Science and Technology B, 2010. **28**: p. 1086.
51. Nishizawa, M. *et. al.*, *Scanning Tunneling Microscopy Observation of Individual Boron Dopant Atoms beneath Si(001)-2x1 Surfaces.* Japan Society of Applied Physics, 2005. **44**(48).
52. Liu, L. *et. al.*, *Atom-resolved three-dimensional mapping of boron dopants in Si(100) by scanning tunnelling microspoy.* Applied Physics Letters, 2001. **78**(3).
53. Oberbeck, L. *et. al.*, *STM imaging of buried P atoms in hydrogen-terminated Si for the fabrication of a Si:P quantum computer.* Thin Solid Films, 2004. **464-465**: p. 23-27.

54. Brown, G.W. *et. al.*, *Observation of buried phosphorus dopants near clean Si(100)-(2x1)…surfaces with scanning tunneling microscopy.* Physical Review B, 2004. **70**(121301).

55. Warschkow, O. *et. al.*, *Reaction paths of phosphine dissociating on the silicon (001) surface.* (In preparation).

56. Tochihara, H. *et. al.*, *Low-temperature scanning-tunneling-microscopy observations of the Si(001) surface with a low surface-defect density.* Physical Review B, 1994. **50**: p. 12262(R).

57. Schofield, S.R. *et. al.*, *Phosphine dissociation and diffusion on Si(001) observed at the atomic scale.* Journal of Physical Chemistry B, 2006. **110**: p. 3173-3179.

58. Wilson, H.F. *et. al.*, *Phosphine dissociation on the Si(001) surface*. Physical Review Letters, 2004. **93**(226102).

59. Bennett, J.M. *et. al.*, *Diffusion pathways of phosphorus atoms on silicon (001).* Physical Review B, 2009. **76**(165311).

60. Zavodinsky, V.G. *et. al.*, *Energies of Si-P and P-P dimers on the Si(100)-2x1 surface.* Applied Surface Science, 1999. **141**: p. 193-196.

61. Miwa, J.A. *et. al.*, *Transport through a single donor in p-type silicon.* Applied Physics Lettes, 2013. **103**(043106).

62. Mol, J.A. *et. al.*, *Interplay between quantum confinement and dielectric mismatch for ultrashallow dopants.* Physical Review B, 2013. **87**(245417).

63. McEllistrem, M. *et. al.*, *M. Electrostatic sampl-tip interactions in the scanning tunnelling microscope.* Physical Review Letters, 1993. **70**(16).

64. Randy, M.W. *et. al.*, *Single hydrogen atoms on the Si (001) surface.* Physical Review B, 2007. **76**(155302).

65. Piva, P.G. *et. al.*, *Field regulation of single-molecule conductivity by a charged surface atom.* Nature, 2005. **435**: p. 658.

66. Zheng, J.F. *et. al.*, *Si donors (SiGa) in GaAs observed by scanning tunneling microscopy.* Journal of Vacuum Science and Technology B, 1994. **12**(3).

67. Sze, S.M. *et. al.*, *Semiconductor devices - Physics and Technology*. 2nd ed.

68. Duguay, S. *et. al.*, *Evidence of atomic-scale arsenic clustering in highly doped silicon.* Journal of Applied Physics, 2009. **106**(106102).

69. Giubetoni, D. *et. al.*, *Deactivation of submelt laser annealed arsenic ultrashallow junctions in silicon during subsequent thermal traetment.* 2010.

70. Nobili, D. *et. al.*, *Features of arsenic clusters in silicon.* Phys. Stat. Sol. (c), 2005. **2**(10).

71. Brazdova, V. *et. al.*, *Exact subsurface dopant sites identied by means of scanning tunnelling microscopy on the Si(001):H surface.* (In preparation).

72. Wang, Y. *et. al.*, *Atomic structure and bonding of boron-induced reconstructions on Si(001).* Physical Review Letters, 1995. **74**(3).

73. Komeda, T. *et. al.*, *Atomic configuration of segregated B on Si(001) surface.* Applied Physics Letters, 1997. **71**(16).

74. Komeda, T. *et. al.*, *Atomic structure of segegrated boron on Si(001) surface; scanning tunneling microscopy and cluster model calculation study.* Surface Science, 1998. **405**: p. 38-45.

75. Nielsen, J.F. *et. al.*, *Scanning tunneling microscope studies of boron-doped Si(001).* Journal of Vacuum Science and Technology A, 1999. **17**(4).

76. Fang, H.Y. *et. al.*, *B-induced reconstruction on Si(100)-(2x1) surface studies with scanning tunnling microscopy.* Materials Characterization, 2002. **48**: p. 183-188.

77. Liu, Z. *et. al.*, *Atomic structures of boron-induced protrusion features on Si(100) surfaces.* Physical Review B, 2008. **77**(035322).

78. Blomquist, T. *et. al.*, *Reversal of the charge transfer between host and dopant atoms in semiconductor nanocrystals.* Nano Letters, 2004. **4**(11): p. 2251-2254.

79. Perdew, J.P. *et. al.*, *Generalized Gradient Approximation Made Simple.* Physical Review Letters, 1996. **77**(3865).

80. Kresse, G. *et. al.*, *Ab initio molecular dynamics for open-shell transition metals.* Physical Review B, 1993. **48**(13115).

81. Kresse, G. *et. al.*, *Efficient iterative schemes for ab initio total-energy calculations using a plane-wave basis set.* Physical Review B, 1996. **54**(11169).

82. Blochl, P.E. *et. al.*, *Projector augmented-wave method.* Physical Reveiew B, 1994. **50**(17953).

83. Kresse, G. *et. al.*, *From ultrasoft pseudopotentials to the projector augmented-wave method.* Physical Review B, 1999. **59**(1758).

84. Monkhorst, H.J. *et. al.*, *Special points for Brillouin-zone integrations.* Physical Review B, 1976. **13**(5188).

85. Hubbard, C.R *et. al..*, *A silicon powder diffraction standard reference material.* Journal of Applied Cryst., 1975. **8**(45).

86. Massa, E. *et. al.*, *Measurement of the lattice parameter of a silicon crystal.* New J. Phys., 2009. **11**(053013).

87. Tersoff, J. *et. al.*, *Theory of the scanning tunneling microscope.* Physical Review B, 1985. **31**(805).

88. Pajot, B. *et. al.*, *A spectroscopic investigation of the lattice distortion at substitutional sites for groups V and VI donors in silicon.* Journal of Physics C: Solid State Physics, 1987. **20**(5241).

89. Morley, G.W. *et. al.*, *The Initialization and Manipulation of Quantum Information Stored in Silicon by Bismuth Dopants.* Nature Materials, 2010. **9**: p. 725-729.

90. Benjamin, S.C. *et. al.*, *Quantum Computing without Local Control of Qubit-Qubit Interactions.* Physical Reveiew Letters, 2001. **88**(017904).

91. Sousa, R.d. *et. al.*, *Spin-Dependent Scattering in Silicon Transiator.* Physical Reveiew B, 2009. **80**(045320-9).

92. Miwa, J.A. *et. al.*, *Transport through a single donor in p-type silicon.* Applied Physics Letters, 2013. **103**(043106).

93. .Brown, G.W. *et. al.*, *Observation of buried phosphorus dopants near clean Si(100)-2x1...surfaces with scanning tunneling microscopy.* Physical Reveiew B, 2004. **70**(121301).

94. Iwaya, K. *et. al.*, *Half-filled orbital and unconventional geometry of a common dopant in Si(001).* Physical Review B, 2013. **88**(035440).

95. Studer, P. *et. al.*, *Site-Dependent Ambipolar Charge States Induced by Group V Atoms in a Silicon Surface.* ACS Nano, 2012. **6**(12).

96. Miki, K. *et. al.*, *Atomically perfect bismuth lines on Si(001).* Physical Reveiew B, 1999. **59**(23).

97. Kirkham, C.J. *et. al.*, *Bi on the Si(001) surface.* Physical Review B, 2012. **86**(035328).

98. Fuller, C.S. *et. al.*, *Diffusion of Donor and Acceptor Elecment in Silicon.* Journal of Applied Physics, 1956. **27**(544).

99. Studer, P. *et. al.*, *Studying atomic scale structural and electronic properties of ion implanted silicon samples using cross-sectional scanning tunnelling microscopy.* Applied Physics Letters, 2013. **102**(012107).

100. Zheng, J.F. *et. al.*, *Scanning Tunnelling Microscopy Studies of Si Donors (Si_{Ga}) in GaAs.* Physical Review Letters, 1994. **72**(10).

101. Trappmann, T. *et. al.*, *Observation of P donors on the Si(111) surface by scanning tunnling microscopy.* Euro Physics Letters, 1997. **38**(3): p. 177.

102. Garleff, J.K. *et. al.*, *Identification of P dopants at nonequivalent lattices sites of the Si(111)-(2x1) surface.* Physical Revire B (Condensed Matter and Material Physics), 2007. **76**(12): p. 125322-125325.

103. Haamers, R.J. *et. al.*, *Characterisation of localised atomic surface defects by tunneling microscopy and spectroscopy.* Journal of Vacuum Science and Technology B, 1988. **6**: p. 1462-1467.

104. Brown, G.W. *et. al.*, *Observation of substitutional and interstitial phosphorus on clean Si(100)-(2x1) with scanning tunneling microscopy.* Physical Review B, 2005. **72**(195323).